Cataclysmic Variable Population Studies

Environmental influences on close binary formation and evolution

James D. Neill III

Submitted in partial fulfillment of the
requirements for the degree
of Doctor of Philosophy
in the Graduate School of Arts and Sciences.

COLUMBIA UNIVERSITY

2004

ABSTRACT

Cataclysmic Variable Population Studies

Environmental influences on close binary formation and evolution

James D. Neill III

The theory describing the formation and evolution of cataclysmic variables (CVs) is currently hampered by strong biases in the observational sample. These biases include: selection effects that skew the sample toward brighter, higher mass-transfer rate objects, the uncertainty in the frequency and type of CVs within the sample, and the difficulty in obtaining pure samples from either disk (late-type) or bulge (early-type) populations. These problems make it nearly impossible to discern the effect of environment on the formation and evolution of CVs. This thesis presents the results from a series of studies sampling a range of stellar environments in which CVs are found. We employed new observing techniques that begin to address some of the worst selection biases with the aim of strengthening the observational constraints on models of CV formation and evolution. We have measured the first orbital period for a dwarf nova in a globular cluster (M5 V101). Globular clusters are known to produce and lose many hard binaries through dynamical encounters in their cores, and as such, may be important contributors to the CV population of their host galaxy. We have produced the most accurate nova rate and spatial distribution for an external (late-type) galaxy (M81). We have conducted the first systematic, long-term nova survey of local group dwarf elliptical galaxies (M32, NGC205, NGC147, NGC185). Additionally, we have searched for novae in an environment which has implications for galaxy formation, namely the region between galaxies in a cluster (Fornax).

Our results confirm that CVs with orbital periods similar to Galactic CVs can be produced in globular clusters. We also provide some evidence that M5 V101 is being ejected from its host cluster. We show that our comprehensive, densely time-sampled nova survey of M81 produced a significantly larger and much more accurate global nova rate and spatial distribution than previous techniques. Our nova spatial distribution for M81 implies a bulge-to-disk nova ratio of > 9, in stark contrast to theoretical predictions. We show that local group dwarf ellipticals have a higher nova rate than predicted from assuming a constant nova rate per unit light for galaxies of all luminosities. We have demonstrated that novae exist between the galaxies of the Fornax cluster, and proven the feasibility of using them as probes of cluster tidal debris. We also show that the distribution of novae in the Fornax cluster is consistent with $\sim$25% of the total cluster light being unassociated with any galaxy. Our overarching conclusion is that the biases listed above will be reduced by dense temporal and comprehensive spatial coverage. As astronomical resources begin to shift toward large scale synoptic imaging surveys, we can look forward to a much more complete sample of close binaries, which may be used to inform a much-improved theory of their formation and evolution.

Contents

List of Tables

List of Figures

Acknowledgements

As my involvement in astronomy has been a lifelong one, and I have been alive for 44 years now, I have a long list of people to acknowledge. I apologize in advance for this indulgence, but I cannot overlook this opportunity to thank the people who have helped me on this long strange trip. I will do this in roughly chronological order. For those who begrudge this reverie I can only quote Tom Lehrer's "Irish Ballad":

You've yourselves to blame if it's too long,
You should never have let me begin...

I must, then, begin with my parents and sisters. My father, Don II, always encouraged in me an insatiable curiosity for words and the flow of history as a story about people. I think he is still puzzled about my choice of science as a career, but he gave me the basic storytelling tools that make describing my research an enjoyable task. My mother, Mary, instilled a strong belief in my own creativity which serves me well when I have doubts about my own peculiar path in astronomy and when it comes to trying out new ideas. My sisters, Jane and Glynnis, provided for me, in my childhood, the give and take that sharpened my mind as we negotiated (i.e., bickered) for our own way, and in adulthood, a particularly meaningful encouragement knowing as well as anyone the challenges I have faced in reaching for this goal.

Two other members of my close family that joined us later had a distinct impact on my academic goals. My step-mother Margaret joined our family just as she was finishing her Doctorate. I remember lots of pencils and stacks of graph paper pads, the tools of her research. She showed me in a very personal way that intellectual curiosity should not be confined to traditional academic subjects. My step-father Ed, who joined us a little later, recounted for me his story of persuing a PhD. He also showed me the joys of finding things out by applying the proper tools to good data.

If I owe my interest in astronomy to anyone, I owe it to my third grade teacher, Mrs. Holder. She knew how to channel my energies and curiosities and used the library to particular advantage. I still remember when she introduced me to H. A. Ray's book on the stars and constellations in the library at Vine Street elementary. I still own a copy.

From there astronomy took me to the Kalamazoo Astronomical Society who I thank en mass, but must mention Eric Schreur, Brian Akers, Mike Potter, Joe Medsker and the incomparable Peter Eckels. Being thrown in with a bunch of astronerds laid an important foundation for my career. Not only did I learn a whole host of astronomical basics, but I also immersed myself in observing and literally discovered the universe for myself through a variety of telescopes. It was during this phase of my life that a very deep bond with astronomy was forged. It still remains a bit of a mystery to me.

I was attending the University of Michigan when I first became aware of astronomy as a real way to make a living. Brad Whitmore, the graduate assistant who was teaching the recitation section of astro 101, showed the class slides from his recent observing run at CTIO. He calmly informed me that astronomy was indeed an acceptable major at the university. I promptly declared my major and received a

good grounding in astrophysics from the likes of Al Hiltner, Dick Teske, Dick Sears, Chuck Cowley, Hugh Aller, and Bob Kirshner. Bob sent me on my first professional observing run at the MDM observatory. My first real job doing astronomy I owe to Nancy Houk who hired me to operate a punch card machine to enter comments for stars in the Michigan Spectral Catalog. We got our first video display terminal during this time. It didn't do lower case letters yet, but when you logged out of the data entry program you were informed that you had just advanced science by 0.000001%! I would be remiss if I didn't also thank the graduate students at UofM who were quite friendly to us undergrads and gave us a view of the stages ahead.

I graduated in 1983 with a B.S. in Astronomy. The timing was fortuitous as the Space Telescope Science Institute (STScI) was ramping up prior to an expected launch for Hubble in 1986 (ahem). I must thank my fellow K. A. S. member and UofM undergrad Mike Potter for blazing the trail to Baltimore that I followed. I owe a deep debt of gratitude to my first advisor at STScI, Holland Ford. His scientific thoroughness and integrity is a constant yardstick against which I measure my own research. He also provided an environment of encouragement under which I developed many of the skills and habits which serve me in my research to this day. For his encouragement and instruction, I also thank Robin Ciardullo who was Holland's graduate student at UCLA (Baltimore campus) and co-conspirator on our Local Group survey projects.

From Baltimore I went to New York City just after the first Hubble repair mission. For this I must thank Carole Haswell, who in addition to prying me out of Baltimore, gave me an inside look at how to succeed in graduate school and my first real instruction in astro-politics. Once in NYC, I have to thank Mike Rich for hiring me out of Wall Street (a temporary insanity) and for imparting to me (I hope) some of his energy and scientific creativity. His encouragement started my career as a graduate student.

It was also through Mike that I got to know Edgar Smith, another graduate student at Columbia who was not cut from the standard mold. Edgar was building a state-of-the-art 1.2 meter telescope and asked me to help him. I joined his project and we became good friends. Edgar was another champion of my career advancement and also instrumental in my decision to become a full-time graduate student. Through the years we worked on many projects and published several papers together with Mike. I worked with Edgar and his team to get the Calypso Observatory up and running and producing science. Edgar's generosity toward me has been an important component in my success as a graduate student. My debt to him for the incredible allocation of entire seasons of telescope time on Calypso is one I don't think I'll ever be able to repay.

I am also indebted to the entire Astronomy Department at Columbia. I had an unusual path in that I got to know them as a research assistant and system manager first. When I changed to being a student, I always received the same respect that I got as a colleague which I appreciate deeply. In particular, I am indebted to Jacqueline van Gorkom who was chair of the department when I started as a student and encouraged my application. I also owe a debt of gratitude to David Helfand for very helpful conversations on career choices in astronomy and general guidance (not to mention great pasta dinners). Millie Garcia-Kramer has been a constant

source of guidance in the ways of Columbia bureaucracy and is an essential part of every graduate student's success. I would like to thank Joe Patterson for many useful conversations concerning cataclysmic variables and methods for analyzing the periodic signal in photometric data. I wish to thank Chuck Hailey who shepherded my 2nd year research project on Abell 262. I was also given encouragement and support by Steve Kahn who hired me as a system manager for the astrophysics lab at Nevis.

I wish to thank all my fellow students at Columbia for their friendship and help in the trenches. I thank Eilat Glickman for being a great office-mate, willing to swap therapy stories as well as talk about hydrostatic enebriation. I thank my fellow members of Hale-Bopp for their tolerance of the band's prima-donna guitar player and for letting him pretend to be Sting; Karl Forster, David Schiminovich, Andrew Chen, Eric Ford, and of course DJH (chanelling Janis). I thank Ben Sugerman for inviting me to his wedding to Jenny – I mean Sonja – it was great fun, and for providing the template for this thesis.

The next major advance for me came when the American Museum of Natural History (AMNH) started its astrophysics department. The hiring of Mike Shara by AMNH as the head of the new department was a singular stroke of luck for me. We had already collaborated on projects at STScI when I was there and he was a natural choice to be my advisor. His support in bringing me to the Museum as a research fellow and his encouragement and direction catalyzed the final stages of my transformation from research assistant to fully realized independent scientist. We immediately found ourselves in concord over the basic strategy of my thesis, namely to publish as much of the research as possible, as soon as possible. He provided the right mix of project seeds and support for new branches that has produced the final tree of my thesis. He performed that advisorly magic that supported my growth and yet allowed me ownership of my research program. His excitement about research was infectious and it was always a pleasure to share ideas and drafts of proposals, papers, and chapters of my thesis with him.

Among others at AMNH, I want to thank Diane Bynum in Grants and Fellowships for taking care of me and for her part in dealing with the Columbia bureaucracy. I thank Neil Tyson for hiring me as an instructor at the Hayden Planetarium and for comradeship as a fellow amateur-turned-pro. I thank all the denizens of the AMNH astro department for interesting lunch conversations and making the nascent department a fun and stimulating environment to do research in.

I cannot begin to thank enough the core support structure of my life, without which even the thought of this thesis would be impossible: Charity, my wife. Her constant belief in my abilities during my darkest hours calmed the storms of self-doubt that assailed me. Not only was she willing to hear constantly about the problems of research, politics, and career that I faced, but she is now willing to join me on the wild ride that will bring our family to a new city in a new country once I finish. It was an amazing stroke of luck to meet her, yet another unpayable debt I owe to Edgar Smith. Charity also brought forth our son, Leo who I also thank. He was born at nearly the same time as my graduate career and has grown with it. In his own way, he has always expressed belief in the importance of my work. It is inspiring to see

the effect my success has on his vision of the future. I also owe him thanks for the great excuse to indulge in playtime after a hard day at work.

In carrying out the research for my thesis, I would like to make the following additional acknowledgments. I acknowledge the enthusiastic support of the Calypso engineers, Bruce Truax and Frank Scinicariello, who made the projects carried out with Calypso possible. I also gratefully acknowledge the support of the Calypso observing team, Elaine Halbedel and Viktor Malnushenko, whose observing abilities and dedication through numerous trials made my research possible. I thank Robin Ciardullo for a comprehensive and rapid referee's report on the M81 nova survey paper and for excellent suggestions. I also thank Alan Shafter for valuable comments on the M81 manuscript. I also thank the anonymous referee of the M5 V101 paper for useful comments that made it a better paper. I am very grateful to John Thorstensen for obtaining the spectra of M32 Nova 1, allowing us to confirm its nature. We are also thankful to him for obtaining and astrometrically calibrating the I-band epoch of this nova, allowing us to refine its position. I also acknowledge the valuable assistance of the Tenagra Observatory team, Michael Schwartz, and Paulo Holvorcem, in determining coordinates for the Local Group novae and in preparing the IAU circulars announcing their discovery. Both Mike Shara and I wish to thank Bill Oegerle for the collaboration that resulted in the 1993 epochs of the Fornax cluster survey. We also thank Martin Bureau, Jeremy Mould, Tim Abbott, Knut Olsen, and Chris Smith for their role in acquiring Fornax cluster survey epochs in 2003 and 2004.

James D. Neill
neill@astro.columbia.edu
April, 2004

Dedication

I dedicate this thesis to my wife, Charity, and my son, Leo, who's patience, understanding, and support made it possible.

Chapter 1
Introduction

Two of the fairest stars in all the heaven, having some business
do entreat her eyes to twinkle in their spheres till they return.
William Shakespeare, *Romeo and Juliet*, Act II, scene 1.

1.1 Advancing Binary Star Theory

One of the greatest intellectual achievements of the previous century was the understanding of what powers the stars. The great union of stellar observation and nuclear theory brought a synthesis that now explains the structure and evolution of the majority of single stars in the universe. What happens when you add another star to our well understood single star? Like human couples, the answer to this question depends strongly on the initial conditions. It is clear that when our two stars are close enough to interact, the picture from single star theory begins to break down and cataclysms mark the evolution of what could have been quite ordinary stars. In humans, these cataclysms inspire literature. In astrophysics, the interacting binaries known as Cataclysmic Variables (CVs) inspire research.

As such, CVs are useful laboratories for gaining a more complete understanding of stellar evolution. Since $\sim$ 70% of all stars exist in multiple star systems and a large fraction of binaries undergo this tempestuous interacting phase, the study of CVs can give us insight into exactly how these interactions change the evolution of a large class of stellar objects. Observationally, the field has well-plowed areas at the brighter end of the population, but there are indications that the mother-load of CVs may exist at the fainter, lower mass transfer ($\dot{M}$) end. The field of CV studies is one where thorough observational work will be rewarded with significant advances in our understanding of how this important sample of stellar objects form, evolve, and die.

The luminous output (L) of an interacting binary goes up dramatically compared to the L of its non-interacting past, making CVs important tracers of binary populations. Mass accretion flow and disk-stream interactions produce observable phenomena that allow the derivation of some of the physical parameters of the interacting system. The small separations of the interacting components increases the probability of eclipses. When such eclipses are observed, we can derive the sizes of the components and produce a detailed physical description of the system.

In addition, CVs are laboratories in which many diverse physical phenomena can be studied. They offer a chance to observe mass transfer, accretion disks, thermonuclear shell burning, Roche lobe dynamics, gravitational perturbation of accretion disks, accretion column dynamics, and other processes that cannot be observed in any other way. These physical processes operate in many other objects and the knowledge gained from CVs contributes to a wider understanding of these phenomena. For example, type Ia supernovae may be understood as the end point of the evolution of

a class of CVs. Another example is provided by the Active Galactic Nuclei (AGN), powered by accretion disks that have much in common with the accretion disks found in CVs.

1.1.1 CV Formation and Early Evolution

Current models of close binary formation begin with a range of initial separations for the parent binaries. The more massive component of the binary evolves more rapidly into a red giant with a radius that can engulf both stars in a common envelope (CE). The observed masses of CV primaries implies a range of red giant core masses of $0.5M_{\odot} < M_{core} < 1.4M_{\odot}$. Since the radius of a red giant is largely determined by its core mass, this translates into an orbital separation range for the pre-interacting binaries of $130 < a/R_{\odot} < 2000$ and a period range of $0.3 < P_{orb}(\mathrm{yr}) < 165$ (Warner 1995). The CE phase provides the drag force required to decrease the separation and orbital period of the binary down to the range where magnetic braking can be important, providing the stars do not coalesce. The timescale for orbital separation decay becomes longer than the age of the universe if magnetic braking and gravitational radiation provide the only losses of orbital angular momentum from the parent binaries.

The lost orbital energy goes into heating the CE until it is ejected. Spin-up of the envelope by the secondary helps ensure that most CE binaries will eject their envelopes before the cores coalesce (Warner 1995). Complete ejection takes $\sim 10^3$ yr, produces a planetary nebula (PN), and exposes a pre-cataclysmic close binary consisting of the red giant core as the white dwarf (WD) primary and a low mass main sequence red dwarf (RD) secondary. The amount of matter accreted onto the secondary by the end of this phase is only ~ 0.01 $M_{\odot}$ (Hjellming & Taam 1991), and therefore does not affect its evolution appreciably. The separation of this binary is now such that magnetic braking can bring the pair closer together in $\sim 10^7$ yr to where the secondary starts to overfill its Roche lobe and mass transfer can begin. Warner (1995) calculates the timescales for both gravitational radiation and magnetic braking and finds that magnetic braking is the more important, if lesser understood, process for angular momentum loss at this stage of the CV's evolution. A recent study of the angular momentum loss rate in CVs due to magnetic braking has shown that the timescale derived from older data may be an overestimate (Andronov, Pinsonneault & Sills 2003). Thus, the timescale required to turn a WD-RD pair into an erupting nova is uncertain and may be longer than previously thought.

1.1.2 Classical CVs and Later Evolution

Once mass transfer begins, the object increases in brightness. Matter is transferred from the secondary to the primary via an accretion disk or an accretion column. In an accretion disk the matter is heated enough through viscosity to produce significant luminosity, sometimes outshining both stars. The point where the matter stream intersects the accretion disk (called the hot-spot) is often very bright due to the release of gravitational potential energy as the free-falling matter is slowed and shocked. In

an accretion column, luminosity is produced as energy is released where the matter impacts the surface of the primary. The total brightness and the amplitude of the light fluctuations of these systems depends very strongly on the mass accretion rate (Kolb 1993).

The mass transfer rate is Eddington-limited at the high end. If this rate is exceeded another CE phase ensues. At the low end, mass transfer is limited by the interplay between angular momentum transfer and angular momentum loss. As the matter moves closer to the center of gravity the system expands to conserve angular momentum. If the rate of angular momentum loss cannot overcome this expansion, the mass transfer is turned off when the secondary loses contact with its Roche lobe until magnetic braking or gravitational radiation brings the pair closer again. If the angular momentum loss rate is high enough to keep the secondary in contact with its Roche lobe, then a phase of relatively steady mass transfer is attained.

The mass accretion flow and disk-stream interactions provide instabilities that produce a 'flickering' in the light from CVs. Orbital variations are also present as the accretion hot-spot changes its aspect. The separation of the components in these systems is a few stellar radii and so eclipses occur in $\gtrsim 15\%$ of these objects. At such close orbital separations, the secondary rotation period becomes tidally locked to the orbital period in relatively few orbits. Once tidally locked, the uneven illumination caused by the close proximity of the hot primary causes one side of the secondary to be brighter than the other. This, combined with the distortion of the secondary as it fills its Roche lobe, produces photometric modulations at the orbital period called ellipsoidal variations (see Chapter 2). These are particularly important for low accretion rate systems, where the light flickering may be of low amplitude and the accretion hot-spot may not be particularly bright. All these effects ensure that a significant fraction of all CVs show detectable light variations.

For systems with a small magnetic field, the accretion onto the primary occurs through an intermediate accretion disk. The accretion disk can behave like a reservoir holding the material until an instability in the disk causes the matter to crash onto the primary. The gravitational energy of this material is released and this causes the primary to brighten by ~ 3 - 5 magnitudes in a dwarf nova outburst. No thermonuclear runaway is believed to occur and the amount of material ejected is small. After this disruption, accretion begins again and the entire process can repeat at 10-day to decades-long intervals.

For systems with a high magnetic field the accretion disk never forms because the accreting material is a plasma that is constrained to follow magnetic field lines. In this case there is an accretion column covering a small fraction of the white dwarf surface near the magnetic pole of the primary. These are the 'polars' and include objects such as AM Her. An intermediate case occurs if the magnetic field is weaker allowing an accretion disk to form at larger radii that is truncated at smaller radii by magnetically channeled accretion before reaching the surface of the primary. These are the 'intermediate-polars' an example of which is FO Aqr.

If the accretion rate onto the surface of the white dwarf primary (either through an accretion disk, or along field lines) is low enough ($\dot{M} < 10^{-8}$ M$_\odot$ yr^{-1}), the base of the accreted envelope becomes degenerate without nuclear burning. Degeneracy

prevents the expansion while the temperature of the envelope increases until nuclear burning ignites. Once ignited, all the energy goes into heating the envelope, since degeneracy prevents expansion of the envelope. The CNO cycle nuclear reaction rate is a strong function of temperature ($\propto T^{16}$) producing a feedback loop that accelerates the nuclear reaction rate. The resulting thermonuclear runaway is characterized by a rapid transition from a degenerate equation of state to that of a perfect gas at a high temperature and this causes a violent expansion and ejection of the envelope. This is the classical nova outburst that can brighten the object by up to 20 magnitudes (e.g., Nova Cyg 1975).

The nova outburst lasts from a few weeks to a few months. The decline rate in B magnitudes is correlated with the brightness of the outburst, with brighter outbursts having a more rapid decline (Shara 1981), making novae interesting as standard candles. The luminosity at outburst can reach $M_V = -10$, ensuring that novae can easily be observed in external galaxies. These properties make novae the most suitable class of CV for galaxy-wide population studies, since a large sample can be gathered by observing any nearby galaxy.

Current theories of mass transfer evolution predict that most CVs will evolve from a brighter, higher mass accretion rate ($\sim 10^{-6}$ $M_\odot$ yr^{-1}), longer orbital period (2 - 8 hours) system to a fainter, lower mass accretion rate ($\sim 10^{-11}$ $M_\odot$ yr^{-1}), shorter period ($<$ 2 hours) system due to the loss of angular momentum. The orbital period is predicted to reach a minimum of about 70 minutes (Kolb & Baraffe 1999). The rate of period evolution slows down as the period gets shorter such that most CVs should spend $\sim 90\%$ of their lifetime near this minimum (Kolb 1993).

In this low $\dot{M}$ state, CVs are faint ($M_V > 10$), show no UV excess, have extremely long outburst intervals or show no outbursts at all. It is probably no accident that the closest known CV, WY Sge (at 45 parsecs), is just such a system, with outbursts decades apart. Finding these objects relies on detecting low amplitude, mass transfer induced 'flickering', ellipsoidal variations, the eclipses of high inclination systems, or very infrequent outbursts.

1.1.3 Environmental Influences

What this outline of CV evolution does not include is any hint of the effect of environment on the properties of the CV population. Clues are there, but remain obscure due to problems acquiring environmentally 'pure' samples of any statistical size. The Milky Way offers three broad environments; disk, bulge, and halo, but difficulties in measuring distances to CVs make the secure placement of any system in one of these environments problematic. Older populations mix with younger in the disk of the Milky Way and an error of less than 1 kpc, common in Galactic nova distances, can move a system from the younger part of a spiral arm to the older inter-arm region.

The studies presented here focus on several unique environments in an effort to deduce their effect on the CVs contained within them. We start by studying the globular cluster environment because of its potential as a source for hard binaries and its association with older bulge populations. We then use nova surveys of external

galaxies to probe distinct populations by mapping the spatial distribution of the novae against the distribution of bulge and disk populations. The advantage here is that projection errors are less important than the distance errors in the Milky Way. We also study the trend in nova rate versus the dominant stellar population of host galaxies. We end by surveying the regions between galaxies in a cluster of galaxies for novae, which are thus tracers of intergalactic 'tramps'. Using what we have learned about nova populations, we have the potential to constrain the amount and source of the stellar tidal debris in the cluster, and thereby constrain the theory of galaxy cluster formation and harassment-driven evolution.

1.2 CVs in Globular Clusters

Dynamical theory predicts that the evolution of globular clusters is characterized by ever increasing central densities until close encounters between core stars become frequent. Hard binaries then form by tidal capture (Fabian, Pringle & Rees 1975) and by three-body encounters (Hut 1985). A few dozen binaries contain as much binding energy as a typical globular cluster. These binaries control the dynamical evolution of globular clusters by ejecting cluster stars in close encounters, and becoming harder binaries.

This picture of dynamical evolution is supported by the large number of binary systems being found in globular clusters (e.g., Grindlay et al. 2001). White dwarfs with a Main-Sequence companion should be much more common than the brighter neutron star binary X-ray sources found in these globular clusters, and therefore finding and studying CVs in globular clusters is important for understanding the cluster's dynamical evolution.

Dynamical theory also predicts that globular clusters should evaporate by ejecting stars during very close stellar encounters. This is the most important dynamical process dominating the long-term evolution of globular clusters. This implies that globular clusters may also be important as a source for hard binaries in the parent galaxy as pointed out by Ciardullo et al. (1987). In order to understand the formation and evolution of CVs, we must understand how important globular clusters are as contributors to the CV population, and to what population the ejected hard binaries are contributed.

1.2.1 A Tidal Capture CV in the Globular Cluster M5

The vast majority of CVs in globular clusters are located within one or two core radii of the cluster centers. This is expected because most captures occur in the dense environments of cluster cores, and because energy equipartition segregates the most massive objects, including CVs, towards the core. The dwarf nova (DN) M5 V101 is unique because it is located an extraordinary 10 core radii from the center of M5 (Margon, Downes & Gunn 1981). How did it get there? It is most likely that V101 has suffered a recent violent encounter near the center of M5, perhaps its formation event, and is now being ejected from the cluster.

V101, therefore, offers a unique opportunity to study a member CV that may have been recently formed from tidal capture. Spectra taken of V101 show very broad (3000-5000 km s^{-1}) Balmer lines which imply that the inclination of the system is high and eclipses may be seen (Naylor et al. 1989).

A power spectrum of preliminary photometry shows two significant peaks at 23 and 5 hours, with the 23 hour peak being about twice as large as the 5 hour peak (Zurek 2001). The low-state magnitude of the object is V = 22.5 (Kukarkin & Mironov 1970) and it exhibits outbursts to V $\sim$ 18 (Shara, Potter & Moffat 1987). There has been no campaign to determine the outburst period although two outbursts separated by 65 days were observed by the discoverer of V101 (Oosterhoff 1941). Subsequent campaigns to determine the orbital period have been frustrated by outbursts (Shara, Potter & Moffat 1987).

We executed a program of photometry with sufficient time resolution and coverage to produce an orbital period for M5 V101, the first for a dwarf nova in a globular cluster (Neill et al. 2002). The published results of this survey are presented in Chapter 2.

1.3 CVs in External Galaxies

Using novae in our Milky Way galaxy to investigate the distribution of the parent population for close binary systems is problematic. Extinction, sampling, and distance effects prevent the gathering of a complete and uniform sample. Extragalactic novae allow the collection of a large sample at a uniform distance from all parts of the observed galaxy in a short period of time. Extinction effects can be mitigated by observing early-type galaxies or more face-on late-type galaxies.

Comparing the nova rates and spatial distributions in different galaxy types tell us if the interacting binary fraction varies with such underlying properties as ambient metallicity and/or star formation history or if there is a universal binary fraction for all stellar populations. Determining the fraction of fast, bright novae tells us how many high-mass white dwarfs have been recently ($\sim 10^9$ yr) produced and how many low-mass white dwarfs exist in binaries, since it has been shown that nova brightness is largely a function of white dwarf mass (Prialnik & Kovetz 1995).

1.3.1 Novae in M81 and Local Group Dwarf Ellipticals

In spite of the promise of extragalactic novae to trace binary stellar populations, after nearly a century of observing them, controversies still exist about the most basic features of their parent populations. The luminosity specific nova rate (LSNR) of a galaxy is the nova rate normalized to the galaxy's integrated infrared luminosity. The infrared luminosity is less susceptible to the influence of a few young stars than the blue or visual luminosities and facilitates the comparison of nova rates between galaxies of different sizes and types. Studies comparing this LSNR with Hubble type have found both a strong correlation (della Valle et al. 1994), and no correlation (Shafter, Ciardullo & Pritchet 2000)! A correlation might be expected because of the

trend in the age of the predominant galaxy population with Hubble type. Studies analyzing the nova spatial distribution in M31 have found both a bulge-to-disk nova ratio of ≥ 9 (Ciardullo et al. 1987) and a bulge-to-disk nova ratio of 1/2 (Hatano et al. 1997). Intrinsic differences between putative disk novae and thick disk/bulge novae observed in the Milky Way (della Valle & Livio 1998) are hinted at in surveys of M31 (Arp 1956; Ciardullo, Ford & Jacoby 1983; Tomaney & Shafter 1992), but have never been conclusively verified with an unbiased sample in any galaxy.

The near-impossibility of acquiring long observing runs on telescopes of sufficient size has limited extragalactic nova surveys to short, widely spaced runs with incomplete spatial coverage of the target galaxies. A few nights of telescope time every few months at National Observatories is the norm, and provides terrible time-sampling for nova surveys. These conditions require researchers to model the relationship between mean nova lifetimes and survey limiting magnitude and to make assumptions about the spatial distribution of novae outside their survey area. Earlier photographic surveys of M31 that did have dense time sampling (Arp 1956; Rosino 1973) were limited by the fact that the central region of the galaxy was saturated and so most novae in the bulge were missed. This produced a long standing spurious notion that a 'nova hole' existed in the center of M31. This notion survived for many decades and was only disproved in 1987 using a CCD Hα survey of M31's bulge (Ciardullo et al. 1987). Even with modern detectors, incompleteness still exists in the centers of galaxies and the time sampling remains too sparse for definitive conclusions about the parent populations of these close binary tracers.

The errors produced by these limitations have been responsible for our inability to resolve the controversies delineated above. Most importantly, they prevent extragalactic novae from being used as close binary population tracers. The newly available Large Galaxy Atlas (Jarrett et al. 2003) derived from the 2MASS has the potential to provide a consistent normalization of nova rates to host galaxy infrared luminosity, once issues concerning the determination of the infrared background are resolved (Ferrarese, Côté & Jordán 2003). This will certainly reduce the scatter in our analysis of how LSNR varies with Hubble type. However, the most pernicious effect in trying to compare nova rates in different galaxies is the systematic underestimation of the bulk nova rates of the galaxies studied, particularly in the central regions.

Until we can address the systematic errors in bulk nova rates, we will not know how nova rate correlates with the star formation history of the parent galaxy or any other property of the underlying population. Until we have a large unbiased sample of novae from all parts of the galaxies studied, we will not know how novae are associated with either bulge or disk populations. Without comprehensive light curves for these novae we will not be able to detect intrinsic differences between bulge and disk novae. The potential of using novae as tracers of close binaries in galaxies will remain unfulfilled.

In an effort to confront these issues, we completed a preliminary survey of M81 that was able to cover the entire galaxy every clear night for a period of 5 months (Neill & Shara 2004a). The published results from this survey were revealing and are presented in Chapter 3. In addition, we surveyed 4 local group dwarf ellipticals in their entirety, every clear night for over 4 months (Neill & Shara 2004b). Because

these galaxies are nearby, and nearly dust free, the survey completeness for these objects approaches 100%. The results from this survey were equally revealing, have been submitted for publication, and are presented in Chapter 4.

1.4 CVs Between Galaxies

A fundamental problem in understanding the evolution of galaxy clusters and their constituent galaxies is the importance of dynamical processes such as tidal stripping. Theoretical models of cluster evolution have considered collisions, mergers, dynamical friction and tidal stripping in order to explain the galaxy morphology-density relation and the presence of luminous halos around supergiant D galaxies. It is generally accepted that tidal stripping will remove the more loosely bound stars in the outer envelopes of galaxies (Richstone 1976). Merritt (1984) has argued that the extensive envelopes of cD galaxies consist of this tidal debris moving in the potential well of the cluster. However, the efficiency of tidal stripping is not well understood, because of uncertainties in the velocities, the mean tidal field, the distribution of dark matter, and the orbits of stars in the outer envelopes of the stripped galaxies. Typical theoretical estimates indicate that $\sim 30\%$ of the total cluster light should be in the intergalactic medium. Miller (1983) and Dressler (1984) have therefore stressed the importance of obtaining reliable measurements of the intracluster light (ICL) as a direct indicator of the tidal damage suffered by galaxies.

The stars stripped from galaxies in the cluster formation process should contain the same binary fraction as their parent galaxies, and therefore the same fraction of CVs. The brightest eruptive CVs (i.e., novae) may be useful tracers of the ICL. If novae are detected between galaxies, we can use what we know about the nova-to-light ratio from other galaxies to calculate the amount of ICL within a cluster.

1.4.1 Intra-Cluster Novae in Fornax

Attempts to measure the ICL date back to the early 1970s, originally being done with photographic plates. More recently CCD surveys have been employed by Partridge (1990), Boughn, Kuhn & Uson (1990), and Vilchez-Gomez, Pello & Sanahuja (1994), with results ranging from non-detections to $\sim 20\%$ of the total cluster light (surface brightnesses of $\mu_V \sim 29$ mag arcsec^{-2}). Even with CCDs, detecting the ICL directly is notoriously difficult and fraught with uncertainties such as the contributions from overlapping galaxy halos. An independent means of measuring the ICL, not subject to the same problems as measuring the extremely low surface brightness diffuse emission is needed.

Methods using planetary nebulae (PNe) have been developed and applied to Virgo (Feldmeier, Ciardullo & Jacoby 1998) and Fornax (Theuns & Warren 1997). The brightest intergalactic red-giant-branch stars have also been detected in Virgo (Ferguson, Tanvir & von Hippel 1998). Novae typically range in brightness from $M_V = -6$ to -10 while the bright end of the PN luminosity function reaches $M^*_{5007} = -4.5$ (Ciardullo, Jacoby, Ford & Neill 1989) and red-giant-branch stars typically reach

$M_V = -3$. Novae can be detected with a brighter limiting magnitude and can thus be observed to greater distances than PNe or red-giant stars. The transient nature of novae and their Hα brightness also limit the contamination problem suffered by PNe or red-giant-branch stars due to background emission line objects or unresolved compact galaxies.

Novae represent an opportunity to trace the ICL out to distances beyond Virgo. We can apply our understanding of how the novae trace the light of individual galaxies to the novae in and between galaxies in the Fornax cluster. Using a diverse set of observations obtained over more than a decade, we present a feasibility study (Neill, Shara & Oegerle 2004c) in Chapter 5 that proves that this method will indeed provide a useful measure of the ICL.

Chapter 2
The First Orbital Period for a Dwarf Nova in a Globular Cluster: V101 in M5

2.1 Introduction

Close binaries in globular clusters contain a significant fraction of the total cluster binding energy. This makes them critically important in unraveling the dynamical evolution of their host clusters. In order to place constraints on cluster evolution theory, one must determine the binding energy of the binaries in a cluster; i.e., their orbital periods and component masses. Determining the evolutionary states of cluster binaries is also important, and this also demands component masses and periods. The high stellar densities in the cores of many globular clusters, where most of the close binaries reside, make this an observational challenge. UV and X-ray observations have improved our population census of cluster close binaries (Knigge et al. 2002; Grindlay, Heinke, Edmonds & Murray 2001; Pooley et al. 2002), but without knowing the periods of these new binaries we cannot calculate the binding energy they contain or constrain their evolutionary state.

The cataclysmic variable (CV) V101 in the globular cluster M5 has many properties that make it an ideal candidate for period determination. It lies 280" from the center of M5 (10 core radii) and is relatively uncrowded compared to the objects near the core of a globular cluster (see Figure 2.1). It is classified as a dwarf nova (DN), a particularly well studied class of CV for which empirical relations exist relating the period to the luminosity, spectral type, and mass of the secondary.

The literature on M5 V101 is not extensive. It was first reported as a possible SS Cygni type variable star by Oosterhoff (1941). He reported seven observations, including two pairs of measurements in outburst separated by 66 days in 1934. Since then Margon, Downes & Gunn (1981) performed the initial identification of V101 in quiescence and obtained a low resolution spectrum showing strong, broad Balmer and He I emission lines, confirming the identification and the DN classification. Shara, Potter & Moffat (1987) reported B-band observations in outburst and quiescence and predicted a fairly long orbital period (P $\sim$ 11 hr) based on the minimum observed magnitude (V = 22.5, Kukarkin & Mironov 1970) and the duration and rise and fall time of the outburst. Spectral observations of V101 in outburst were published by Naylor et al. (1989) and showed Hα in absorption with a fairly red continuum. They also showed a radial velocity curve covering 1.75 hrs from which they concluded that the orbital period must be longer than twice their sampling interval (P $\geq$ 3.5 hr, see their Figure 2). Shara, Potter & Moffat (1990) published the highest resolution spectrum to date of V101 in quiescence and noted that the high velocity width of the Balmer lines hinted that the system might be highly inclined and eclipses might be observable.

The possibility of using these eclipses to determine the orbital period for M5 V101

Table 2.1. M5 V101 Observations

JD	Date	N exp	Comments
	1995 SAAO V-band Data		
2449833	25 Apr	11	outburst decline
2449835	27 Apr	21	outburst decline
2449837	29 Apr	19	
2449838	30 Apr	18	
2449839	01 May	16	
	2001 Calypso I-band Data		
2451988	20 Mar	1	
2451990	22 Mar	3	
2451992	24 Mar	1	
2451994	26 Mar	2	
2451999	31 Mar	1	
2452026	27 Apr	27	
2452028	29 Apr	13	outburst rise?
2452050	21 May	17	
2452051	22 May	19	
2452052	23 May	23	
2452053	24 May	23	
2452054	25 May	34	
2452055	26 May	29	
2452056	27 May	19	
2452058	29 May	38	
2452059	30 May	52	
2452060	31 May	32	
2452084	24 Jun	29	
2452086	26 Jun	3	
2452087	27 Jun	36	outburst rise
2452088	28 Jun	23	outburst rise
2452089	29 Jun	21	outburst rise
2452090	30 Jun	15	outburst rise

Note. — All observations are in quiescence unless otherwise noted.

motivated this study. The availability of many nights on the Calypso Observatory 1.2m telescope using the high-resolution camera allowed us to achieve the photometric accuracy and time sampling required to determine the orbital period. We describe below the photometric analysis and the method for finding the period, and present the physical properties of V101 derived from our observations.

2.2 The Calypso Telescope Observations

The Calypso Telescope is a 1.2m telescope of Ritchey-Chretien design on a computer controlled altitude-azimuth mounting located on Kitt Peak, Arizona. Two instruments are mounted at the Naysmith foci: a high resolution camera (HRCAM) with tip/tilt adaptive correction and a field of view of 85", and a non-adaptive camera (WFCAM) with a 10' field of view. The aperture of the telescope was matched to the atmospheric cell size during the best quartile of seeing at the site allowing the tip/tilt to theoretically correct 87% of the atmospheric distortion on the optical axis. The optical components are figured so that the total wavefront error at the focal plane, including all error budgets, is less than 1/17th of a wavelength at 5500Å. The telescope is mounted on a 10.2 meter high pier with an enclosure that rolls completely away, allowing it to operate in the open air. The site is placed so the prevailing winds during the best seeing reach the telescope unhindered by any ground obstruction providing a laminar flow of air over the telescope.

The HRCAM was used for this study of V101. It uses a single Loral 2048 square CCD with 15μ pixels. Its native resolution is 0.04" per pixel in order to over-sample the point spread function (PSF) at the best seeing measured at the site of 0.25". However, the average seeing ranges between 0.6 and 0.8", as measured in the I-band. Therefore, the CCD was binned 4x4 (giving a pixel size of 0.16") to better accommodate these atmospheric conditions during the observing campaign. Since the secondary component of V101 was thought to be a late-type main-sequence (M-S) star, we chose the I-band to maximize the chances that ellipsoidal variations would be visible. We used 10 minute exposures back-to-back to allow us to sample the light curve densely enough to detect low amplitude eclipses or ellipsoidal variations. This exposure time gave us a limiting magnitude of I $\sim$ 21.5 under typical conditions. Table 2.1 presents the log of I-band observations for the Calypso data. Figure 2.1 presents three finder charts for V101 in the B, V, and I-bands taken with the HRCAM on Calypso.

2.3 South African Astronomical Observatory Observations

Observations taken in 1995 with the TEK4 CCD on the South African Astronomical Observatory (SAAO) 1.9m telescope in the V-band were also analyzed for this study. For five nights, V101 was observed with 15 minute exposures back-to-back over the entire night yielding a limiting magnitude of V $\sim$ 22.7 under typical conditions. Table 2.1 presents the log of observations for the SAAO V-band data. These observations proved valuable for confirming the orbital period seen in the Calypso data (see below).

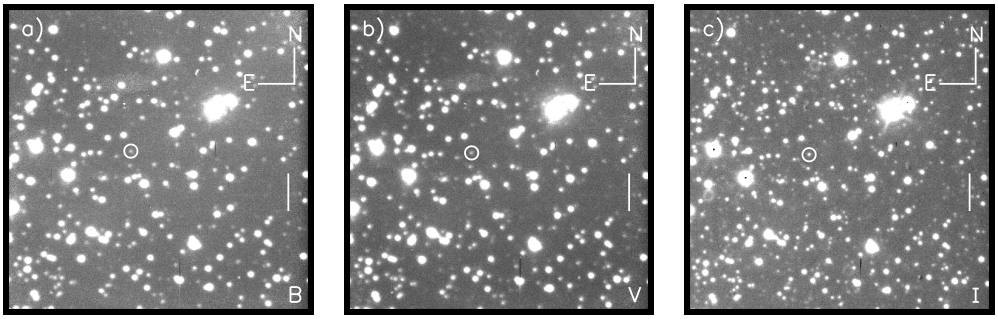

(a) *(b)* *(c)*

Figure 2.1: Calypso images of V101 produced by coadding three 600 second HRCAM exposures. The scale bar on the right is 10 arcseconds long, and V101 is circled. (a) B-band data taken on JD 2451994 (26 March 2001) with point spread function (PSF) that has a full width at half maximum (FWHM) of 0.8 arcseconds. (b) V-band images taken on JD 2451993 (25 March 2001) with a PSF that has a FWHM of 0.8 arcseconds. (c) I-band images taken on JD 2452051 (22 May 2001) with a PSF that has a FWHM of 0.6 arcseconds.

2.4 Reduction and Photometry

All frames were reduced in the standard way to remove instrumental artifacts. In order to minimize the impact of cosmic rays, each image was shifted to a standard reference position and coadded in the following way: first, all images were ordered in time sequence, then a running set of three images was coadded from the beginning to the end of the night incremented by one image at a time. This produced a smoothing of the light curve but kept the time sampling interval at roughly the exposure time of the individual images (plus read time).

The coadded frames were photometered using the APPHOT package in IRAF (Tody 1986). A set of isolated, well-exposed stars near V101 with low variability ($\leq$ 0.02 mag) was used to tie all the epochs together onto the same instrumental magnitude system. Calibration was achieved by comparing our instrumental magnitudes with Peter Stetson's photometry of M5[1] (Stetson 2000) in the I and V-bands. Due to the small fields of the Calypso and SAAO detectors, the calibration was boot-strapped to the Stetson standards through intermediate wider-field images taken under photometric conditions. A wide-field I-band image of M5 taken with the 8K mosaic camera on the Hiltner 2.4m telescope at the MDM observatory on 01 June 2001 by JDN was used to bootstrap the Calypso photometry. The SAAO photometry was bootstrapped using a V-band image kindly taken for us by Ron Downes with the T1KA camera on the 2.1m telescope at Kitt Peak National Observatory on 28 May 1998. In each case and at each step at least 25 stars were used and a final absolute photometric calibration with a root-mean-square error of less than 0.1 mag was achieved for all

[1]available at http://cadcwww.dao.nrc.ca/cadcbin/wdb/astrocat/stetson

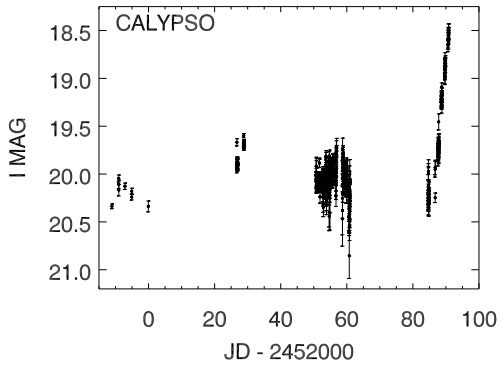

Figure 2.2: Calypso photometry summarized showing the individual I-band observations.

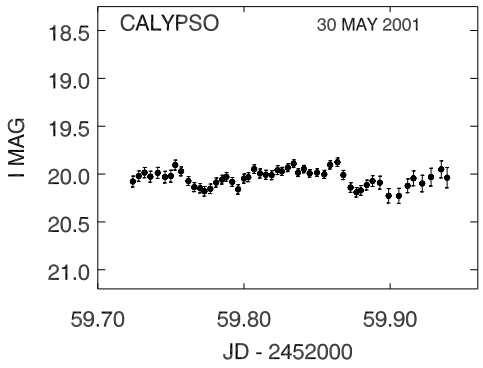

Figure 2.3: One night from the Calypso observations during quiescence showing the 'flickering' typical of CVs.

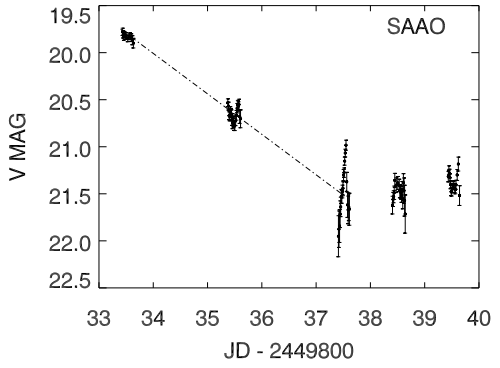

Figure 2.4: SAAO photometry summarized showing the individual V-band observations. The empirical relation between orbital period and outburst decline rate from equation 3.5 of Warner (1995) overplotted as a dot-dashed line (see § 2.6.1).

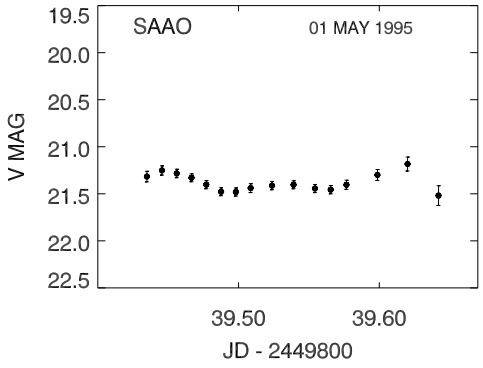

Figure 2.5: One night from the SAAO observations during quiescence.

photometry. The final calibrated I-band magnitudes are presented in Table 2.2, and the final calibrated V-band magnitudes are presented in Table 2.3.

The I-band photometry is summarized in Figure 2.2 with a single night during quiescence shown in Figure 2.3 to illustrate a typical night's I-band light curve. The V-band photometry is summarized in Figure 2.4 and a single night's V-band observations during quiescence are shown in Figure 2.5. Figure 2.2 shows what may be the beginning of an outburst on JD 2452028 and one well-observed outburst rise starting at JD 2452087. Figure 2.4 shows a decline from outburst to a V magnitude of 22.0 on JD 2449837.

Table 2.2. Calypso I-band Photometry

Julian Day (day)	I (mag)	Error (mag)
2451988.938	20.34	0.03
2451990.986	20.05	0.04
2451990.995	20.11	0.05
2451991.002	20.17	0.06
2451992.882	20.13	0.03
2451994.914	20.18	0.03
2451994.925	20.24	0.03
2451999.937	20.34	0.06
2452026.752	19.67	0.04
2452026.760	19.93	0.04
2452026.767	19.88	0.03
2452026.774	19.96	0.03
2452026.781	19.92	0.03
2452026.789	19.91	0.03
2452026.804	19.90	0.03

Note. — Table 2.2 is presented in its entirety in the electronic edition of the Astronomical Journal (Neill et al. 2002). A portion is shown here for guidance regarding its form and content.

2.5 Orbital Period Analysis

To derive the orbital period we used the algorithm of Scargle (1982) and Horne & Baliunas (1986), accelerated by the technique described in Press & Rybicki (1989). The calibrated magnitudes were converted to flux units for the period analysis. Residual long term trends were removed by taking each night, calculating the mean flux for the night, and subtracting this mean flux from the individual fluxes from the night.

2.5.1 Calypso Data

We used all data with errors ≤ 0.2 magnitudes to generate the periodogram shown in Figure 2.6. The most significant peak is at $\omega(1/\mathrm{d}) = 8.281 \pm 0.026$ (P = 2.898 $\pm$ 0.009 h). The half-width of the periodogram peak at 85% of its peak value was

Table 2.3. SAAO V-band Photometry

Julian Day (day)	V (mag)	Error (mag)
2449833.436	19.78	0.04
2449833.447	19.81	0.04
2449833.459	19.83	0.04
2449833.469	19.81	0.03
2449833.500	19.82	0.04
2449833.530	19.85	0.04
2449833.560	19.83	0.03
2449833.573	19.83	0.04
2449833.594	19.84	0.04
2449833.615	19.87	0.05
2449833.634	19.90	0.05
2449835.374	20.53	0.04
2449835.386	20.57	0.04
2449835.397	20.67	0.04
2449835.408	20.68	0.05

Note. — Table 2.3 is presented in its entirety in the electronic edition of the Astronomical Journal (Neill et al. 2002). A portion is shown here for guidance regarding its form and content.

used to derive all frequency error estimates in this paper. Experience has shown that this measure corresponds to a 1σ error in the frequency while the half-width at half maximum is closer to the 3σ error (Patterson 2004).

If the periodic signal is due to the ellipsoidal variations (Bochkarev, Karitskaya & Shakura 1979), then the period found in the periodogram is half the orbital period because there are two modulations per orbit. In the I-band this would be especially true since the low mass M-S secondary would be prominent. An odd-even effect, where one modulation is deeper than the other, is expected because the two sides of the secondary are unequally luminous either due to gravity darkening or heating by the primary. This, plus the radial velocity curve published by Naylor et al. (1989) which strongly indicates an orbital period ≥ 3.5 h, motivated us to explore both the peak frequency from our periodogram and half this frequency: $\omega(1/\mathrm{d}) = 4.140 \pm 0.026$ ($\mathrm{P} = 5.796 \pm 0.036$ h).

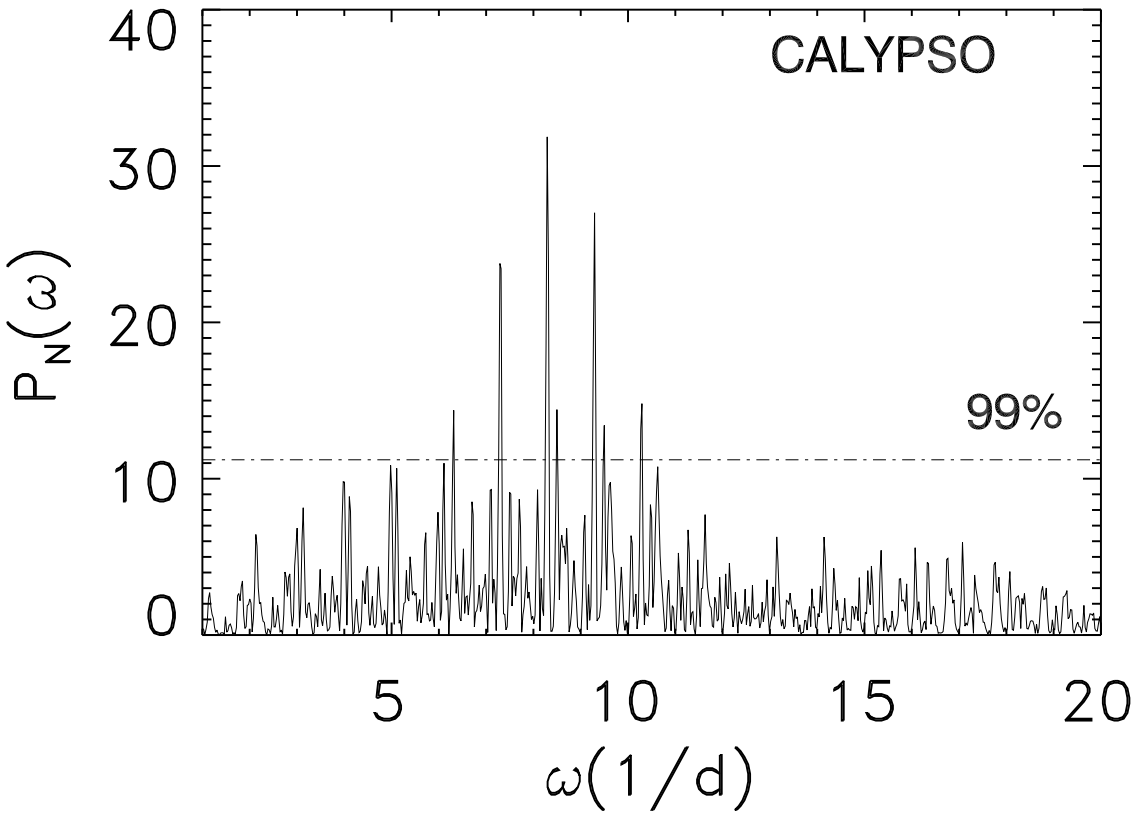

Figure 2.6: Periodogram generated from the Calypso data with errors ≤ 0.2 magnitudes. The line of 99% confidence (false alarm probability = 10^{-2}) is indicated as a dot-dashed line. The largest peak is at $\omega(1/\mathrm{d}) = 8.281 \pm 0.026$ (P = 2.898 ± 0.009 h) and has a false alarm probability of $10^{-10.9}$. All other other significant peaks have corresponding peaks in the alias periodogram shown in Figure 2.9 and are aliases due to the time sampling of the Calypso data (see § 2.5.1).

We produced the binned phase diagrams shown in Figures 2.7 and 2.8 using the error-weighted mean counts within each of 50 phase bins. Figure 2.8 clearly shows the expected odd-even effect of two unequal modulations per orbital period. We fit both sets of phase data with a periodic function of the form:

$$y = a + b\cos(c\phi + d) + e\sin(f\phi + g), \tag{2.1}$$

where ϕ is the phase, and plotted them on the phase data. The reduced χ^2 of the fit in Figure 2.7 is 2.15, while that in Figure 2.8 is 1.25, which supports the longer orbital period.

The fit of equation (2.1) to the phase data was sampled the same way as the Calypso data and used to generate the alias periodogram shown in Figure 2.9. All significant peaks from Figure 2.6 have a corresponding peak in Figure 2.9 and, apart from the highest one, are aliases due to our time sampling.

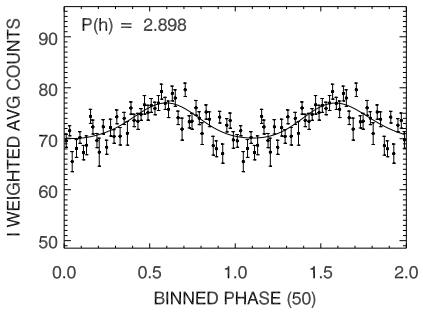

Figure 2.7: Phase diagram generated from error-weighted counts in 50 phase bins using the period of the largest peak in the Calypso periodogram. The solid line is the fit of equation (2.1) to the phase points and is used to generate the alias periodogram shown in Figure 2.9. The fit has a reduced χ^2 of 2.15.

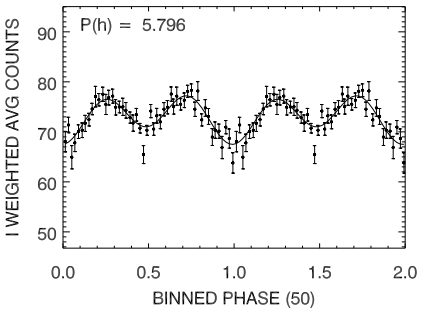

Figure 2.8: Phase diagram generated from error-weighted counts in 50 phase bins using twice the period of the largest peak in the Calypso periodogram. The solid line is the fit of equation (2.1) to the phase points and is used to analyze the orbital inclination of V101 (see § 2.6.2). The fit has a reduced χ^2 of 1.25.

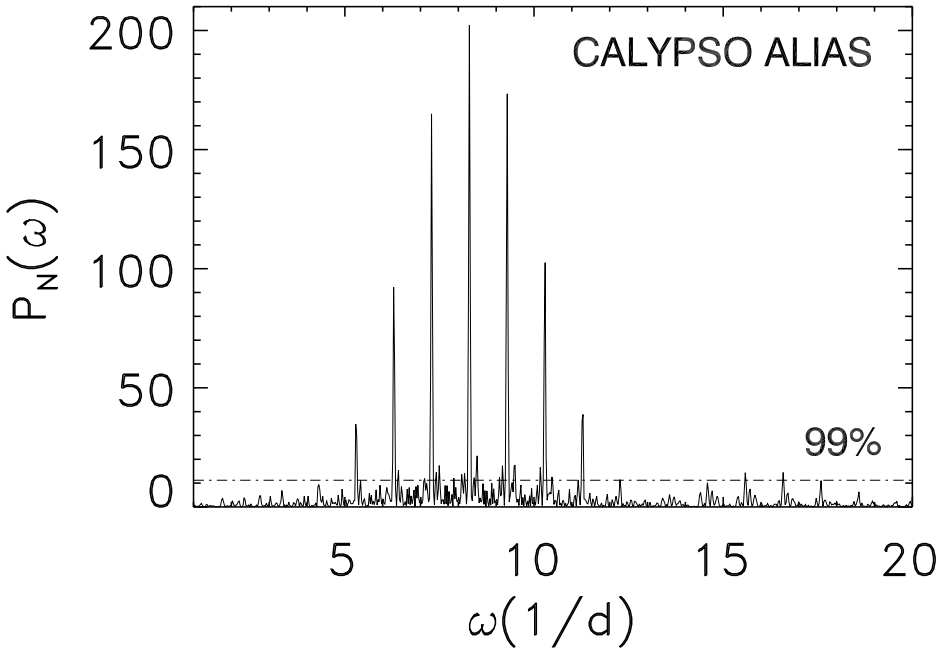

Figure 2.9: Periodogram generated from the fit in Figure 2.7 sampled the same way as the Calypso observations and showing the alias peaks.

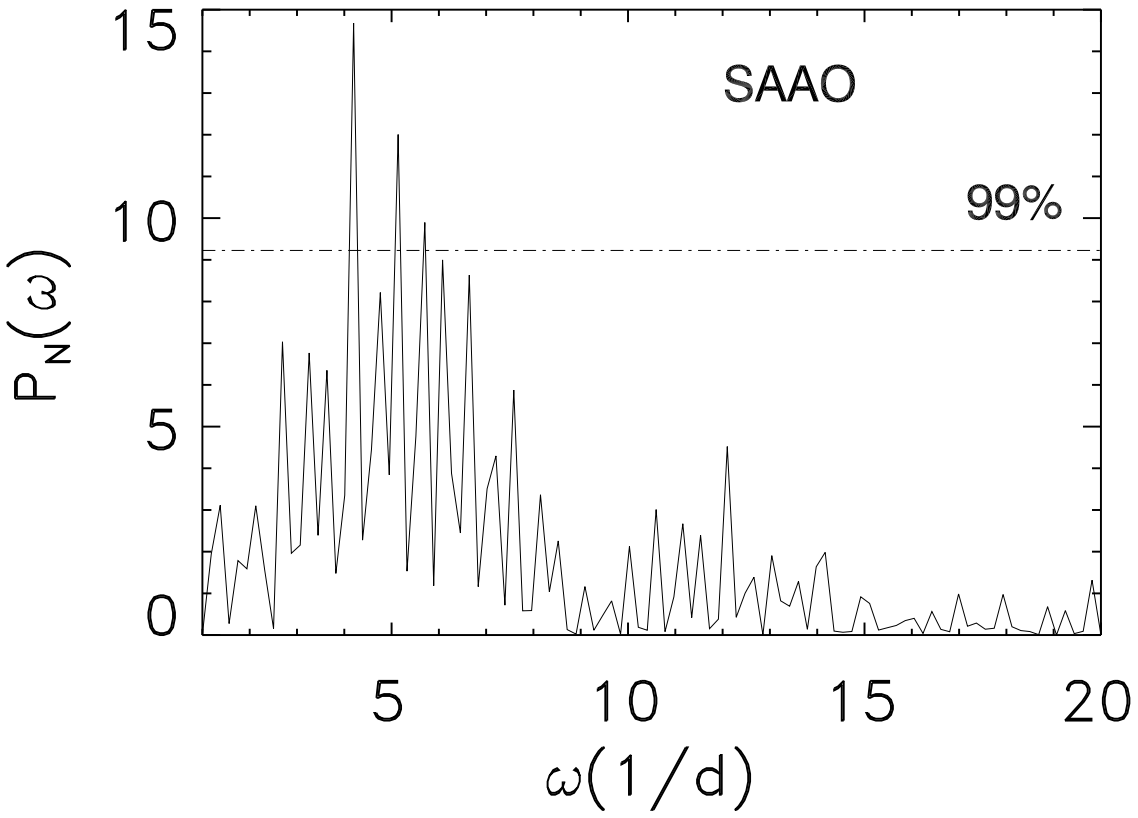

Figure 2.10: Periodogram generated from the SAAO data. The largest peak is at $\omega(1/\mathrm{d}) = 4.20 \pm 0.19$ (P = 5.72 ± 0.25 h) and has a false alarm probability of $10^{-4.5}$.

2.5.2 SAAO Data

We applied the same techniques to the V-band data taken at the SAAO. We assumed that the orbital modulations would be present during the decline from outburst and used the run of observations from JD 2449833 to JD 2449839. Figure 2.10 presents the periodogram derived from these data.

While this periodogram is not as clean as the periodogram derived from the Calypso data, its most significant peak at $\omega(1/\mathrm{d}) = 4.20 \pm 0.18$ (P = 5.72 ± 0.25 h) does support the 5.796 hour period from the Calypso data. The binned phase diagram using the weighted mean counts within each of 50 phase bins is presented in Figure 2.11.

We also fit this phase diagram with equation (2.1) in order to investigate aliases in the periodogram. The fit is presented as the solid line in Figure 2.11. The alias test periodogram is presented in Figure 2.12. Most of the significant peaks can be explained as aliases from our time sampling.

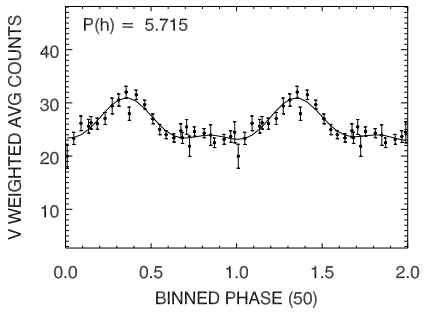

Figure 2.11: Phase diagram generated from error weighted counts in 50 phase bins using the period of the largest peak in the SAAO periodogram. The solid line is the fit of equation (2.1) to the phase points and is used to generate the alias periodogram shown in Figure 2.12. The fit has a reduced χ^2 of 1.09.

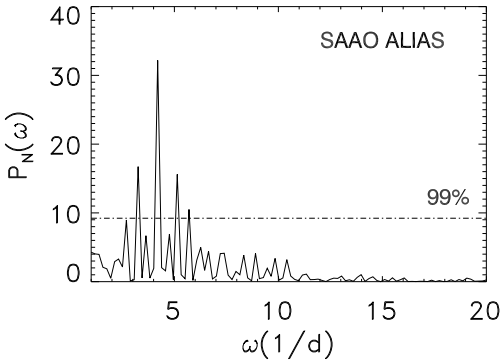

Figure 2.12: Periodogram generated from the fit in Figure 2.11 sampled the same way as the SAAO observations and showing the alias peaks.

2.6 Interpretation

2.6.1 The Orbital Period of V101

The phase diagram presented in Figure 2.8 shows the odd-even phenomenon from the ellipsoidality effect, caused by the changing geometry of the distorted secondary during the orbital cycle and the unequally luminous halves of the secondary. This effect has a small amplitude and only with many observations can the superposed stochastic variations from the accretion process be average out.

Figure 2.45 from Warner (1995), showing the observed relationship between spectral type and P_{orb}, places the secondary of V101 in the range of spectral types from K5 to M0. This is consistent with spectral observations published by Margon, Downes & Gunn (1981), Naylor et al. (1989), and Shara, Potter & Moffat (1990) which show a red continuum in quiescence.

The phase diagram for the SAAO V-band data presented in Figure 2.11 shows a modulation of the same period. We expect the secondary to be much fainter in the V-band, since the secondary is of spectral type K5 to M0 with $V - I \simeq 2.2$, and so we see only one modulation per orbit, perhaps due to the changing visibility of the primary star or the changing aspect of the accretion disk.

As a further consistency check, we compare the decay from outburst shown in Figure 2.4 with equation 3.5 from Warner (1995), which relates the outburst decay timescale, τ_d, to P_{orb}:

$$\tau_d = 0.53\ P_{orb}^{0.84}(h)\ \text{day mag}^{-1}. \tag{2.2}$$

We have overplotted this relation for an orbital period of 5.796 hours on Figure 2.4

as a dot-dashed line which follows the decline well. This orbital period places V101 well above the period gap for CVs and at the high end of the distribution for CVs above this gap (Warner 1995).

2.6.2 The Orbital Inclination of V101

Having a constraint on the spectral type of the secondary allows us to use the light curve to explore the orbital inclination of the system using the tables in Bochkarev, Karitskaya & Shakura (1979), assuming that the modulations shown in Figure 2.8 are purely due to the ellipsoidality effect. The fit shown in Figure 2.8 as the solid line and the average deviation from this fit was used to determine the amplitude of the variation ($A = 0.114 \pm 0.020$ mag), the difference between the two minima ($\Delta m = 0.055 \pm 0.021$ mag), and their corresponding errors.

Knowing that the secondary is a K5 to M0 dwarf constrains the effective temperature which, combined with the filter bandpass and the fact that the envelope of the secondary star is convective, allows us to use Figure 2 from Bochkarev, Karitskaya & Shakura (1979) to determine the gravity darkening coefficient: $\beta \simeq 0.4$. The limb darkening coefficient is also determined by the effective temperature and using Figure 17.6 from Gray (1976) we get u $\simeq$ 0.5. We know that the secondary is filling its Roche lobe so we can set the Roche lobe filling factor to be $\mu = 1$. We can also assume that the mass ratio, q $= M_p/M_s$ is in the range 1.6 - 2.3, by using the mass of a K7 dwarf for the secondary star mass, $M_s \simeq 0.6$ M$_\odot$, and assuming the primary star mass, M_p, is in the range 1.0 to 1.4 M$_\odot$ (see § 2.6.5). Note that the q used by Bochkarev, Karitskaya & Shakura (1979) is the inverse of that used traditionally in the CV literature where q $= M_s/M_p$.

Using these values to examine Table 1 from Bochkarev, Karitskaya & Shakura (1979), we can constrain the inclination angle, i, by A (see above) to be in the range $30^\circ < i < 60^\circ$. Using Table 2 from Bochkarev, Karitskaya & Shakura (1979) we can constrain the inclination angle by Δm to be in the range $50^\circ < i < 90^\circ$. These two constraints overlap in the range $50^\circ < i < 60^\circ$ and are consistent with the fact that no eclipses are seen.

2.6.3 The Distance to V101

We can now use the empirical relation between orbital period, P_{orb}, and secondary luminosity, $M_V(2)$, to determine the distance modulus to V101. Using equation 2.102 from Warner (1995),

$$M_V(2) = 16.7 - 11.1 \log P_{orb}(h), \tag{2.3}$$

we determine the absolute magnitude of the secondary to be M$_V = +8.2$. Figure 2.46 in Warner (1995) shows that the scatter in this relation is about ± 0.5 magnitudes. From the minimum published V magnitude of 22.5 (Kukarkin & Mironov 1970) and M$_V = +8.2$, we get a distance modulus of $(m - M)_V = 14.3 \pm 0.5$, consistent with the distance modulus for M5 of $(m - M)_V = 14.41 \pm 0.07$ (Sandquist, Bolte, Stetson & Hesser 1996).

2.6.4 The Outburst Period of V101

If the rise seen in Figure 2.2 on JD 2452028 is indeed the beginning of an outburst, then the two outbursts we observe separated by 60 days with an intervening quiescent period supports the outburst period first proposed by Oosterhoff (1941) of 66 days. Many observations of individual outbursts have been reported (Margon, Downes, & Gunn 1981; Shara, Potter, & Moffat 1987; Naylor et al. 1989). Using these data to examine the periodicity of the outbursts shows that no regular period for the outbursts exists, but a 'typical' outburst interval is in the range of 60 to 66 days. This is expected behavior for DN outbursts which don't exhibit strict periodicity.

2.6.5 The Mass and Location of V101

A recent mass-spectral type study (Baraffe & Chabrier 1996) concludes that an M0 star has a mass of 0.6 $M_\odot$. The mass-orbital period relation, equation 2.100 from Warner (1995),

$$M_1(2) = 0.065\, P_{orb}^{5/4}(h) \qquad 1.3 \leq P_{orb}(h) \leq 9, \tag{2.4}$$

yields 0.58 $M_\odot$ as the secondary mass of a CV with a 5.796 hour period. These are consistent with the 0.6 $M_\odot$ derived earlier from the system luminosity (and type K5-M0) near minimum. We can estimate the primary mass for V101 from the average primary mass of a sample of 21 DN with periods greater than 2.5 hours, which is 0.91 ± 0.08 $M_\odot$ (Webbink 1990). This implies a system mass of ~ 1.5 $M_\odot$ for V101. This system mass nearly twice that of the main sequence turnoff in M5, which should place V101 in the inner one or two core radii of the cluster.

M5 V101 stubbornly refuses to conform to this logic. It is, in fact, located 10 core radii from the center of M5. What is it doing out there? Perhaps the simplest explanation is dynamics.

Stars lead extremely promiscuous lives in clusters, especially near the centers where stellar densities are highest. Mate swapping is commonplace, as are strong, close encounters between binaries and single stars (e.g., Hurley & Shara 2002). These encounters often lead to the high speed recoils of the emerging binary and single stars. Such a scenario could place V101 far from the core of M5. It also makes the intriguing prediction of the existence of a low mass M dwarf on the opposite side of M5, considerably farther out than 10 core radii, escaping the cluster at high speed.

2.7 Conclusions

1. The orbital period for V101 is P = 5.796 ± 0.036 h. Using this orbital period to determine a distance modulus yields $(m - M)_V = 14.3 \pm 0.5$ which supports the membership of V101 in M5.

2. The secondary of V101 is a low mass M-S star whose spectral type is in the range K5 to M0.

3. The orbital inclination of V101 is high, but not high enough for the system to exhibit eclipses.

Chapter 3
The Hα Light Curves and Spatial Distribution of Novae in M81

3.1 Introduction

Extragalactic novae are particularly appealing objects for studies of close binary evolution. They are *the* tracer of interacting close binary stars, visible to much greater distances than any other well studied standard candle except supernovae (novae display M_v up to -10). By studying the novae in a nearby galaxy, one can gather a homogeneous sample of objects, all at the same distance, that is not plagued by the selection effects hampering an analysis of the cataclysmic variable (CV) population in our own Galaxy.

Given the large fraction of all stars that exist in binaries, the effort to understand binary formation and evolution has wide-reaching implications for understanding stellar populations. There are currently many unsolved problems in the theory of close binary formation and evolution that are difficult to tackle using CVs in our own Galaxy because of the selection effects mentioned above.

The prediction that the nova rate should correlate with the star formation history in the underlying stellar population (Yungelson, Livio & Tutukov 1997) is one example. This prediction is based on our understanding of how close binaries form and evolve, combined with our understanding of how the mass of a nova progenitor influences the nova outburst. Massive white dwarfs come from massive progenitors. These massive white dwarfs erupt as novae frequently as they need only accrete a small amount of hydrogen from their companions to explode as novae. This, in turn, implies that stellar populations with a currently low star formation rate should have a correspondingly low nova rate; i.e., early-type galaxies with older stellar populations should have a lower luminosity-specific nova rate (LSNR) than late-type galaxies with ongoing star formation.

Efforts have been made to detect a trend in LSNR with galaxy type (della Valle et al. 1994; Shafter, Ciardullo & Pritchet 2000), but the random errors are too large to date for a meaningful comparison. Typical extragalactic nova surveys are carried out using short runs, and significant assumptions must be made about the mean lifetimes of novae in order to derive nova rates (Shafter & Irby 2001). It is also rare that an extragalactic survey has been able to spatially cover an entire galaxy and avoid making some assumption about the distribution of novae with light to derive a galactic nova rate. The resulting errors in the nova rates are large, but systematic biases are far more pernicious.

In order to accurately compare nova rates with the underlying stellar population, we are pursuing a research program that uses the comprehensive time and spatial coverage afforded by a dedicated observatory. We have begun our program with M81 and used 5 continuous months of observing time to produce a survey that requires no

Table 3.1. M81 Observations

	Center (J2000)						
Field	RA	Dec	Epochs[a]	# Exp.	Hours	Novae	Bulge/Disk
1N	09 56 24.6	68 58 24	19	89	29.7	0	Disk
1S	09 56 24.1	68 53 44	18	87	29.0	0	Disk
2N	09 55 31.8	69 01 34	18	82	27.3	3	Bulge
2S	09 55 30.1	68 56 52	5	23	7.7	0	Disk
3N	09 54 39.9	69 03 12	17	79	26.3	1	Disk
3S	09 54 40.6	68 58 29	10	48	16.0	0	Disk
4N	09 56 25.2	69 07 35	18	80	26.7	0	Disk
4S	09 56 25.3	69 02 57	5	25	8.3	0	Disk
5N	09 55 31.1	69 10 58	6	29	9.7	0	Disk
5S[b]	09 55 31.7	69 06 14	15/21	68/94	22.7/31.3	7	Bulge
6N	09 54 39.1	69 12 32	8	36	12.0	0	Disk
6S	09 54 39.4	69 07 50	21	94	31.3	1	Disk

[a]Except where noted, epochs range from December 31, 2002 (JD 2452638.8) to June 6, 2003 (JD 2452796.6).

[b]The additional 15 epochs for field 5S were acquired between June 6, 2003 and June 26, 2003 to follow the declines of Nova 11 and Nova 12 (see text). No additional novae were found in this interval.

assumptions about nova spatial distribution or mean lifetimes. Not since Arp (1956) surveyed the central parts of M31 has such extensive, continuous coverage of a galaxy for novae been attempted.

Our survey updates the five-year photographic survey of M81 for novae reported by Shara, Sandage & Zurek (1999). They found 23 novae, evenly divided over the disk and central bulge. Significant incompleteness must be present in that survey due to photographic saturation in the bright central regions of the galaxy and due to large gaps in their time coverage. The results we present below supercede those of Shara, Sandage & Zurek (1999), and show that a comprehensive spatial and temporal survey is essential to minimize the systematic effects of incompleteness.

3.2 Observations

We used the WFCAM 2048x2048 pixel CCD on the Calypso 1.2m telescope at 4x4 binning for our observations of M81. This configuration yields a pixel scale of 0".6 px^{-1} and a field size of 5' on a side. The seeing for our observations had a median of 1".5 and ranged from 1".0 to 2".5. In an effort to cover the entire spatial extent of M81 in our search for novae we divided M81 into 12 fields covering roughly 15' in Right Ascension and 23' in Declination. Figure 3.1 is an Hα mosaic of the 12 fields showing

the extent of our spatial coverage, the identification of the fields, and the location of the 12 novae discovered.

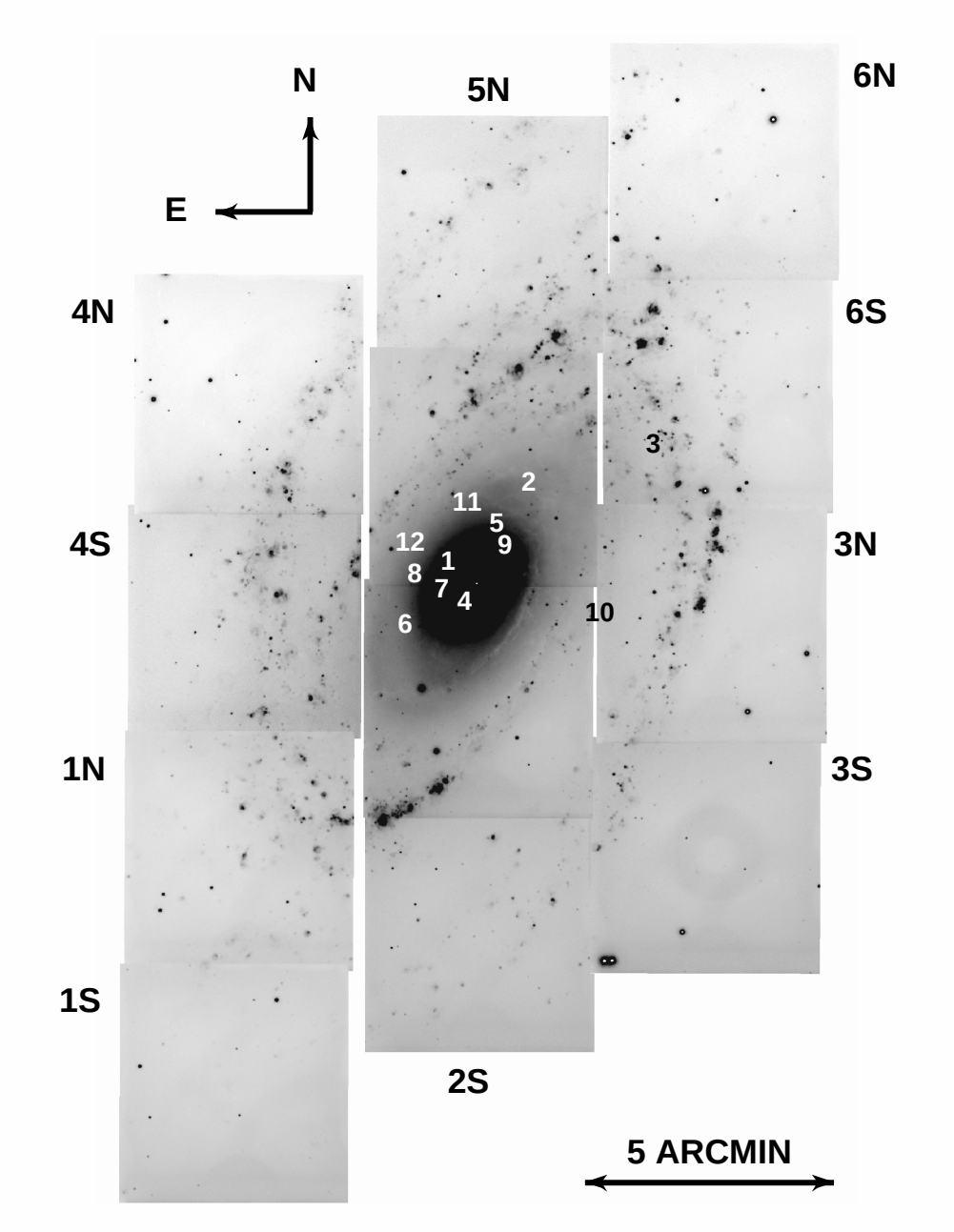

Figure 3.1: Hα mosaic of the twelve M81 survey fields (labeled) with the positions of the 12 novae discovered in the 2003 season indicated as white or black numbers. Note that most of the novae are close to the nucleus of the galaxy and the asymmetry of the nova distribution across the major axis. The predominance of bulge or spiral-arm novae has been hotly debated for twenty years. This image finally resolves that debate in favor of the bulge.

All observations were taken through an Hα filter with a 30Å full width at half-maximum (FWHM) bandpass. This filter was chosen for several reasons. Because of the longer duration of novae in Hα compared to the B-band (Ciardullo et al. 1987), we minimize the possibility of missing novae due to inevitable gaps in coverage. The redder wavelengths observed with the Hα filter means that our images are less influenced by internal extinction in M81, and less influenced by scattered moonlight during the fuller phases of the moon. To illustrate this point, Figure 3.2 shows the distribution of frame limits (described in § 3.4) with days from New Moon. Only within 1.5 days of the full moon is any effect seen. It is also our goal to explore the Hα light curve as a tool for understanding the physics of nova outbursts. So far attempts to do this have failed, but with our dense time sampling the possibility opens up that features of the Hα rise, previously poorly observed, may correlate with properties of the nova progenitor.

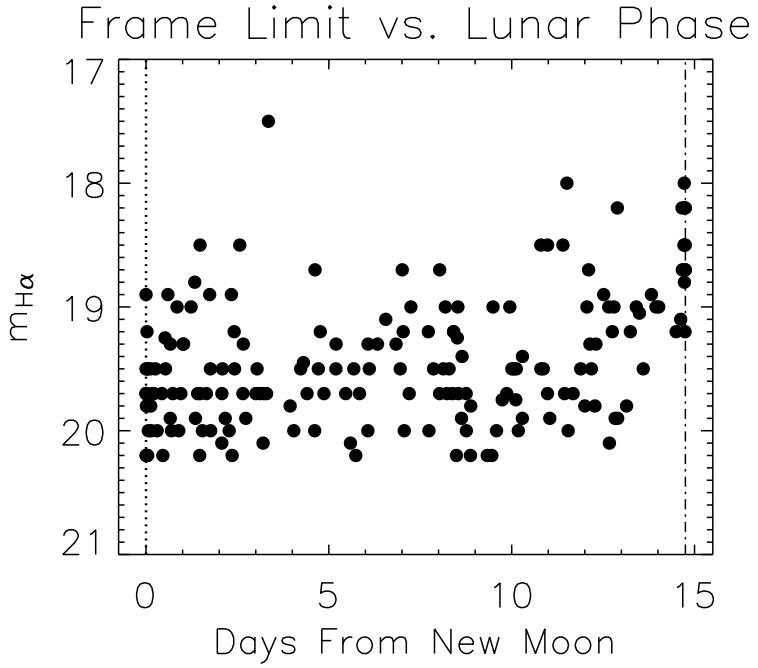

Figure 3.2: Frame limits in $m_{H\alpha}$ versus days from the New Moon. The dotted line indicates the New Moon, while the dot-dashed line indicates the Full Moon. The moon's impact on the survey depth is limited to the three days centered on Full Moon and has a maximum amplitude of less than a magnitude. Since novae last longer in Hα, the chance that we missed a nova because of the moon is very small.

Each individual exposure was 1200s and we attempted to get at least 5 exposures on a given field in one night for a total exposure time of 100 minutes per epoch. Although most of our epochs reached this goal, observing conditions varied considerably and so the number of useful exposures per epoch ranges from 2 to 9.

Ideally we would have observed all 12 fields every clear night. This was impossible

to achieve with the requirement that we get 100 minutes of exposure per epoch. Thus, we cycled through the 12 fields over the course of a varying number of nights depending on the time available on a given night subject to weather, M81's availability, and occasional equipment problems. Guide stars were not readily available for some of the fields or were faint, with the result that the number of usable survey epochs for each field varies from 5 to 21.

Our survey ran from December 31, 2002 (JD 2452638.8) to June 6, 2003 (JD 2452796.6) covering a total of 158.8 days. At the end of this time, two novae were still observable in decline in one of the fields (5S). An additional 15 epochs were obtained of this field to follow the declining novae until June 26, 2003 (JD 2452816.7), during which time no new novae were discovered in this field. This period from June 6 to June 26, 2003 is not included in our nova rate calculations.

Table 3.1 summarizes the observations in our survey. The field designations correspond to those in Figure 3.1, with the exception that field 5S and 2N are unlabeled (but their location is obvious). The fields with Bulge in the last column also contain a significant amount of M81's disk as can be seen from Figure 3.1.

3.3 Reduction

All exposures were bias-subtracted and flat-fielded using the standard tools in IRAF (Tody 1986). The exposures for a given epoch (from 2 to 9) were then registered and combined to produce a coadded image for each epoch using the following DAOPHOT programs (Stetson 1987): DAOPHOT to measure the point sources, DAOMATCH and DAOMASTER to derive and refine the transformations, and MONTAGE2 to perform the registration and coaddition. The registration master was chosen to be the best coadded image from the entire set for a given field based on measurements of the seeing in each coadded image over the entire survey. The coaddition process removed all but a few cosmic rays.

3.4 Nova Detection

The coadded images were blinked against each other to detect changing point sources. Nova candidates were required to be observed in at least two epochs *and* to be missing on an epoch of sufficient depth coverage to confirm its transient nature. We also used the raw images for an epoch to confirm the presence of the candidate in each individual frame.

For the bulge region of M81 (Fields 2N and 5S), where the intensity gradient makes detection more difficult, we used the following technique. We produced a spatial median-filtered image of the coadded frame using a box size of 11 by 11 pixels to remove point sources and preserve the low frequency structure of the image. This was then subtracted from the coadded image of the bulge fields after which they were blinked against each other. Since most of the novae were detected in the bulge region, the subtraction proved to be important for detecting novae in M81.

Table 3.2. M81 Nova Positions

	Position (J2000)				Nuclear Distance (arcsec)	
Nova	RA	Dec	Field	Detections	Uncorrected	Corrected
1	09 55 39.2	69 04 22	5S	11	42	84
2	09 55 21.5	69 05 60	5S	9	140	141
3	09 54 53.6	69 06 49	6S	5	274	317
4	09 55 35.3	69 03 34	2N	2	24	24
5	09 55 28.5	69 05 10	5S	10	79	85
6	09 55 48.5	69 03 05	2N	3	96	123
7	09 55 40.5	69 03 49	2N	6	40	66
8	09 55 46.7	69 04 07	5S	8	73	140
9	09 55 26.5	69 04 44	5S	4	61	61
10	09 55 04.4	69 03 24	3N	4	157	304
11	09 55 34.8	69 05 34	5S	14	99	144
12	09 55 47.4	69 04 44	5S	16	91	183

For each coadded image of each field we determined the frame limit by using artificial stars and the exact techniques outlined above for detecting the novae. Closer to the nucleus of M81, frame limits were derived from the flattened images. For field 2N, an additional set of frame limits was derived near the position of Nova 4. For field 5S, two additional sets of frame limits were derived near the positions of Nova 1 and Nova 5.

Table 3.2 summarizes the 12 novae discovered with our survey. Astrometry was derived for each nova using the WCSTOOLS package (Mink 2002) and the Guide Star Catalog-II[1]. Positions are accurate to better than 2" based on the fit residuals to the GSC-II stars. The corrected nuclear distances were calculated using the equations and parameters given in Shara, Sandage & Zurek (1999).

Could our candidates be anything other than novae? Their positions in M81 rule out foreground or background objects. We checked the position of each candidate against the list of known Hubble-Sandage (HS) variables in M81 (Sandage 1984) and found no coincidences. These bright blue HS variables are the only known non-nova variables that approach the brightnesses of our candidates. In fact, the brightest

[1]The Guide Star Catalog-II is a joint project of the Space Telescope Science Institute and the Osservatorio Astronomico di Torino. Space Telescope Science Institute is operated by the Association of Universities for Research in Astronomy, for the National Aeronautics and Space Administration under contract NAS5-26555. The participation of the Osservatorio Astronomico di Torino is supported by the Italian Council for Research in Astronomy. Additional support is provided by European Southern Observatory, Space Telescope European Coordinating Facility, the International GEMINI project and the European Space Agency Astrophysics Division.

B-band magnitude for the HS variables in M81 is 19.1 (Sandage 1984). These are massive stars and are likely to be much fainter in the red at the Hα passband than in the B-band. Considering the peak magnitudes of our candidates (see below), there is little chance that any of our nova candidates is actually one of these bright blue variables... or anything other than a nova.

3.5 Nova Photometry

Since crowding was not an issue, aperture photometry was used to measure point source brightnesses in each coadded image. We used the IRAF *apphot* package to measure point source brightnesses. Variable seeing was accounted for by setting the measurement aperture radius in each image to 1/2 the FWHM of the stellar profile to maximize the signal-to-noise ratio. The FWHM was measured from a set of well isolated stars in each image.

The photometric calibration was achieved using a two-step process, which was required because of the negligible overlap between fields, and the lack of Hα standards in many of the fields. The first step was to tie all the frames to a common system. This was achieved using the R-band photometry of Perelmuter & Racine (1995). An offset from our instrumental Hα magnitudes to the calibrated R magnitudes was calculated for each epoch of each field using from 18 to 70 stellar sources per field with an accuracy of better than 0.1 magnitude. Non-stellar sources (HII regions) were excluded by virtue of their much brighter instrumental Hα magnitude relative to R than the stellar sources.

Once all magnitudes were on this common R system, an offset was needed to the standard AB system where $m_{H\alpha} = 0.0$ for $f_\lambda = 2.53 \times 10^{-9}$ erg cm^{-2} s^{-1} Å^{-1}. For our filter with a FWHM of 30Å, this gives a zero-point flux of 7.59×10^{-8} erg cm^{-2} s^{-1}. We used the foreground extinction- corrected and standardized flux measurements of M81 planetary nebulae (PNe) published by Magrini et al. (2001) to calculate this offset. They used a 90Å FWHM Hα filter which would include [NII] if present. Our filter excludes [NII] so we had to assume that for the set of PNe used, the [NII] fluxes are small. Using our filter zero-point flux, we converted the fluxes from Magrini et al. (2001) into Hα filter magnitudes for the 107 PNe we were able to measure in 7 of our fields. We then compared these Hα filter magnitudes with the common R system magnitudes for the PNe to calculate an offset between the two systems. We calculated a mean offset from 78 PNe of -0.26 ± 0.13 magnitudes. We excluded 29 outliers that showed evidence of stronger [NII] by virtue of their having a lower instrumental Hα magnitude than predicted from the conversion of the flux to Hα filter magnitude. Without individual spectra of the PNe, this exclusion is less than perfect and limited our photometric accuracy.

As a check on this calibration, we used the one object which is in both the R catalog of Perelmuter & Racine (1995) and the Hα flux catalog of Magrini et al. (2001). Object 2111 from Perelmuter & Racine (1995) with an R magnitude of 19.64 is object 93 from Magrini et al. (2001) which has an Hα magnitude (using the zero point flux above) of 19.42. This gives an offset of -0.22, in good agreement with our

calibration.

This calibration should allow comparison of our Hα nova light curves with the M31 Hα light curves of Ciardullo et al. (1990a) with one important caveat. Because our filter is 2.5 times narrower, many of the faster novae with expansion velocities $>$ 685 km s^{-1} have overfilled our 30Å bandwidth. The M31 novae can have expansion velocities up to 1715 km s^{-1} and not overfill the 75Å filter bandwidth used by Ciardullo et al. (1990a). Because nova ejection velocity is a function of nova luminosity (Shara 1981), a direct comparison of the nova luminosity distribution between M31 and M81 is precluded for this survey.

Table 3.3 presents our calibrated photometry for each nova at each observed epoch. The errors in Column 3 are the 1-σ internal photometric errors. The three points in parenthesis for Nova 6 are unfiltered magnitudes from the KAIT telescope (Weisz & Li 2003). Filippenko & Chornock (2003) report that the spectrum of this nova exhibited strong double-peaked hydrogen Balmer emission lines and that many Fe II, Ca II, and O I lines also appeared in emission, and thereby confirm this object as a nova.

3.6 The Hα Light Curves

Figure 3.3 and Figure 3.4 present our calibrated Hα light curves for the 12 novae discovered in M81 during our survey. Figure 3.3 presents the 6 novae for which we have observed the maximum $m_{H\alpha}$, while Figure 3.4 presents the 6 novae observed days or weeks after maximum $m_{H\alpha}$. The frame limits are plotted as short horizontal lines with downward pointing arrows, while the solid circles with error bars are the nova observations from Table 3.3.

A simple linear fit was made to the decline portion of each light curve to calculate the decline rates in $m_{H\alpha}$ day^{-1}. The thin lines in Figure 3.3 and Figure 3.4 show the resulting fits. Table 3.4 presents the properties of the nova light curves including the rise time and decline rate for each nova. We consider the Hα rise times to be lower limits because we do not have the continuum light curves with which to to accurately define the outburst time.

Table 3.3. M81 Nova Photometry

Nova	J. D. (+2452000)	$m_{H\alpha}$	Err($m_{H\alpha}$)	Pl. Limit $m_{H\alpha}$
1	641.80	18.02	0.17	18.5
	644.79	18.46	0.17	18.8
	653.88	18.16	0.13	18.8
	668.78	18.50	0.11	18.9
	679.64	18.33	0.15	18.7
	689.88	···	···	18.3
	693.76	18.93	0.15	19.0
	707.60	18.69	0.25	18.7
	709.78	18.88	0.14	19.3
	711.89	19.20	0.22	19.2
	720.78	···	···	18.9
	723.79	18.88	0.17	19.0
	728.63	18.97	0.21	19.0
	735.63	···	···	18.5
	753.79	···	···	18.7
	758.79	···	···	18.4
	769.69	···	···	19.3
2	641.80	18.28	0.12	18.9
	644.79	18.05	0.09	19.3
	653.88	18.26	0.10	19.5
	668.78	18.67	0.10	19.7
	679.64	18.62	0.13	19.3
	689.88	19.02	0.23	19.0
	693.76	19.27	0.14	19.7
	707.60	19.41	0.23	19.5
	709.78	19.38	0.16	19.7
	711.89	···	···	19.4
	720.78	···	···	19.7
3	642.76	18.05	0.08	19.5
	652.76	18.66	0.23	19.5
	657.74	···	···	18.5
	670.78	18.87	0.11	20.0
	680.71	19.37	0.29	19.5
	705.75	···	···	19.9
	707.91	···	···	19.5
	710.68	···	···	19.0
	718.79	···	···	19.0
	721.80	19.87	0.33	20.0
	724.89	···	···	19.5
	725.61	···	···	19.5
	728.79	···	···	20.0
4	639.84	···	···	19.2
	643.78	18.45	0.23	19.0
	653.77	···	···	18.5
	668.68	19.66	0.54	19.7
	671.88	···	···	19.5
5	668.78	···	···	19.5
	679.64	18.72	0.15	19.1
	689.88	···	···	18.7
	693.76	18.55	0.10	19.5
	707.60	18.57	0.15	18.8
	709.78	18.55	0.09	19.5
	711.89	18.88	0.14	19.2
	720.78	18.79	0.15	19.4

Table 3.3—Continued

Nova	J. D. (+2452000)	$m_{H\alpha}$	Err($m_{H\alpha}$)	Pl. Limit $m_{H\alpha}$
5–Continued	723.79	18.29	0.09	19.4
	728.63	18.20	0.09	19.2
	735.63	18.37	0.13	18.7
	753.79	18.98	0.18	19.0
	758.79	···	···	18.9
6	671.88	···	···	20.2
	676.90	(19)[a]	···	···
	679.90	(17.8)[a]	···	···
	680.90	(17.9)[a]	···	···
	687.99	17.34	0.07	18.7
	692.63	17.37	0.04	19.7
	706.84	19.20	0.17	19.7
	709.63	···	···	18.7
	711.72	···	···	19.5
7	692.63	···	···	19.7
	706.84	18.26	0.12	19.7
	709.63	17.42	0.08	18.7
	711.72	16.97	0.04	19.5
	720.62	17.66	0.09	19.5
	723.61	17.79	0.13	19.0
	734.79	18.82	0.14	20.2
	758.70	···	···	19.3
	765.65	···	···	19.7
8	693.76	···	···	19.5
	707.60	17.76	0.09	18.8
	709.78	17.79	0.05	19.5
	711.89	17.95	0.07	19.2
	720.78	18.46	0.13	19.4
	723.79	18.64	0.12	19.4
	728.63	18.91	0.17	19.2
	735.63	···	···	18.7
	753.79	···	···	19.0
	758.79	···	···	18.9
	769.69	···	···	19.5
9	693.76	···	···	19.5
	707.60	18.69	0.20	18.8
	709.78	18.74	0.12	19.5
	711.89	19.12	0.19	19.2
	720.78	19.36	0.29	19.4
	723.79	···	···	19.4
10	728.71	···	···	19.7
	735.85	···	···	18.5
	754.77	18.59	0.10	19.2
	759.65	18.92	0.12	19.7
	770.69	18.78	0.17	19.5
	778.74	···	···	19.2
	785.75	19.68	0.40	19.7
	796.63	···	···	18.7
11	758.79	···	···	18.9
	769.69	17.61	0.06	19.7
	777.66	17.47	0.08	18.9

Table 3.3—Continued

Nova	J. D. (+2452000)	$m_{H\alpha}$	Err($m_{H\alpha}$)	Pl. Limit $m_{H\alpha}$
11–Continued	778.66	17.59	0.04	19.9
	783.65	17.98	0.11	19.5
	794.64	18.23	0.08	20.1
	797.64	18.47	0.12	19.5
	798.65	18.90	0.19	19.2
	800.64	18.21	0.24	18.5
	801.68	18.64	0.22	18.9
	802.68	18.61	0.19	19.5
	805.67	···	···	19.1
	807.67	18.72	0.17	19.2
	808.64	18.82	0.20	19.3
	809.67	···	···	18.5
	810.65	···	···	19.0
	811.66	···	···	18.7
	812.66	···	···	19.1
	813.66	18.74	0.16	19.3
	815.67	18.57	0.14	19.3
	816.67	···	···	18.9
12	783.65	···	···	19.5
	794.64	18.60	0.11	20.1
	797.64	18.18	0.10	19.5
	798.65	18.29	0.12	19.2
	800.64	18.25	0.29	18.5
	801.68	18.48	0.19	18.9
	802.68	18.08	0.11	19.5
	805.67	17.96	0.15	19.1
	807.67	17.90	0.10	19.2
	808.64	17.98	0.09	19.3
	809.67	17.90	0.14	18.5
	810.65	18.04	0.13	19.0
	811.66	17.91	0.11	18.7
	812.66	18.43	0.14	19.1
	813.66	18.54	0.14	19.3
	815.67	18.52	0.14	19.3
	816.67	18.70	0.21	18.9

[a]Nova 6: Unfiltered magnitudes from the KAIT Telescope (Weisz & Li 2003).

We cannot compare the brightness distribution of our novae to that for M31, because of the filter-overfilling described above, but we can compare the nova decline rates. Figure 3.5 shows the comparison of our decline rates with the M31 decline rates reported in Ciardullo et al. (1990a) and Shafter & Irby (2001). We see that the distribution is similar, but there is an indication of incompleteness in our slowest decline rate bin. Both M31 surveys spanned at least two years and therefore had longer overall time baselines. Our survey is continuous, but only covers a five month period. At the slowest reported decline rate for an M31 nova of 0.0018 $m_{H\alpha}$ day^{-1} (Ciardullo et al. 1990a), in five months a nova would only change by 0.3 magnitudes in Hα and would not be seen in our survey as a transient point source. In fact, it would take over 500 days before such a slow nova would change by one magnitude. Based on Figure 3.5, and accounting for small-number statistics, we estimate that there are roughly 10 very slow novae that remain to be detected in the present survey. As we

Table 3.4. M81 Nova Light Curve Properties

				Decline		
Nova	Max ($m_{H\alpha}$)	Baseline (days)	Rise Time (days)	Baseline (days)	Pts (N)	Rate ($m_{H\alpha}$ day^{-1})
1	< 18.0	87	$\cdots$	87	11	0.010
2	18.0	68	> 3	65	8	0.021
3	< 18.0	79	$\cdots$	79	5	0.027
4	< 18.4	25	$\cdots$	25	2	0.049
5	18.2	74	> 49	25	3	0.031
6	17.3	19	> 11	14	2	0.129
7	17.0	28	> 5	23	4	0.078
8	< 17.8	21	$\cdots$	21	6	0.058
9	< 18.7	13	$\cdots$	13	4	0.058
10	< 18.6	31	$\cdots$	31	4	0.022
11	17.5	46	> 8	38	13	0.036
12	17.9	22	> 13	9	9	0.087

extend our survey in time, we will continue to blink epochs from the season reported here in an effort to discover these very slowly declining novae.

Two of the light curves show that, in Hα, novae can take a long time to reach maximum brightness; Nova 12 took more than 13 days , and Nova 5 took at least 50 days. Nova 12 can be compared with Nova 26 in Ciardullo et al. (1990a) which took $\sim$15 days from outburst to reach maximum. Our Nova 5 is unprecedented; its 50 day rise is, as far as we know, the longest ever observed for a nova in Hα. Nova 20 from Ciardullo et al. (1990a) shows a small decline before reaching maximum light, like our Nova 5, and could have taken a similar length of time to reach maximum.

Figure 3.6 shows a comparison of nova rise times in Hα and the continuum. The Hα data consist of the 6 novae from this paper (see Table 3.4) and the three novae with well observed rises from Ciardullo et al. (1990a). The continuum data are from the photographic light curves presented in Arp (1956). Of the 30 novae discovered by Arp, we used 21 for which we could determine a reliable rise time. The continuum distribution has a sharp peak at 1 day, but extends out to nearly as long a rise time as the longest one for Hα. The Hα distribution shows no peak, and does seem to cluster in the range from 3 to 15 days. The arithmetic mean of the continuum rise times is 9.0 days. The arithmetic mean for the Hα rise times is 13.3 days, but should only be considered a lower limit given that all the rise times from Table 3.4 are lower limits. For the four novae from Ciardullo et al. (1990a) that have both B-band and Hα photometry (including Nova Cyg 1975), we see that the Hα maximum always occurs after the B-band maximum. It appears that Hα rise times are generally longer than

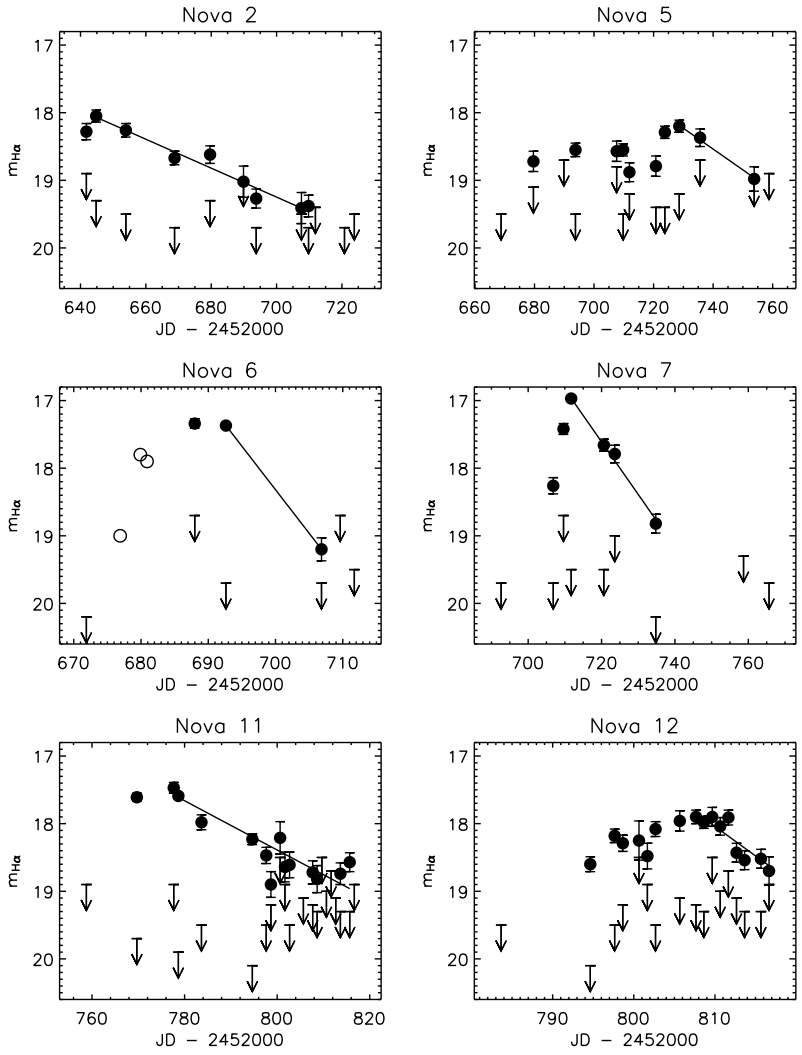

Figure 3.3: Hα light curves of six M81 novae observed to reach maximum $m_{H\alpha}$. The solid points are $m_{H\alpha}$ and the frame limits are indicated by the horizontal line with the downward pointing arrow. The open circles for Nova 6 are unfiltered magnitudes from the KAIT telescope (Weisz & Li 2003). The thin lines are linear fits to the decline rates for each nova.

continuum rise times, but without a large set of light curves in both continuum and Hα for each nova, we cannot say more. We hope to remedy this in future observing seasons for M81.

The slow rise times in Hα of some novae may lead to inaccuracy in the calculation of nova rates if only the maximum light and decline rates are used, especially with a survey such as ours with many closely spaced epochs. Nova light curves which cover the rising portion of the outburst and allow determination of the decline rate are needed for calculating accurate completenesses and nova rates.

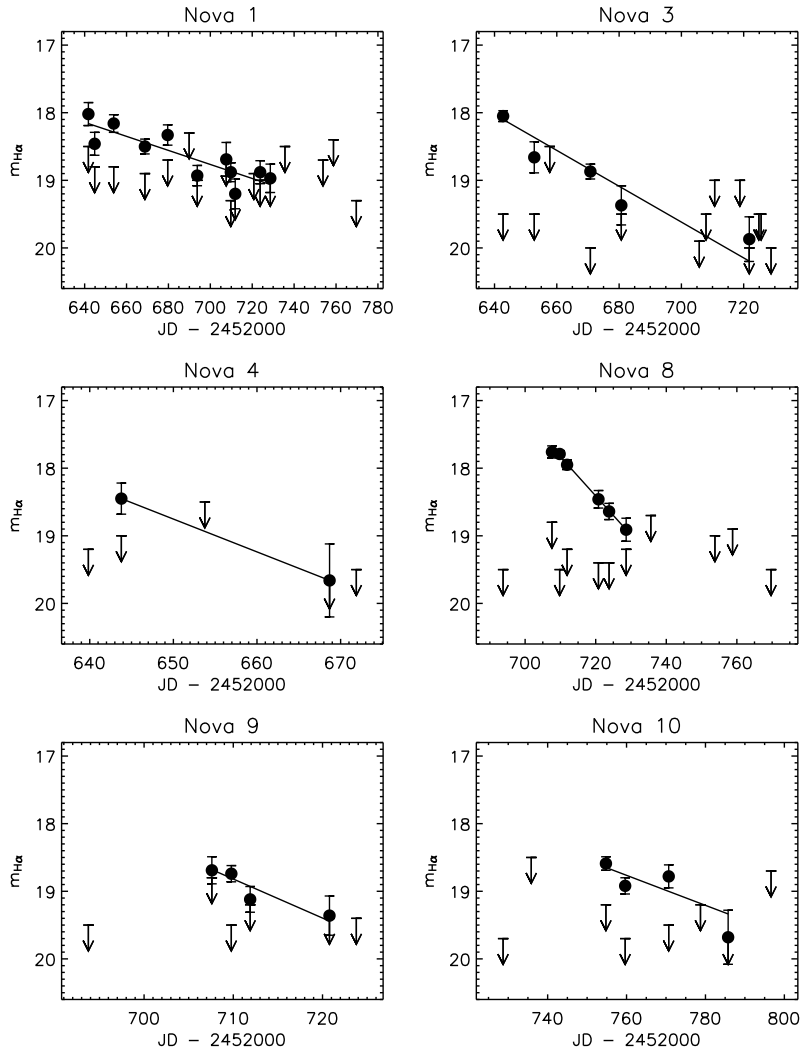

Figure 3.4: As for Figure 3.3, but for the novae observed days or weeks after maximum $m_{H\alpha}$.

3.7 Completeness

Because of the dense time sampling and variable depth of our survey, we developed an approach to finding the completeness of each field that is more appropriate than assigning a single frame limit to the entire survey. With a set of relatively complete Hα nova light curves and the frame limit for each epoch of each field, we can calculate the completeness for a given field by simulating the random outburst times of a large sample (10^5) of novae. This approach assumes that we have a set of Hα light curves that is representative of the nova population in M81.

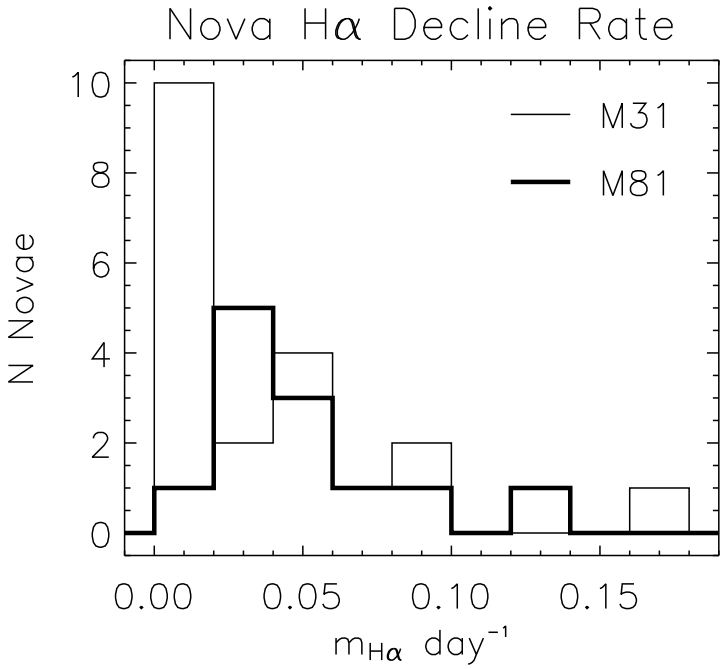

Figure 3.5: Histogram comparing the Hα decline rates for our M81 novae and the M31 novae of Ciardullo et al. (1990a) and Shafter & Irby (2001). Note the incompleteness in our M81 survey in the slowest bin. As noted in the text, this is due to the five month overall time baseline of our survey. The M31 surveys had overall time baselines of two years or more.

3.7.1 Representative Hα Light Curves

Of the 12 light curves reported in this work, three novae have sufficient coverage of the rising part of the light curve and have reasonably well determined decline rates to qualify for this set: Novae 5, 7, and 12 (see Figure 3.3). We can combine these with the Hα photometry of the 8 novae listed in Table 11 of Shafter & Irby (2001) to get a representative set of 11 Hα nova light curves to use in our random outburst simulation.

In order to include the M31 light curves in our representative set, we need to correct for the difference in galaxy distances and the difference in filter bandwidths. Using the distance moduli quoted in Shafter, Ciardullo & Pritchet (2000) we apply a correction to the M31 novae of +3.48 magnitudes to place them at the distance of M81. The filter bandpass we used is 2.5 times narrower than that used by Ciardullo et al. (1990a) for the M31 novae and so they would appear 1 magnitude brighter in our survey making the correction +2.48 magnitudes. If the M31 novae had, in fact, been observed with our filter, they would have overfilled the bandpass by varying amounts and therefore been fainter by up to a factor of 2. Spectroscopic observations of M31 novae by Ciardullo, Ford & Jacoby (1983) show typical emission line widths of 40-60 Å. However, spectra of novae in M31 reported by Tomaney & Shafter (1992) show

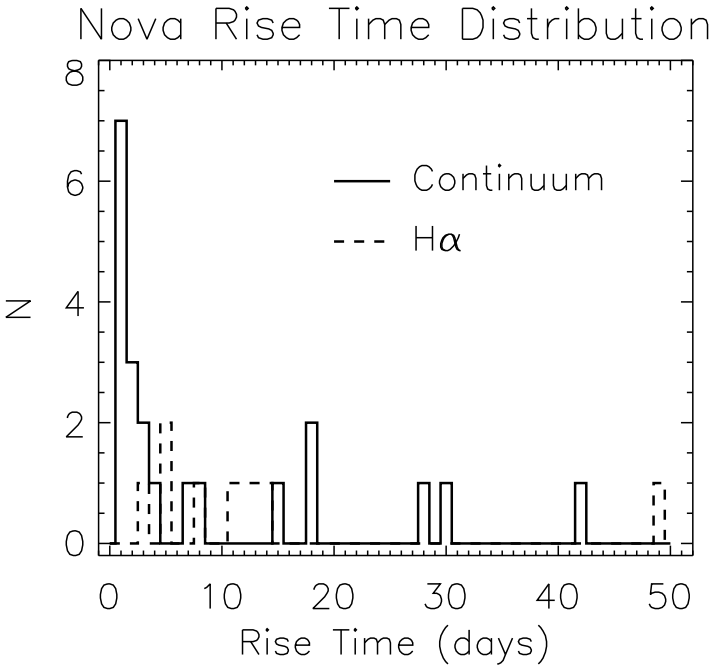

Figure 3.6: Histogram comparing continuum and Hα rise times. The continuum rise times, shown by the solid histogram, are from the photographic light curves in Arp (1956). The Hα rise times, shown by the dashed histogram, are from Table 3.4 and from Ciardullo et al. (1990a). The arithmetic mean of the continuum rise times is 9.0 days, while the arithmetic mean for the Hα rise times is 13.3 days. Note that the Hα rise times presented in this work are lower limits.

the slowest, and therefore faintest, novae to have expansion velocities of less than 685 km s^{-1}, which would not overfill our filter. Since we are interested in calculating the completeness at the faint end, we elect not to apply an uncertain overfilling factor to the M31 novae. Therefore, our total correction to the M31 novae to include them with our M81 photometry through a 30 Å filter is +2.48 magnitudes.

To see if this set is truly representative of novae in M81, we can compare the range of decline rates in this set (0.0044 to 0.087 mag day^{-1}) with Figure 3.5. We see that this range covers the majority of the novae in this figure. By adding the slower novae from M31, we account for the very slow novae we are apparently missing, according to Figure 3.5. We can also compare the range of maximum magnitudes in this set ($m_{H\alpha}$ from 17.0 to 20.9) with the maximum magnitudes reported in Ciardullo et al. (1990a) for M31. After accounting for the magnitude offset as described above, we see that our set spans the majority of the range of novae in M31. For the following analysis, we will assume that our 11 novae are a representative set for M81.

Table 3.5. Completeness of Frame Limit Sets

Field	Nuclear Distance[a] (arcsec) Uncorrected	Corrected	Epochs (N)	Completeness (%)
1N	430	444	19	76
1S	669	685	18	80
2N	141	199	18	80
2N[b]	24	24	18	48
2S	423	591	5	41
3N	289	550	17	78
3S	431	841	10	79
4N	355	716	18	78
4S	285	464	5	30
5N	424	564	6	40
5S	140	182	21	89
5S[c]	79	85	21	85
5S[d]	42	84	21	72
6N	593	595	8	50
6S	372	431	21	79

[a]This distance is from the field center unless otherwise noted.

[b]at position of Nova 4

[c]at position of Nova 5

[d]at position of Nova 1

3.7.2 Random Outburst Simulations

We used each nova in this representative set to make a random outburst simulation for each set of frame limits we measured. This produced 11 simulations for each of the 15 frame limit sets for a total of 165 simulations. To create each simulation, which consisted of 10^5 trials, we used a uniformly distributed random number generator to shift the representative nova light curve in time so that its outburst occurred within the 159 days of our survey. The frame limit set being studied was then compared with each shifted light curve to determine if it would have been a valid nova candidate in that field. A valid candidate must pass the criteria describe above: it must be brighter than at least two frame limits in the set, *and* it must be fainter than at least one of the frame limits, to confirm its transient nature. The number of times a simulated nova was identified as a candidate was divided by the number of trials to produce

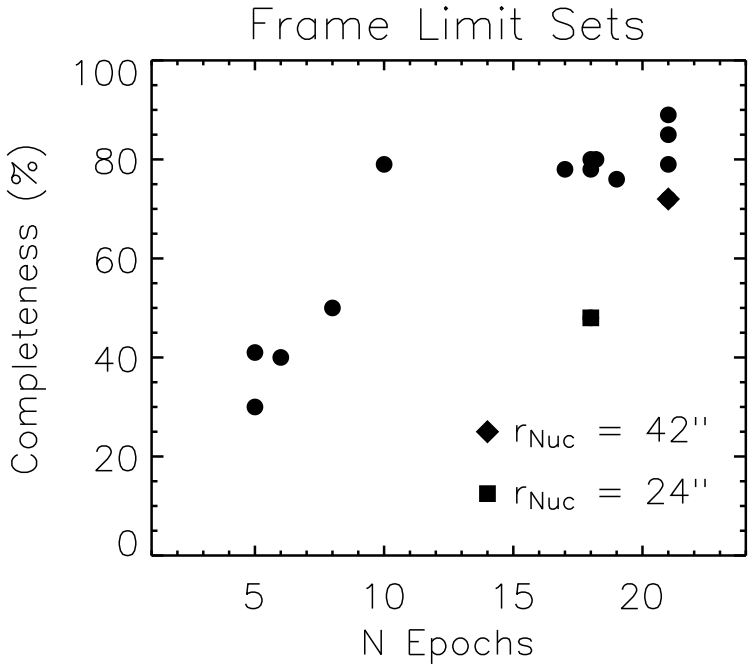

Figure 3.7: Completeness of the 15 frame limit sets as a function of the number of epochs from the random outburst simulations. The trend with the number of epochs is obvious. A trend with nuclear distance, r_{Nuc}, is also shown using the two frame limit sets closest to the nucleus of M81. For Field 5S, the lowest completeness frame limit set is indicated by a diamond. For Field 2N, the lowest completeness frame limit set is indicated by a square. These points illustrate that, in spite of having many epochs, within an arcminute of the nucleus of M81 a significant incompleteness exists.

a fractional completeness for that representative nova in the frame limit set being studied.

In order to compare the randomly shifted nova light curve with the frame limits in the set, and determine if the simulated nova would have been a candidate in the field being studied, the following algorithm was adopted. Any nova magnitude on a frame epoch before outburst was set to 99.9 (i.e., a non-detection). Nova magnitudes on frame epochs between two light curve points were calculated using linear interpolation. Nova magnitudes on frame epochs after the last point in the light curve were calculated using the measured decline rate for the nova. This is much more accurate than extrapolating beyond the end of the light curve since the last points in a nova light curve tend to be the faintest and therefore the noisiest.

The completeness as a percentage, averaged over the 11 representative novae, is given for the 15 frame limit sets in Table 3.5 and plotted in Figure 3.7. Two correlations are apparent. The first and strongest is the correlation with the number of observed epochs. The lowest completeness is obtained for the fields with the smallest number of observed epochs and suggests a substantial incompleteness for

Table 3.6. Completeness of Representative Novae

Nova[a]	Max ($m_{H\alpha}$)	Completeness (%)	Decline Rate ($m_{H\alpha}$ day^{-1})
5	18.2	79	0.031
7	17.0	80	0.078
12	17.9	74	0.087
CFNJS 6	18.2	65	0.080
CFNJS 20	19.8	54	0.0044
CFNJS 26	17.6	82	0.029
CFNJS 31	18.5	80	0.013
N1992-07	19.0	71	0.0070
N1995-06	18.9	78	0.015
N1995-07	19.4	71	0.0090
N1995-09	21.2	3.5	0.046

[a]Novae from this work are identified with a number, while novae from Shafter & Irby (2001) have the identifications from their Table 11. The magnitudes from Shafter & Irby (2001) have been corrected by +2.48 magnitudes to account for the difference in Hα filter widths, and the different distances of M31 and M81.

these fields. The other correlation is with nuclear distance. For fields 2N and 5S, the completeness drops considerably as the distance to the nucleus decreases. For a frame limit set measured at 42" from the nucleus of M81, and plotted in Figure 3.7 as a filled diamond, we derive a completeness of 72%. For the closest frame limit set at 24" from the nucleus, and plotted in Figure 3.7 as a filled square, we derive a completeness of only 48%. This suggests that a significant incompleteness exists in our survey within an arcminute of the nucleus of M81.

The completeness as a percentage, averaged over the 15 frame limit sets, is given for the 11 representative novae in Table 3.6 and plotted in Figure 3.8. The effect of maximum magnitude on completeness is readily apparent. This trend is not without scatter, however, due to the complex interaction between the shape of the light curve and the depth of the survey as a function of epoch.

3.8 The Nova Rate

The effects noted above demonstrate that assigning a single limiting magnitude to our survey is overly simplistic. This fact, combined with our dense time coverage, indicates that we can improve on the mean nova lifetime approach of Ciardullo et al.

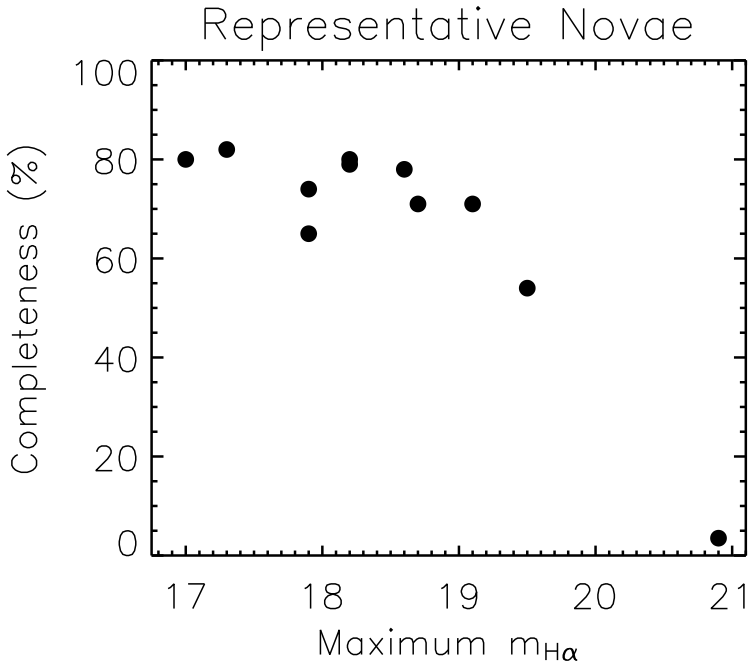

Figure 3.8: Completeness of each of the 11 representative novae as a function of maximum $m_{H\alpha}$ from the random outburst simulations. The trend with maximum $m_{H\alpha}$ is obvious, and implies a survey limit of just fainter than 19 $m_{H\alpha}$. There is scatter even for novae with the same maximum $m_{H\alpha}$. This is due to the different shapes of the nova light curves and illustrates the difficulty in assigning a single frame limit to a survey such as ours.

(1990a) for calculating the nova rate for M81. A raw global nova rate can be obtained simply by dividing the observed number of novae that erupted during the survey by the time covered. Excluding the two novae that erupted before the start of the survey (Nova 1 and Nova 3), gives $R = 10/0.43\text{yr} = 23$ yr^{-1} and is obviously a hard lower limit on the M81 nova rate. This rate also requires no correction for partial spatial coverage since we are covering the entire galaxy. For comparison, Moses & Shafter (1993) report a nova rate for M81 of $R = 24 \pm 8$ yr^{-1}, based on 15 novae discovered over a three year period. Shafter, Ciardullo & Pritchet (2000) refer to an unpublished study whose preliminary results indicate that the nova rate in M81 may be somewhat lower than this.

We can adjust our raw rate by the completenesses shown in Table 3.5. Since the novae in fields 2N and 5S were distributed closer to the nucleus of M81, we must account for the lower completenesses found. For field 2N, we use a completeness which is the average of the two positions measured, or 64%. For field 5S, we also average the completeness measurements to get a 82% average completeness. Dividing the number of novae that erupted in each field by the appropriate completeness fraction and adding, we derive a completeness-corrected number of novae during our five month survey of 13. Using this corrected number of novae, we find a global M81

nova rate of $R = 13/0.43\text{yr} = 30$ yr^{-1}. This is still a conservative lower limit because by averaging the completenesses in the two Bulge fields, we are assuming that the number of novae at each measurement location is the same. Figure 3.1 shows that the novae are more likely to come from the regions of lower completeness nearer to the nucleus of M81 and hence the true completeness correction is probably larger than what we have used here.

3.8.1 The Monte Carlo Approach

Shafter & Irby (2001) describe a Monte Carlo technique which uses the maximum magnitudes and decline rates of the novae in their Table 11 and their survey limit to find the most probable nova rate in their survey region. We used the 11 representative nova light curves described above combined with our frame limits in a similar Monte Carlo experiment to derive nova rates for each of our fields.

This technique makes many independent estimates of the observed nova rate in the given field as a function of the true nova rate $[N_{obs}(N_t)]$. For a given trial estimate of N_t, the true rate, we choose a random set of light curves and outburst times and use the frame limits to calculate the number of observed novae, using the candidate criteria described above. We repeat this 10^5 times and record how many times we recover the number of nova candidates actually observed for that field. The estimate of the true nova rate N_t is then incremented and the process is repeated. This produces a probability distribution for N_t in the given field. The best estimate for N_t is that which corresponds to the peak of this distribution.

Figure 3.9 shows the probability distributions for an interesting subset of fields. The two distributions at the top of the figure, for Field 1S and Field 4S, show the difference between two disk fields with no observed novae, but very different time coverage and depth. This is reflected in the widths of the distributions and consequently the errors on the estimated true nova rate. The middle two distributions are for fields 3N and 6S, having one nova observed in each. The bottom two distributions are for the two fields that had the bulk of the observed novae with 3 for Field 2N and 7 for Field 5S.

Table 3.7 presents the results of the simulations for each of 15 sets of frame limits. To derive a global nova rate from these data, we add up the nova rates in all the fields. Without accounting for the incompleteness near the center of M81 (i.e., using the frame limit sets derived at the field centers of the two bulge fields), we find a global nova rate of 28^{+10}_{-4} yr^{-1} which is in good agreement with our corrected nova rate of 30 yr^{-1}. If we include the rates from the frame limit sets closer to the nucleus of M81, as we did for the completeness, we get a higher nova rate. Averaging the two rates for Field 2N we get a rate of 11^{+7}_{-5} yr^{-1}. Averaging the three rates for Field 5S we get 18^{+7}_{-6} yr^{-1}. Adding these rates to the nova rates for the other fields, we derive a Monte Carlo, completeness-corrected nova rate for M81 of 33^{+13}_{-8} yr^{-1}. We point out again that this is a conservative estimate because we have not accounted for the distribution of novae in our simplistic averaging of nova rates for fields 2N and 5S.

Table 3.7. Field Nova Rates

	Nuclear Distance[a] (arcsec)				
Field	Uncorrected	Corrected	Epochs (N)	Novae Obs. (N)	Nova Rate (yr^{-1})
1N	430	444	19	0	$0^{+1.7}_{-0.0}$
1S	669	685	18	0	$0^{+1.6}_{-0.0}$
2N	141	199	18	3	$8^{+3.2}_{-2.3}$
2N[b]	24	24	18	3	$14^{+5.9}_{-4.4}$
2S	423	591	5	0	$0^{+3.5}_{-0.0}$
3N	289	550	17	1	$2^{+2.6}_{-0.9}$
3S	431	841	10	0	$0^{+1.6}_{-0.0}$
4N	355	716	18	0	$0^{+1.6}_{-0.0}$
4S	285	464	5	0	$0^{+4.9}_{-0.0}$
5N	424	564	6	0	$0^{+3.5}_{-0.0}$
5S	140	182	21	7	$16^{+3.6}_{-2.9}$
5S[c]	79	85	21	7	$17^{+3.7}_{-3.2}$
5S[d]	42	84	21	7	$20^{+5.0}_{-3.7}$
6N	593	595	8	0	$0^{+2.8}_{-0.0}$
6S	372	431	21	1	$2^{+2.6}_{-0.9}$

[a]This distance is from the field center unless otherwise noted.

[b]at position of Nova 4

[c]at position of Nova 5

[d]at position of Nova 1

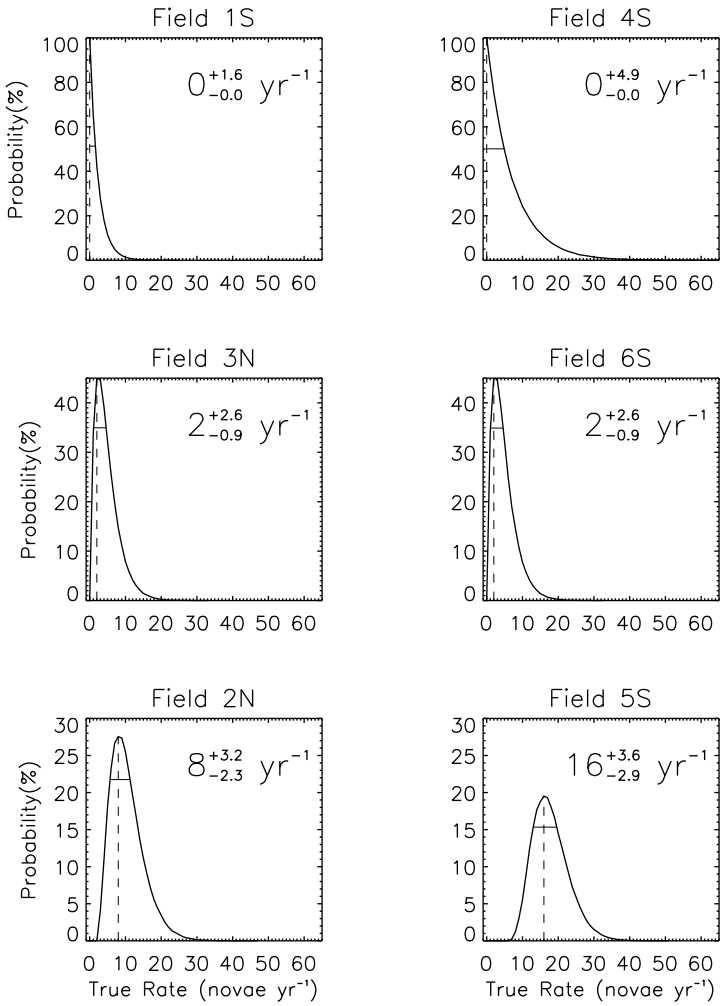

Figure 3.9: Monte Carlo probability distributions of the true nova rate, N_t, for 6 of the 12 M81 fields. The dashed vertical lines show the locations of the most probable N_t. The solid horizontal lines show the limits encompassing half the probability and define the errors for each estimate of N_t.

3.8.2 The Luminosity Specific Nova Rate

The 2-micron All Sky Survey (2MASS) offers a uniform infrared photometric system for normalizing nova rates from different galaxies to their underlying stellar luminosity. This has the potential to remove one of the major uncertainties in the study of how the luminosity specific nova rate (LSNR) in a galaxy varies with Hubble type, once issues concerning the level of the infrared background are resolved (See § 4.8.2). The Large Galaxy Atlas of the 2MASS (Jarrett et al. 2003) gives a K-

band integrated magnitude for M81 of 3.831±0.018[2]. Using this we derive a K-band luminosity for M81 of $L_K = 8.34 \pm 0.14 \times 10^{10} L_{\odot,K}$. We derive a LSNR of $\rho_k = 3.96^{+1.8}_{-1.1}$ yr^{-1}[$10^{10} L_{\odot,K}$]$^{-1}$ from our nova rate of 33^{+13}_{-8} yr^{-1} obtained from the Monte Carlo experiment.

This LSNR moves the position of the data point for M81 in Figure 6 from Shafter, Ciardullo & Pritchet (2000) up from $\rho_k = 1.80 \pm 0.71$. This does not change the conclusion they drew: namely, that no correlation exists between ρ_k and galaxy $B - K$ color. There are many systematic and random errors that could mask such a correlation. The normalization of nova rate to infrared luminosity using 2MASS should reduce the scatter in this diagram caused by non-uniform infrared galaxy magnitudes. We maintain that the biggest source of error in this diagram is that nova rates are systematically underestimated for the inner regions of galaxies where most of the novae may well occur. This figure could change substantially as global nova rates are improved and normalized to a uniform measurement of stellar luminosity for these galaxies. We now show that novae seem to prefer the bulge over the disk of M81.

3.9 The Spatial Distribution

We do not yet have enough novae in M81 to perform a reliable maximum likelihood decomposition of bulge and disk novae as did Ciardullo et al. (1987) for M31. We can, however, do a simple test comparing the distribution of light and novae. We used the bulge/disk decomposition of Simien & de Vaucouleurs (1986), Table 4, to calculate the cumulative radial distributions of the bulge, the disk, and the total light of M81. We then compared these with the cumulative radial distribution of the novae. We used the Kolmogorov - Smirnov (KS) test to determine at what confidence level we can rule out the hypotheses that the nova distribution is identical to the three different light distributions. Figure 3.10 shows the results of this comparison.

The "best match" with the nova distribution of the three is the bulge light distribution which can only be ruled out at the 21% confidence level. The total light fares considerably worse by over a factor of two and can be ruled out at the 57% confidence level. The disk light distribution is the worst match and can be ruled out at the 99% confidence level. Even though the bulge light does the best, the confidence level of 21% is still high. This is most likely due to the incompleteness in the central regions of the galaxy (see Figure 3.7).

Another diagnostic for the bulge-to-disk ratio of novae was described in Hatano et al. (1997). They used a model for dust in M31 and predicted its effect on the distribution of novae in the bulge region. They state that if novae arise primarily in the bulge, a large asymmetry in their distribution would be apparent because the dust in the disk obscures the bulge novae behind the disk. In this case there would

[2]This publication makes use of data products from the Two Micron All Sky Survey, which is a joint project of the University of Massachusetts and the Infrared Processing and Analysis Center/California Institute of Technology, funded by the National Aeronautics and Space Administration and the National Science Foundation.

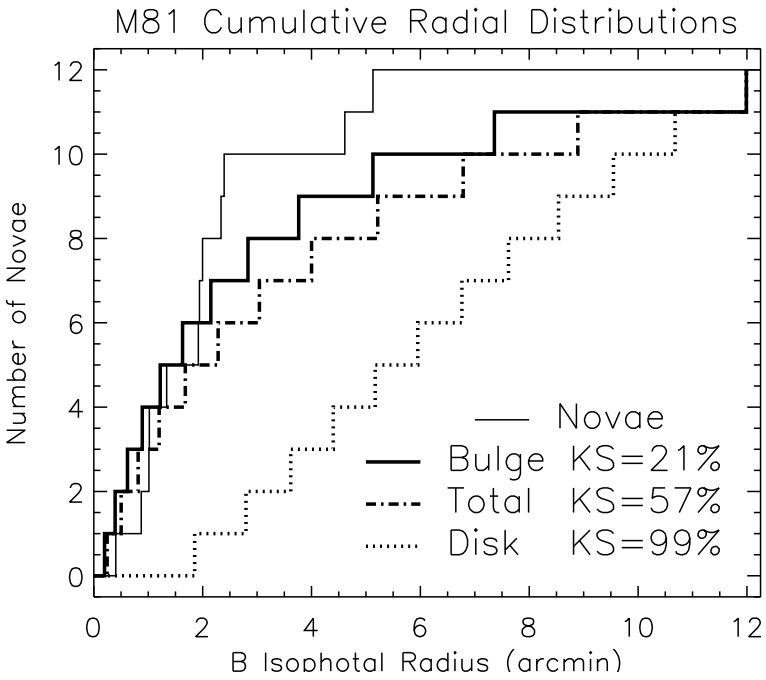

Figure 3.10: Cumulative radial distribution of novae compared with the bulge/disk decomposition of Simien & de Vaucouleurs (1986) in B-band light. Using their parameters we calculated the K-S statistic to test how well we can rule out the hypotheses that the radial distribution of the novae, indicated by the solid thin line, differ from the radial distributions of the various components of M81. The bold solid line represents the bulge light and can be ruled out at only the 21% confidence level. The total light shown by the bold dot-dashed line can be ruled out at the 57% confidence level. The exponential disk, shown by the bold dotted line can be excluded with a confidence of 99%. While the bulge of M81 does the best, its high KS statistic may be due to incompleteness of nova detection in the inner part of the galaxy.

be fewer novae seen on one side of the bulge than on the other. They use the major axis of M31 as the dividing line between novae on top of the disk and novae on the bottom and compared the number of novae below the disk, on the bottom of the bulge, with the number of novae in the bulge above the disk. This ratio is called the bottom-to-top ratio (the BTR). If disk novae predominate, the asymmetry is much less pronounced across this line since the fraction of novae obscured by the disk is the same on each side of the major axis. Using their dust model, Hatano et al. (1997) calculated the BTR for two different scenarios for M31: one with a bulge-to-disk nova ratio of 9 which produced a BTR of 0.33, and one with a bulge-to-disk nova ratio of 1/2 which produced a BTR of 0.63.

If we look at our sample of novae in M81, we can calculate the same BTR diagnostic. M81 clearly has dust in the disk that extends into the bulge (Jacoby et al. 1989). Its inclination of 60.°4 (Shara, Sandage & Zurek 1999) is not that different from the inclination of 77.°0 for M31 (Ciardullo et al. 1987). By examining the image

of M81 from the Hubble Atlas (Sandage 1961), one can see that the top of the bulge is on the north-east side of the major axis line. If we say that the 10 novae within 2'.5 of the nucleus of M81 are the apparent bulge novae, we see that 2 of these novae are south of the major axis line (on the bottom) and 8 of these novae are north of it (on the top) giving a BTR of $2/8 = 0.25$. This BTR is much closer to the model for M31 from Hatano et al. (1997) with a bulge-to-disk nova ratio of 9 and clearly rules out the scenario with a bulge-to-disk nova ratio of 1/2. One thing we must consider is that our novae were discovered using Hα light, while the models of Hatano et al. (1997) were based on novae in M31 discovered in the B-band. Using the redder Hα light should reduce the effect of dust on the discovery rate of novae in the bulge. One would expect that, for the same bulge-to-disk nova ratio, the distribution in Hα light would be more symmetric, not less, than the distribution in the B-band. In addition, the fact that M81 is slightly more face on than M31 should also reduce the asymmetry, since a face on galaxy would show no asymmetry regardless of the bulge-to-disk nova ratio. The fact that our distribution is even more asymmetric than the M31 scenario with a bulge-to-disk nova ratio of nine argues for an even higher bulge-to-disk nova ratio in M81.

Unless the disk of M81 has a vastly different distribution of dust than the disk of M31, one must ask why Hatano et al. (1997) conclude that M31 has a bulge-to-disk nova ratio close to 1/2 while, using the same assumptions, we conclude that M81 has a bulge-to-disk nova ratio greater than 9. One possibility is that Hatano et al. (1997) used data from photographic surveys which have been shown to be incomplete in the inner regions of M31 (Ciardullo et al. 1987). Another problem, compared with our survey, is that M31 has never been surveyed comprehensively. Thus, calculations of the ratio of disk to bulge novae must account for differences in disk and bulge discovery rates from fundamentally different surveys, adding large uncertainties to the calculation. A uniform, comprehensive survey, such as presented here, removes these uncertainties.

The spatial distribution of the novae in M81 adds more weight to the idea that novae are associated with older stellar populations. It is important to continue to test this idea because, if verified beyond a doubt, it would strongly constrain the theory of how these objects form and evolve. We would have to consider that novae take much longer to form than previously thought and may not appear at all in young stellar populations.

3.10 Bulge versus Disk Novae

We can examine our novae sample in M81 to test the idea that bulge novae are preferentially fainter and slower than disk novae. della Valle & Livio (1998) found that for novae in the Milky Way, the bulge novae were spectroscopically distinct, having Fe II lines in the early emission spectrum, slower expansion velocities, and slower decline rates, while the disk novae had He and N lines, larger expansion velocities, and faster decline rates. Unfortunately, the two unambiguous disk novae reported here, Novae 3 and 10, were not covered well enough to determine their maximum

magnitudes, although their decline rates are toward the slow end of the distribution (see Table 3.4). The presence of Fe II lines in the spectrum of Nova 6 (Filippenko & Chornock 2003) implies that it could be one of the slow bulge novae. The decline rate for this nova is, however, the fastest one observed in M81 and argues that it may be one of the hybrid objects that evolve from showing Fe II lines to the faster He/N class and more properly be a member of the fast/bright novae class (della Valle & Livio 1998). Nova 6 is 1.'6 from the nucleus of M81 and could be either a disk or a bulge nova. These facts are suggestive, and illustrate the difficulty in testing this idea conclusively. Clearly we need more comprehensive light curves for both bulge and disk novae in order to provide a more definitive test.

3.11 Future Work

Adding to the database of complete Hα nova light curves will improve the accuracy of the nova rates derived with Monte Carlo simulations as the parent population becomes better sampled. Once we accumulate enough novae in both the bulge and the disk of M81, we will be able to perform a decomposition and derive an accurate bulge-to-disk nova ratio. If we have enough complete light curves, we should begin to detect the differences in the bulge and disk novae one would expect from the results of della Valle & Livio (1998). We will see if the asymmetry in the bulge novae across the major axis line persists. Adding continuum observations for the novae in the database will allow us to directly compare the maximum magnitude decline rate (MMDR) relation in M81 with the MMDR relation for M31 and determine a nova distance to M81. We will also be able to directly compare continuum and Hα rise times.

3.12 Conclusions

1. The raw nova rate for M81 provides a hard lower limit of 23 yr^{-1}. Using a set of representative nova Hα light curves in random outburst simulations we derive a completeness corrected nova rate of 30 yr^{-1}. Monte Carlo simulations using the same set of light curves provide our most reliable nova rate for M81 of 33^{+13}_{-8} yr^{-1}. The high nova rate found here for M81, with a survey technique that uses comprehensive time and spatial coverage, implies that the nova rates for other galaxies derived from surveys with incomplete spatial coverage and widely spaced epochs are, at best, rough values and may be serious underestimates.

2. The LSNR for M81 is $\rho_k = 3.96^{+1.8}_{-1.1}$ yr$^{-1}[10^{10}L_{\odot,K}]^{-1}$ using our best nova rate and the 2MASS K-band photometry for M81. This raises the LSNR for M81 by a factor of two from that published by Shafter, Ciardullo & Pritchet (2000), and implies that the LSNR for other galaxies could be systematically low by similar or greater amounts. A definitive comparison between galaxies of different Hubble type must await the results of comprehensive nova surveys such as that presented here.

3. The cumulative radial distribution of the novae matches the bulge light distribution significantly better than either the total or the disk light distribution, which is

ruled out at a 99% confidence level. The BTR value for M81 of 0.25 derived from the asymmetry in the spatial distribution of the apparent bulge novae across the major axis line implies a bulge-to-disk nova ratio for M81 of > 9, according to the models of Hatano et al. (1997) for novae in M31. Both these facts lead to an association of the novae in M81 with the older bulge stellar population, in sharp contradiction to the theoretical predictions of Yungelson, Livio & Tutukov (1997).

4. The disk novae reported here, Nova 3 and 10, have decline rates that place them in the slow class of novae, but their maximum magnitudes were not determined. Nova 6 is most likely a fast hybrid nova, is 1.'6 from the nucleus of M81, but cannot be unambiguously assigned to either the bulge or the disk. More comprehensive light curves of both bulge and disk novae are required to test for differences in their average maximum magnitudes and decline rates.

Chapter 4
A High Nova Rate for Two Local Group Dwarf Galaxies: M32 and NGC 205

4.1 Introduction

Extragalactic novae are potentially important as tracers of close binary stars in other galaxies. The brightness of the nova outburst (M_V of -6 to -10 at maximum) betrays their presence to beyond the Virgo cluster with current telescopes. By observing extragalactic novae it is possible to trace the frequency and distribution of the close binaries that produce them in many extragalactic environments, thus allowing an exploration of close binary populations and the factors that influence their formation.

One of the most basic investigations into these factors is to plot the normalized nova rate versus the luminosity of the host galaxy and see if any trend can be detected. Various versions of this plot have been produced over the years (della Valle et al. 1994; Shafter, Ciardullo & Pritchet 2000; Ferrarese, Côté & Jordán 2003), but systematic effects continue to dominate the published nova rates. We have found that nova rates are subject to biases that tend to underestimate the bulk rate for a given galaxy (Neill & Shara 2004a). Most severe of these biases is the one imposed by telescope scheduling, which, until recently, provided only short, widely spaced runs for sampling nova rates in external galaxies.

As noted in Chapter 3, we have attempted to overcome this bias by using a dedicated telescope to observe the target galaxy in its entirety, every clear night for many months. Our first survey of this type was of M81 (Neill & Shara 2004a) producing a bulk nova rate 40% higher than previous studies (Shafter, Ciardullo & Pritchet 2000). However, we also demonstrated the effects of dust in the disk on the detection of novae in the bulge, implying that our bulk rate could be low by as much as a factor of 2.

If one examines the plot of normalized nova rate versus galaxy luminosity, such as presented in the references above, it is clear that at the low luminosity end, there is much uncertainty. This is for obvious reasons. In particular, low luminosity systems produce few novae per year and so the sample is small. The low luminosity systems must be nearby and so often subtend very large solid angles on the sky and hence making it difficult to survey them in their entirety (e.g., M33, LMC, SMC).

We took advantage of the availability of telescope time on an hourly basis, provided by the Tenagra Observatory, to perform a comprehensive, nightly survey of four local group dwarf galaxies with the aim of refining the nova rates at the low end of the galaxy luminosity scale. We surveyed M32, NGC205, NGC147, and NGC185 for over four months, every clear night.

These surveys will continue for several years and will provide accurate nova rates for the low luminosity systems, allowing us to determine if there is indeed a trend

in nova rate with luminosity. In order to constrain binary formation and evolution theory, this kind of survey must be accompanied by comprehensive, densely time-sampled surveys of higher mass galaxies. Only by removing systematic biases can we determine if there is a universal nova rate per unit luminosity, or if the nova rate is influenced by the mass of the host galaxy.

4.2 Observations

We used the SITe based 1024x1024 pixel CCD camera on the Tenagra 0.8m telescope for our observations of the local group dwarfs. This configuration yields a pixel scale of 0".87 px^{-1} and a field size of 15' on a side, allowing us to cover each galaxy in its entirety for each epoch of observation.

The majority of the survey observations were taken through a standard Johnson V filter. This filter was chosen to maximize the sensitivity of the telescope and detector combination. Once a nova was discovered, we initiated additional observations through the standard Johnson B filter to derive nova colors. Each individual exposure was 300s, except for M32 which required a shorter exposure time of 150s to avoid saturating the nuclear region. We attempted to have 15 minutes total exposure time per epoch. Most epochs reached this goal, with only a few having less exposure time. The seeing for our observations had a median of 2".5 and ranged from 1".7 to 4".5.

Our survey ran from October 04, 2003 (JD 2452916.8) to February 18, 2004 (JD 2453053.6) covering a total of 136.8 days. Two novae were discovered; one in M32 and one in NGC 205. An additional epoch in the I-band was generously obtained for us by John Thorstensen using the Echelle direct CCD camera on the Hiltner 2.4m telescope. In addition, he was able to obtain two spectra using the Modspec on the 2.4m on JD 2453017.60 and two spectra on JD 2453022.60, allowing us to confirm the nature of the M32 nova. We were also fortunate that *HST* images were available in the archive of both nova positions[1]. For M32 Nova 1 we used WFPC2 images taken on JD 2449622 (proposal ID 5464, PI Rich). For NGC205 Nova 1 we used an ACS WFC image taken on JD 2452525 (proposal ID 9448, PI Ferrarese). We also used a 4m MOSAIC image from the NOAO science archive[2] taken on JD 2452528 (PI Massey). Table 4.1 summarizes all the observations presented in this paper.

4.3 Reductions

All Tenagra exposures were bias-subtracted and flat-fielded using the standard tools in IRAF (Tody 1986). The exposures for a given epoch (6 for M32, 3 for the

[1]This research uses observations made with the NASA/ESA Hubble Space Telescope, obtained from the data archive at the Space Telescope Science Institute. STScI is operated by the Association of Universities for Research in Astronomy, Inc. under NASA contract NAS 5-26555.

[2]This research draws upon data provided by Dr. Philip Massey as distributed by the NOAO Science Archive. NOAO is operated by the Association of Universities for Research in Astronomy (AURA), Inc. under a cooperative agreement with the National Science Foundation.

Table 4.1. Local Group dE Observations

Galaxy	Filter	Epochs (N)	Exp. (s)	Start (MJD)	End (MJD)	Span (days)	Novae (N)
			Tenagra 0.8m Observations				
M32	V	90	900	52916.83	53046.60	129.8	1
	B	14	900	53015.63	53037.64	···	
NGC205	V	89	900	52916.83	53053.60	136.8	1
	B	2	900	53047.61	53048.60	···	
NGC147	V	78	900	52927.73	53042.62	114.9	0
NGC185	V	84	900	52927.79	53045.62	117.8	0
			MDM 2.4m Observations				
M32	I	1	60	53014.70	···	···	1
	Spec	2	960	53017.6	53022.6	5.0	1
			HST WFPC2 Observations				
M32	F555W	1	1600	49622.9	···	···	0
	F814W	1	1200	49622.9	···	···	0
	F1042M	1	3000	49622.9	···	···	0
			KPNO 4m Observations				
M32	V	1	2400	52528.3	···	···	0
			HST ACS Observations				
NGC205	F606W	1	497	52525.8	···	···	0

others) were then registered and combined to produce a coadded image for each epoch using the following DAOPHOT programs (Stetson 1987): DAOPHOT to measure the point sources, DAOMATCH and DAOMASTER to derive and refine the transformations, and MONTAGE2 to perform the registration and coaddition. The registration master was chosen to be the best coadded image from the entire set for a given galaxy based on measurements of the seeing in each coadded image over the entire survey. The coaddition process removed all but a few cosmic rays.

The HST images were downloaded from the archive in reduced form. The only processing that was required was to coadd the images to remove cosmic rays. The images were already registered, so this task was easily achieved using the STSDAS wfpc2 combine task. The image from the NOAO science archive required no processing.

The spectra were extracted using the IRAF apsum task, wavelength- calibrated using calibration lamps and night sky lines, and flux- calibrated using flux standard

Table 4.2. Local Group dE Nova Positions

		Position (J2000)			Nuclear Distance
Galaxy	Nova	RA	Dec	Detections	(arcsec)
M32	1	00 42 44.991	+40 53 04.76	33	78.4
NGC205	1	00 40 15.212	+41 37 29.93	24	230.4

observations with the same configuration. The wavelengths are accurate to better than 1Å, but the fluxes are probably only good to about 20% due to unknown slit losses.

4.4 Nova Detection

The coadded Tenagra images were blinked against each other to detect changing point sources. Nova candidates were required to be observed in at least two epochs *and* to be missing on an epoch of sufficient depth coverage to confirm its transient nature. We also used the raw images for an epoch to confirm the presence of the candidate in each individual frame. As a further verification, we checked the images from the archives listed in Table 4.1, and images from the Digitized Sky Survey[3].

For the regions of our target galaxies near the nuclei where the intensity gradient makes detection more difficult, we used the spatial filtering technique described in Chapter 3 (Neill & Shara 2004a), allowing us to detect novae to within 10" of the nuclei of M32 and NGC205 and to within 2" of the nuclei of NGC147 and NGC185. This subtraction technique was performed on each coadded image after which they were blinked against each other. For each coadded image of each galaxy we determined the frame limit by using artificial stars and the exact techniques outlined above for detecting the novae.

Table 4.2 gives the positions and number of detections for the novae discovered in this survey. The nova in M32 was discovered first and is shown in outburst in Figure 4.1. The nova in NGC205 is shown in outburst in Figure 4.2.

[3]The Digitized Sky Survey was produced at the Space Telescope Science Institute under U.S. Government grant NAG W-2166. The images of these surveys are based on photographic data obtained using the Oschin Schmidt Telescope on Palomar Mountain and the UK Schmidt Telescope. The plates were processed into the present compressed digital form with the permission of these institutions.

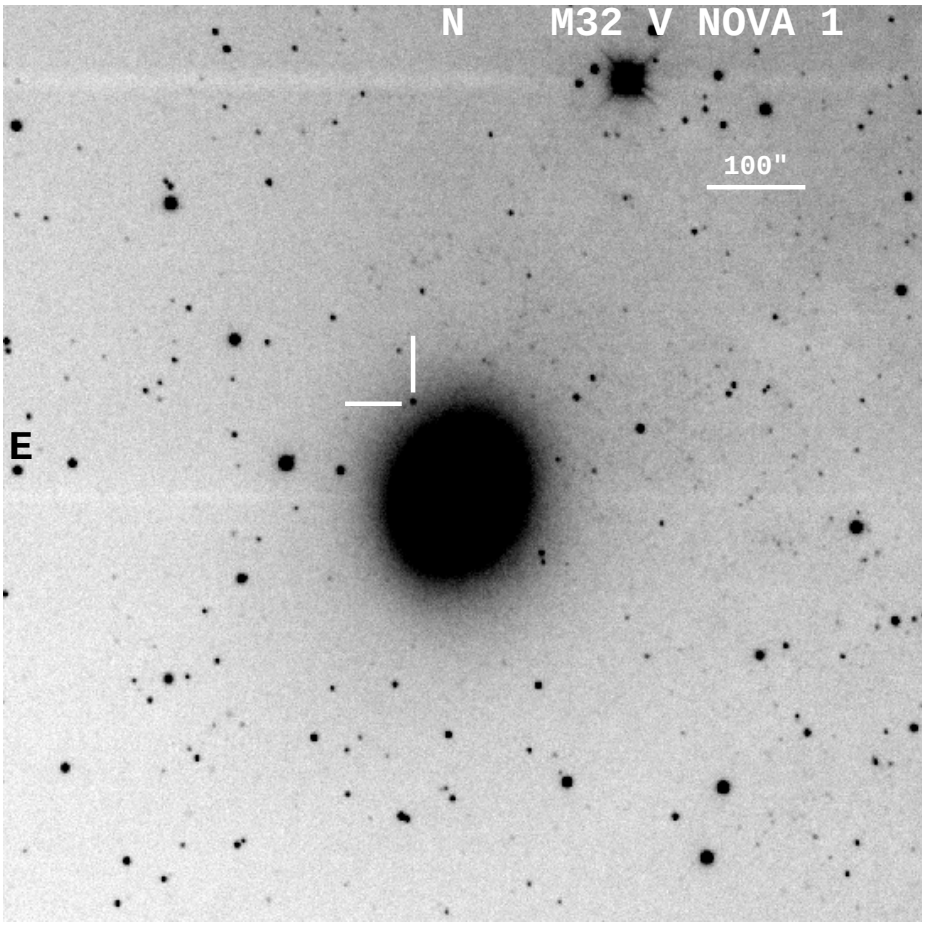

Figure 4.1: Tenagra V image of M32 Nova 1 on JD 2453009.62. North is up and East to the left. The nova is indicated by the two lines at right angles. A scale bar of 100 arcseconds is also shown.

4.5 Nova Photometry

Since crowding was not an issue, DAOPHOT aperture photometry was used to measure point source brightnesses in each coadded image. Variable seeing was accounted for by setting the measurement aperture radius in each image to 1/2 the FWHM of the stellar profile to maximize the signal-to-noise ratio. The FWHM was measured from a set of well exposed, isolated stars in each image.

Calibration required the use of a diverse set of references. For M32, we used the study of Magnier et al. (1992) which has BVRI CCD photometry for 361,281 objects in the field of M31 and also includes M32. For NGC205, the BVRI photometry published in Lee (1996) was used. NGC147 and NGC185 were both calibrated using V-band photometry presented in the study of Nowotny el al. (2003). These studies all made corrections for Galactic extinction. In all cases, the epoch with the best photometric conditions was calibrated using stars in common with the references above and then all other epochs were calibrated to the reference epoch. The number of objects used in the calibrations were as follows: over 100 for M32, 8 for NGC205, 21 for NGC147,

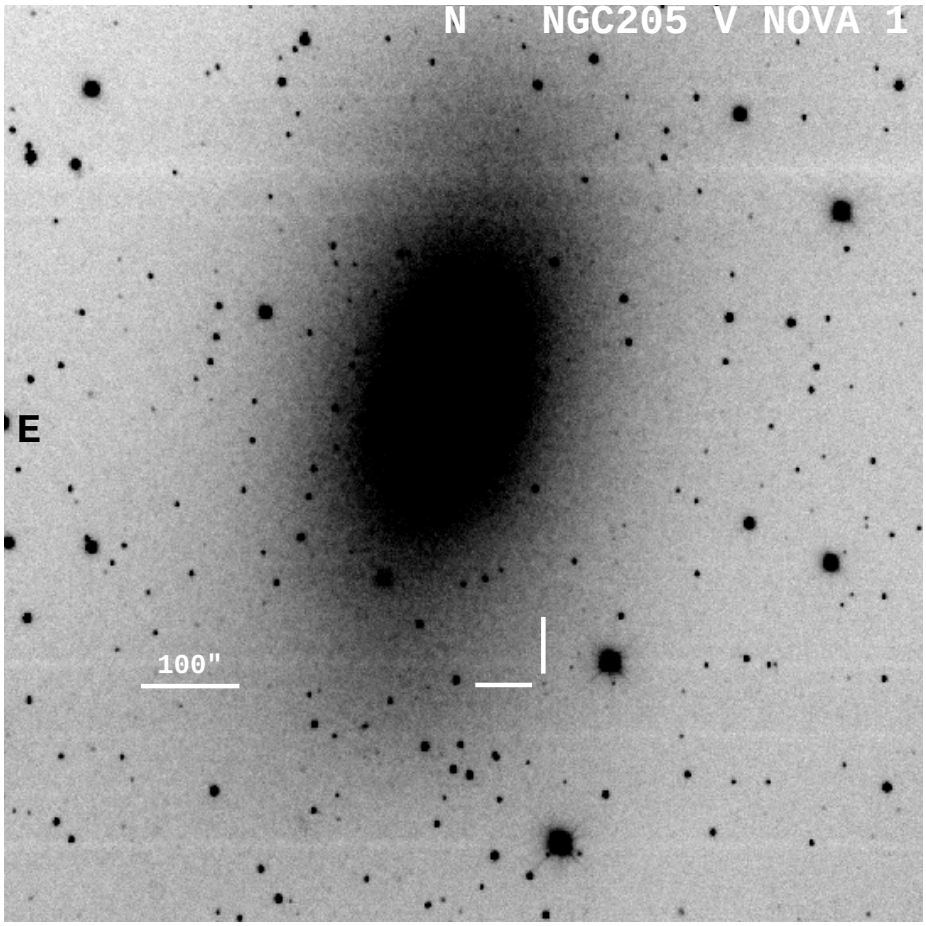

Figure 4.2: Tenagra V image of NGC205 Nova 1 on JD 2453017.64. North is up and East to the left. The nova is indicated by the two lines at right angles. A scale bar of 100 arcseconds is also shown.

and 19 for NGC185. In all cases we achieved a photometric calibration with a RMS error of 0.1 magnitude or less in all filters.

Table 4.3 and Table 4.4 present our calibrated photometry for both novae covering a range of epochs containing the outbursts. The errors presented are 1σ internal photometric errors.

4.6 The Light Curves

Figure 4.3 presents the calibrated light curve for M32 Nova 1, and Figure 4.4 presents the calibrated light curve for NGC205 Nova 1. The frame limits are plotted as short horizontal lines with downward pointing arrows, while the open points with error bars are the nova observations from Tables 4.3 and 4.4.

A simple linear fit was made to the decline portion of each light curve in V to calculate the decline rate in m_V day^{-1}. The thin lines in Figure 4.3 and Figure 4.4 show the resulting fits. Table 4.5 presents the properties of the nova light curves

Table 4.3. M32 Nova 1 Photometry

Nova	MJD	m_V	Err(m_V)	Fr. Limit m_V	MJD	m_B	Err(m_B)	MJD	m_I	Err(m_I)
M32 1	52998.62	···	···	20.96	···	···	···	···	···	···
	53000.65	···	···	20.59	···	···	···	···	···	···
	53001.63	···	···	20.50	···	···	···	···	···	···
	53002.61	···	···	20.50	···	···	···	···	···	···
	53009.62	17.28	0.08	20.21	···	···	···	···	···	···
	53010.62	17.40	0.08	19.28	···	···	···	···	···	···
	53011.62	17.43	0.07	20.54	···	···	···	···	···	···
	53013.62	17.45	0.08	20.63	···	···	···	···	···	···
	···	···	···	···	···	···	···	53014.70	17.30	0.02
	53015.62	17.63	0.10	19.90	53015.63	17.70	0.07	···	···	···
	53016.60	17.59	0.09	20.85	53016.62	17.72	0.06	···	···	···
	53017.60	17.80	0.12	20.97	53017.62	17.87	0.07	···	···	···
	53018.62	···	···	19.24	53018.64	18.50	0.19	···	···	···
	53020.60	18.13	0.15	20.44	53020.62	18.31	0.11	···	···	···
	53021.61	18.38	0.18	20.72	53021.63	18.56	0.11	···	···	···
	53022.60	18.19	0.18	20.88	53022.61	18.22	0.10	···	···	···
	53023.60	18.57	0.22	19.74	53023.61	18.69	0.18	···	···	···
	53031.61	18.77	0.26	19.84	53031.63	19.02	0.27	···	···	···
	53032.59	18.80	0.27	19.85	53032.60	19.05	0.24	···	···	···
	53033.60	···	···	18.80	···	···	···	···	···	···
	53034.59	18.85	0.39	19.34	···	···	···	···	···	···
	53035.59	18.91	0.34	19.61	···	···	···	···	···	···
	53037.61	19.19	0.56	19.12	···	···	···	···	···	···
	53038.59	19.55	0.58	19.44	···	···	···	···	···	···
	53042.60	19.25	0.52	19.66	···	···	···	···	···	···
	53043.60	19.35	0.54	20.74	···	···	···	···	···	···
	53044.60	19.27	0.53	20.71	···	···	···	···	···	···
	53045.60	19.32	0.47	20.86	···	···	···	···	···	···
	53046.60	19.27	0.54	20.81	···	···	···	···	···	···

Table 4.4. NGC205 Nova 1 Photometry

Nova	MJD	m_V[a]	Err(m_V)	Fr. Limit m_V	MJD	m_B	Err(m_B)
NGC205 1	52986.92	···	···	21.45	···	···	···
	52987.63	···	···	20.38	···	···	···
	52988.63	···	···	20.97	···	···	···
	52989.64	···	···	19.87	···	···	···
	52990.64	···	···	20.44	···	···	···
	52991.63	···	···	20.63	···	···	···
	52992.63	21.09	0.39	20.68	···	···	···
	52993.65	21.01	0.35	20.63	···	···	···
	52994.66	21.52	0.41	21.08	···	···	···
	52996.66	···	···	19.04	···	···	···
	52998.64	20.71	0.20	21.07	···	···	···
	53000.67	···	···	20.63	···	···	···
	53001.66	···	···	20.59	···	···	···
	53002.64	20.45	0.22	20.50	···	···	···
	53009.63	20.23	0.25	20.17	···	···	···
	53010.63	20.23	0.31	19.99	···	···	···
	53011.63	19.99	0.13	20.54	···	···	···
	53013.64	20.19	0.17	20.55	···	···	···
	53016.64	20.24	0.17	20.73	···	···	···
	53017.64	20.02	0.11	20.93	···	···	···
	53021.65	20.01	0.13	20.63	···	···	···
	53022.64	20.04	0.13	20.84	···	···	···
	53023.64	···	···	19.59	···	···	···
	53024.64	···	···	17.17	···	···	···
	53031.66	···	···	19.46	···	···	···
	53032.63	19.47	0.21	19.68	···	···	···
	53033.64	···	···	16.59	···	···	···
	53034.61	···	···	19.33	···	···	···
	53035.61	···	···	19.57	···	···	···
	53037.62	···	···	19.05	···	···	···
	53042.61	20.28	0.26	20.11	···	···	···
	53043.61	20.18	0.18	20.63	···	···	···
	53044.61	20.22	0.17	20.78	···	···	···
	53045.61	20.61	0.20	21.02	···	···	···
	53046.62	20.39	0.20	20.83	···	···	···
	···	···	···	···	53047.61	21.50	0.24
	···	···	···	···	53048.60	>21.10	0.21
	53049.60	20.54	0.23	20.97	···	···	···
	53050.60	···	···	19.26	···	···	···
	53051.60	20.39	0.18	21.06	···	···	···
	53052.60	20.50	0.23	20.68	···	···	···
	53053.60	20.52	0.20	20.96	···	···	···

including the rise time and decline rate for each nova. The minimum magnitudes were determined from *HST* observations (see §4.7).

We calculated the average B−V color of the novae over the time that they were observed in two colors and present the results in Table 4.5, column 5. For M32 Nova 1, we used the 9 epochs for which B and V were observed on the same night. This gave <B−V> = 0.14±0.08, which is typical of novae near maximum. Because of bad weather, and the faintness of NGC205 Nova 1, we were unable to get simultaneous B and V measurements. The color we report was derived by using the one B measurement on MJD 53047 and subtracting the average of the two V points on MJD 53046 and MJD 53049. The resulting color for NGC205 Nova 1 is redder than a typical nova

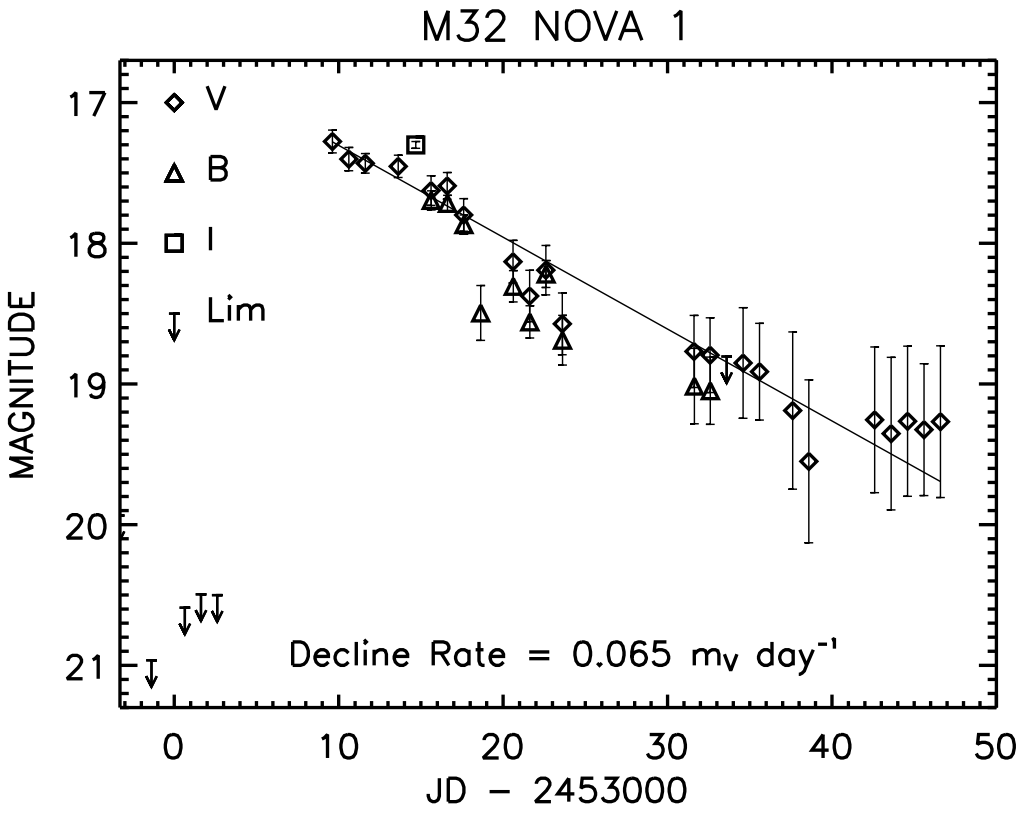

Figure 4.3: Light curve of M32 Nova 1 in V, B, and I-bands. V-band points are indicated by diamonds, B-band by triangles, and the I-band point by the square. Frame limits are indicated by the short line with a downward pointing arrow. The decline rate of 0.065 m_V day^{-1} was determined from an error-weighted linear fit (shown by the thin line) to the V-band points.

(<B−V> = 1.04±0.15), but this could easily be due to short timescale fluctuations during the decline phase.

The light curve of NGC205 Nova 1 has a few unusual features. It has a long rise time, and it never reaches an intrinsic luminosity greater than $M_V = -5.1$. This is possibly the lowest luminosity nova ever observed. We would claim the record for certain, but for an unfortunate gap in coverage leading up to the maximum where higher luminosities may have occured. From the measured decay rate we calculate the time taken to drop 3 magnitudes, t_3, to be 65 days. Using the maximum magnitude-decline rate relation, equation 19 from Shara (1981),

$$M_B = -10.1 + 1.57 \log t_3, \tag{4.1}$$

we calculate $M_B = -7.25$, over 2 magnitudes brighter than the peak for NGC205 Nova 1. Assuming the nova is at the Eddington luminosity at peak light, we can

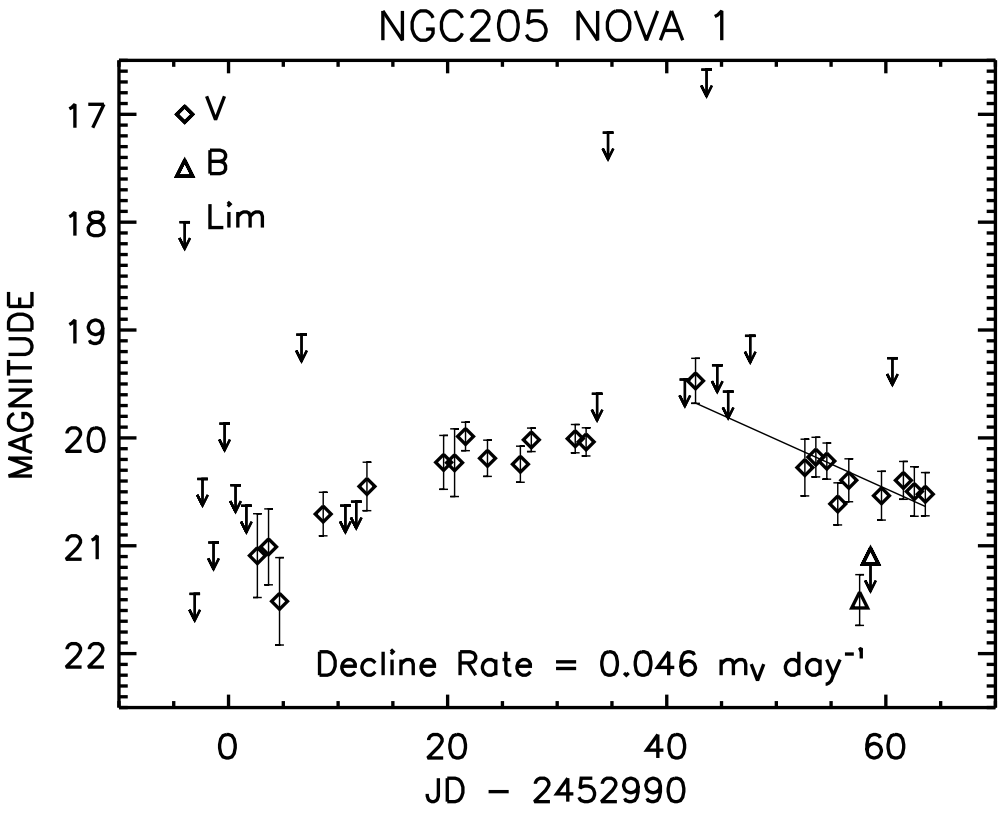

Figure 4.4: Light curve of NGC205 Nova 1 in V and B-bands. V-band points are indicated by diamonds, and B-band by triangles. Frame limits are indicated by the short line with a downward pointing arrow. The decline rate of 0.046 m_V day^{-1} was determined from an error-weighted linear fit (shown by the thin line) to the V-band points after maximum.

estimate the mass of the WD primary using equation 5.15b of Warner (1995),

$$\frac{L(max)}{L_\odot} = 3.0 \times 10^5 \frac{M_1^4(1)}{1+X}, \tag{4.2}$$

with X being the hydrogen abundance ratio, and $M_1(1)$ being the mass of the primary WD in $M_\odot$. Assuming $X = 0.5$, we calculate $M_1(1) = 0.46$. Currently published models of nova outbursts only include WDs down to $0.65M_\odot$ (Prialnik & Kovetz 1995). Models down to $0.4M_\odot$ have been calculated and do show outbursts consistent with that of NGC205 Nova 1 (Shara 2004). These factors prompted us to search the archives to attempt to constrain the progenitor of this nova, and M32 Nova 1.

Table 4.5. Nova Light Curve Properties

							Decline		
Nova	Max (m_V)	Min[a] (m_V)	Ampl. (m_V)	<B−V>	Baseline (days)	Rise Time (days)	Baseline (days)	Pts (N)	Rate (m_V day^{-1})
M32 1	< 17.3	> 26.0	> 8.7	0.14±0.08	37	< 6	37	22	0.065
NGC205 1	19.5	> 27.0	> 7.5	1.04±0.15	61	> 40	21	10	0.046

[a]Derived from archival *HST* observations, see §4.7

4.7 Verifying the Novae

In order to have confidence in our derived nova rates for these galaxies, it is crucial that we be sure that the objects we discovered are indeed novae and not some other kind of variable. Spectroscopy is the best way to verify a nova because of the telltale broad H emission lines. Another way is to place some limits on the amplitude of the outburst.

4.7.1 Verifying M32 Nova 1

Our spectral observations of M32 Nova 1 confirm that it is indeed a nova. They show broad Hα and Hβ in emission with a velocity of expansion of 640 km s^{-1}, typical of a slow classical novae. Figure 4.5 shows the spectrum taken on JD 2453017.60, roughly ten days after maximum. Emission lines of Fe II can be seen just red-ward of Hβ which is also consistent with it being a typical slow nova. The spectra taken five days later is nearly identical, an indication of the slow spectral evolution of this nova.

Because M32 is superposed on the outer disk of the larger M31, we also wanted to confirm that this nova did not originate in M31. We measured the systemic heliocentric radial velocity of the nova from the Hα lines and found it to have a velocity of -170 ± 6 km s^{-1}. This is consistent with the radial velocity of M32 (-200 ± 6 km s^{-1}, Sandage & Tammann 1981), if we account for the velocity dispersion of M32 at a radius of 78". The radial velocity of M31 is -297 ± 1 km s^{-1} (Sandage & Tammann 1981). The part of M31's disk upon which M32 is superposed is where most of the disk's rotation velocity would be transverse to the line of sight and therefore could not make up the difference in velocity between M31 and the nova. This, combined with the proximity of the nova to the nucleus of M32, argues against it originating in M31.

In addition to these spectral confirmations, we also put a limit on the nova outburst amplitude. To do this, we used the *HST* WFPC2 observations in V (F555W) taken nearly a decade prior to outburst. We also used the I (F814W) and F1042M images to verify that the progenitor was not a bright red variable. The nova position in all these filters was in the WFPC2 chip WF3.

There were not enough stars in common with our Tenagra observations to allow the precise determination of the position of the nova in the WF3 images directly. We solved this by using the 4m 8k MOSAIC image from the NOAO archive which went deep enough to pick up a significant number of stars from the WF3 images. First, we registered the MOSAIC image to the WF3 image using 17 stars in common with the IRAF geomap task. This produced a transformation fit with a root mean square (RMS) of 1.0 WF3 pixels. We refined this transformation locally, in the region of the nova, in the following way. We registered the MOSAIC image to the WF3 image using the above transformation. We then extracted a small subimage surrounding the position of the nova (75x87 WF3 pixels) in the transformed MOSAIC image and the WF3 image. The WF3 subimage was convolved with a Gaussian to match the point spread function (PSF) of the MOSAIC image. These two images were then cross

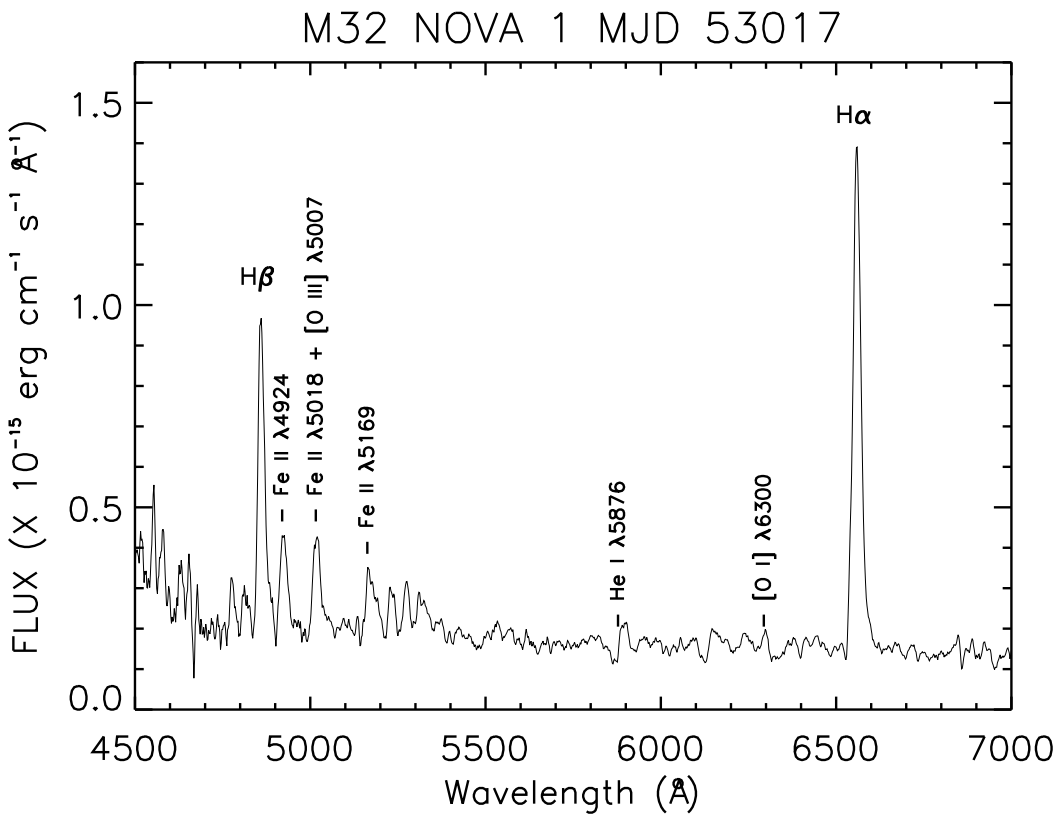

Figure 4.5: Spectrum of M32 Nova 1 taken on JD 2453017.60, 8 days after discovery. The broad H emission lines confirm it as a classical nova. The Hα line has a half width at half intensity of 640 km s^{-1}, at the low end of the velocity range (typically 300 to 3000 km s^{-1}) for classical novae. The strength of the Fe II lines and the weakness or absence of the He and N lines is consistent with the slow nova classification. A spectrum taken on JD 2453022.60, 5 days later, is nearly identical to the spectrum presented here, illustrating the slow spectral evolution of this nova. Note that the He I line (λ5876) has a P Cygni profile and the Hα line also shows a hint of absorption on the blue side.

correlated to detect any offset. An offset in x of 0.35 px, and in y of -0.70 px, was detected with an accuracy of 0.05 WF3 pixels, which improved the transformation locally by at least a factor of ten.

We then produced a transformation from each of 14 Tenagra images (with the nova well observed) to the MOSAIC image using over 400 stars in common. This produced transformations with a typical RMS of less than 0.01 MOSAIC pixels. We used the same cross-correlation technique described above but were unable to detect any local offset in these transformations. We transformed the nova positions to the MOSAIC coordinate system and then used the MOSAIC to WF3 transformation, plus the detected offsets, to put the nova positions in the WF3 coordinate system to better than 0.1 WF3 pixels. We then used an error-weighted average of the 14 positions to get a final position in the WF3 images. This position had an RMS of

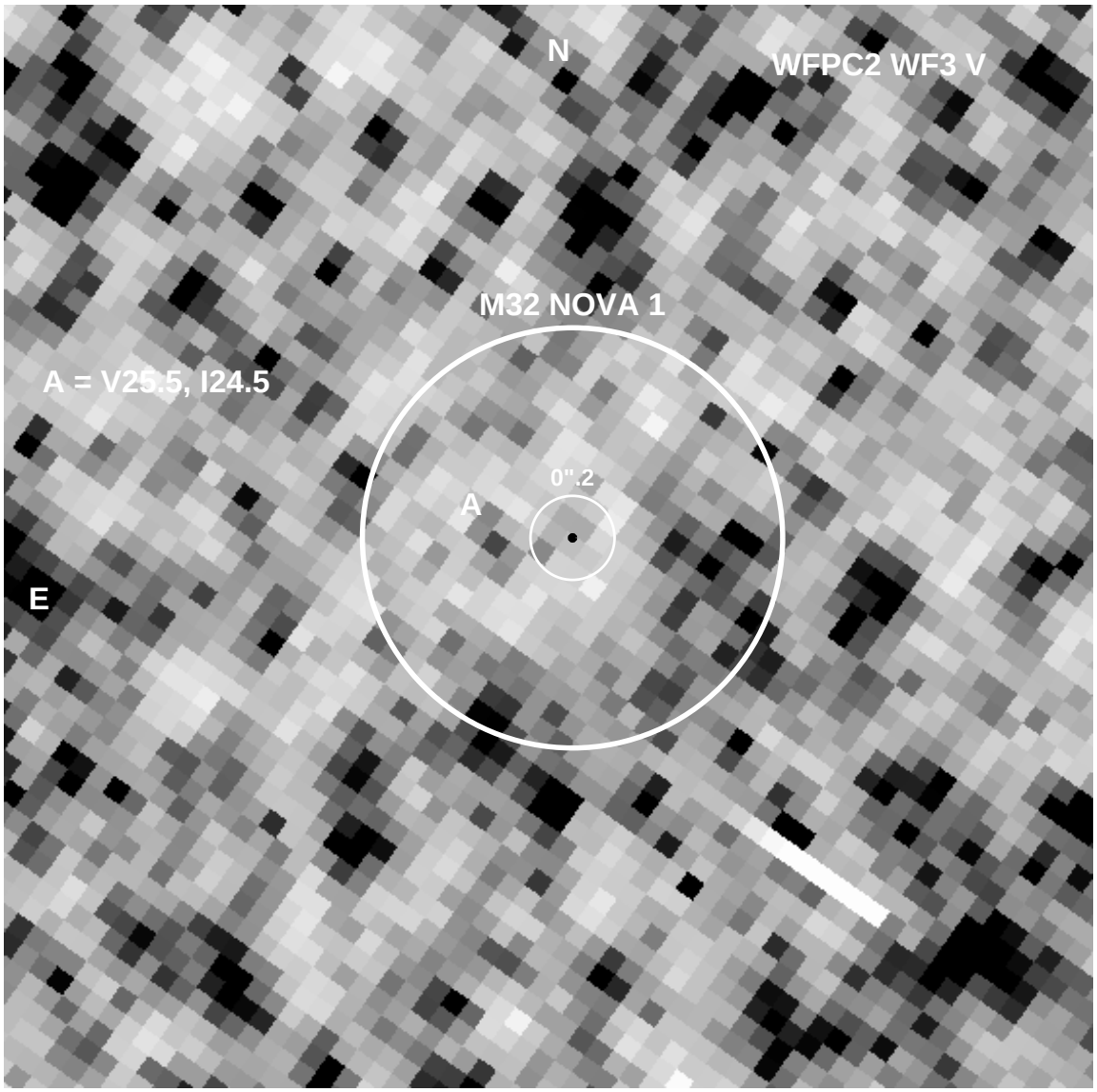

Figure 4.6: *HST* WFPC2 WF3 V-band image of the region around M32 Nova 1 taken on JD 2449622.62. North is up and East to the left. The circles are centered on the position of M32 Nova 1. The larger circle has a radius of 1" and the smaller a radius of 0".2. The positional error of M32 Nova 1 is 0.1 WF pixels or 0".01 and is represented as the black dot at the center of the figure. Star A has a V magnitude of 25.5, but is well outside the 1σ error circle of M32 Nova 1. The progenitor of M32 Nova 1 is fainter than V of 26.0, implying an outburst amplitude of over 8.7 V magnitudes.

0.04 WF3 pixels.

Figure 4.6 shows the region in the WF3 V image surrounding the nova, with a field of view of 3 arcseconds on a side. We do not convincingly detect the progenitor of M32 Nova 1. The star indicated by the letter A is at V of 25.5 and I of 24.5, but is well outside the position error circle defined by the RMS of the nova positions. We estimate that the progenitor of this nova was fainter than V of 26.0 at the epoch that

these data were taken. This gives an amplitude of at least 8.7 magnitudes in V for the nova outburst. The WFPC2 I and F1042M images were well registered with the V image and nothing was detected in them at the position of the nova. We conclude, therefore, that M32 Nova 1 could not be a bright red variable and is, indeed, a nova.

4.7.2 Verifying NGC205 Nova 1

This nova presented more of a challenge. Its faintness precluded spectral observations with the MDM 2.4m. In this case, the *HST* observations were crucial to confirm that it was a nova. We were fortunate that the ACS WFC observations of this area included 14 to 18 stars that could be used to directly register the Tenagra images. We chose 5 of these images in which the nova was well observed to register to the ACS image. Each of the 5 transformations had an RMS of 1 ACS pixel. We used these transformations to place the nova in the ACS WFC image. We then calculated the error-weighted average position for the nova ACS position which had an RMS of 0.64 ACS pixels. To check for local offsets we used two stars within 25" of the nova that were visible in both the Tenagra and the ACS image. We checked the transformed positions of these stars and computed their error weighted average position, which also had an RMS of 0.64 ACS pixels (0".032). These average positions showed no local offset with respect to the ACS to within 0.5 ACS pixels (0".025).

Figure 4.7 shows the position of the nova in the ACS WFC V (F606W) image, with a 3 arcsecond field of view. The small circle shows the 5σ error circle for the nova position. No star is within this circle, but the stars close by are marked on the figure with their magnitudes given in the upper left corner. This bolsters our claim that the object was indeed a nova and not some other kind of bright variable star. We estimate that the progenitor of the nova was fainter than V of 27.0 on the epoch of observation. This gives an amplitude of at least 7.5 magnitudes in V for the outburst. This fact, combined with its observed light curve, argues against any classification other than a very slow classical nova.

4.8 The Nova Rate

Confident that our two objects are indeed novae, we can derive a bulk nova rate and then calculate the luminosity specific nova rate (LSNR) for each galaxy. A raw bulk nova rate for each galaxy can be obtained simply by dividing the observed number of novae that erupted during the survey by the time covered. This gives $R = 1/0.355\text{yr} = 2.82 \pm 1.68$ yr^{-1} for M32 and $R = 1/0.375\text{yr} = 2.67 \pm 1.63$ yr^{-1} for NGC205. For NGC147 and NGC185 we can place a limit on the nova rate by saying that it is no greater than the inverse of the survey time. For NGC147 this gives $R < 1/0.315\text{yr} = 3.18 \pm 1.78$ yr^{-1} and for NGC185 this gives $R < 1/0.323\text{yr} = 3.10 \pm 1.76$ yr^{-1}.

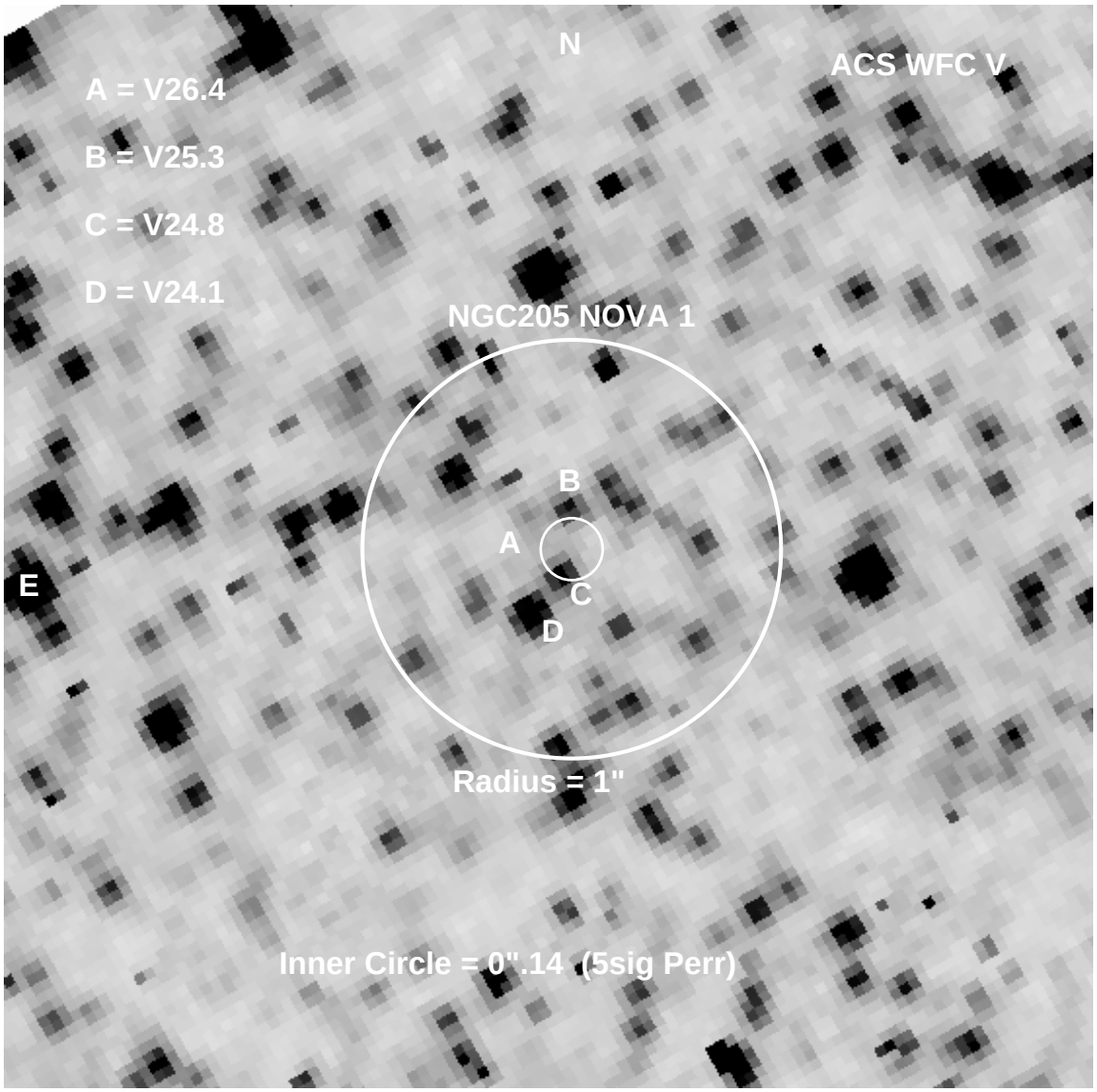

Figure 4.7: *HST* ACS WFC V-band image of the region around NGC205 Nova 1 taken on JD 2452525.83. North is up and East to the left. The circles are centered on the position of NGC205 Nova 1. The larger circle has a radius of 1" and the smaller a radius of 0".14, five times the positional error of NGC205 Nova 1. Star A has a V magnitude of 26.4, B a V magnitude of 25.3, C a V magnitude of 24.8, and D a V magnitude of 24.1. All are well outside the 1σ error circle of the Nova. The progenitor of NGC205 Nova 1 is fainter than V of 27, implying an outburst amplitude of greater than 7.5 V magnitudes.

4.8.1 The Monte Carlo Rate

We used the V-band maximum magnitudes and decline rates reported in Arp (1956) and Rosino (1973), combined with our individual epoch frame limits, to perform a Monte Carlo experiment as described in Chapter 3 to derive more robust nova

rates for each galaxy we observed. Figure 4.8 shows the probability distributions for each galaxy. The differences in the distributions are primarily due to the fact that one nova each was found in M32 and NGC205 and no novae were found in NGC147 and NGC185. Differences between distributions with the same number of discovered novae arise because of differences in the distribution and depths of the individual epochs for each galaxy surveyed.

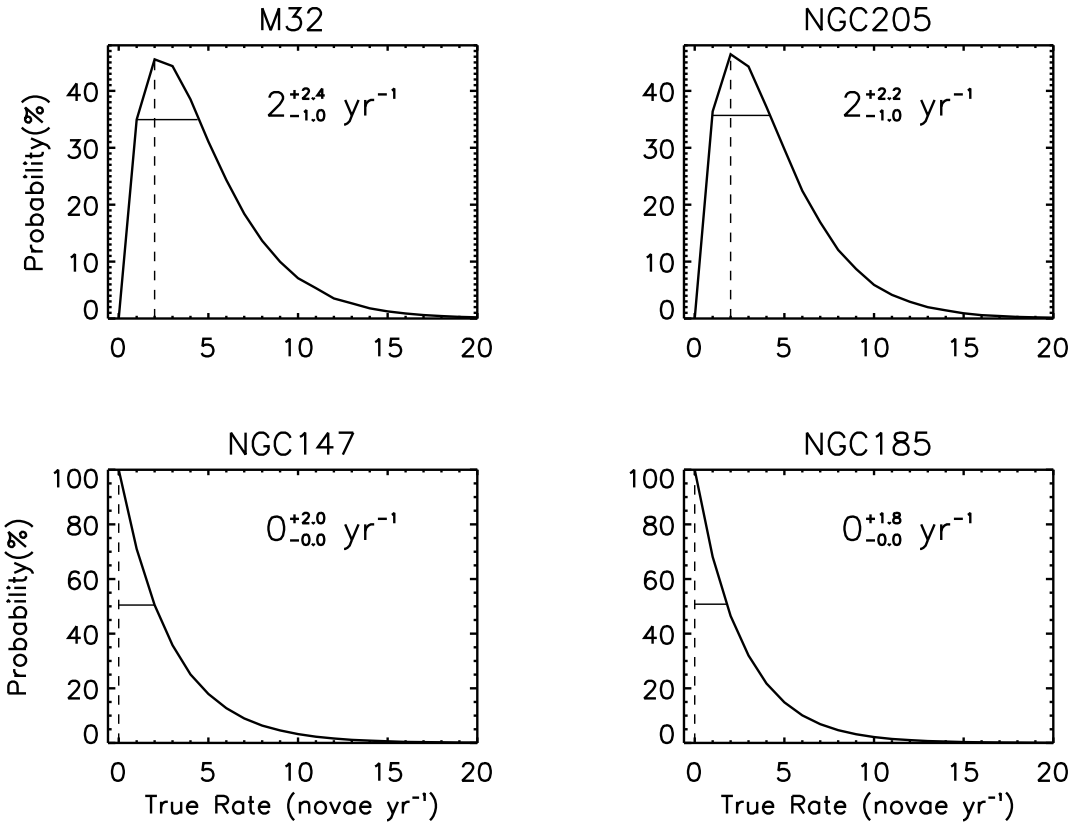

Figure 4.8: Probability distributions from Monte Carlo simulations of the true nova rates in M32, NGC205, NGC147, and NGC185, based on individual epoch frame limits and well observed V-band nova maximum magnitudes and decline rates (Arp 1956; Rosino 1973). The observed number of novae for M32 and NGC205 were one each, while no novae were discovered in NGC147, and NGC185 during our survey. The total bulk nova rate for the combined four systems is $4^{+4.2}_{-1.4}$ novae yr^{-1}.

Column 2 of Table 4.6 presents the results of the simulations for each of the galaxies. Total values for all the local group dwarf ellipticals surveyed are presented at the bottom of the table.

4.8.2 The Luminosity Specific Nova Rate

To facilitate the comparison of nova rates across a broad range of galaxy luminosities, a suitable normalization must be found. The infrared is used as a measure of stel-

Table 4.6. Nova Rates

Galaxy	Bulk Nova Rate[a] (yr^{-1})	$V_{T,0}$[b] (mag)	$(V - K)_0$[c] (mag)	$K_{V,(V-K)}$ (mag)	$K_{2MASS,0}$[d] (mag)	$(m-M)_0$[e] (mag)	L_K ($10^{10} L_{\odot,K}$)	LSNR ($yr^{-1}[10^{10} L_{\odot,K}]^{-1}$)
M81	33^{+13}_{-8}	6.57	3.17±0.1	3.40±0.1	3.802±0.018	27.80±0.08	12.4±1.5	$2.6^{+1.0}_{-0.6}$
M32	$2^{+2.4}_{-1.0}$	7.84	3.13±0.1	4.71±0.1	5.072±0.017	24.43±0.1	0.167±0.023	$12.0^{+14.4}_{-6.0}$
NGC205	$2^{+2.2}_{-1.0}$	7.97	2.12±0.2	5.85±0.2	5.564±0.045	24.60±0.3	0.0682±0.0267	$29.3^{+32.3}_{-14.7}$
NGC147	$0^{+2.0}_{-0.0}$	8.93	···	6.9±0.2[f]	7.137±0.063	24.39±0.05	0.0224±0.0047	< 89
NGC185	$0^{+1.8}_{-0.0}$	8.55	···	6.3±0.2[f]	6.495±0.051	23.96±0.21	0.0269±0.0082	< 67
LGdEs	$4^{+4.2}_{-1.4}$	···	···	···	···	···	0.284±0.036	$14.1^{+14.8}_{-4.9}$

[a]Nova rate references: M81 - Neill & Shara (2004a), others - this study

[b]from de Vaucouleurs et al. (1991)

[c]Color references: M81 - Aaronson (1978), others - Frogel et al. (1978)

[d]from Jarrett et al. (2003), but corrected for reddening using the formula $A(K) \simeq 0.085A(B)$ from Schlegel, Finkbeiner & Davis (1998) with A(B) values from de Vaucouleurs et al. (1991)

[e]Distance references: M81 - Freedman et al. (2001), M32 - Grillmair et al. (1996), NGC205 - Lee (1996), NGC147 - Han et al. (1997), and NGC185 - Lee, Freedman & Madore (1993)

[f]Estimated from $K_{2MASS,0}$ and subtracting the 0.2 systematic offset found by Ferrarese, Côté & Jordán (2003)

lar mass to avoid large fluctuations due to a few bright blue stars. While 2MASS offers a consistent photometric system for this normalization, Ferrarese, Côté & Jordán (2003) found discrepancies between the K-band magnitudes from the 2MASS Large Galaxy Atlas (Jarrett et al. 2003) and those derived from integrated optical magnitudes and optical-to-infrared colors. We chose to use the integrated, extinction corrected V-band magnitudes from de Vaucouleurs et al. (1991) and $(V-K)_0$ colors from Aaronson (1978) and Frogel et al. (1978) to perform our normalization.

Table 4.6 lists the relevant data and references for M81 and the four dwarf ellipticals of this study. We included the 2MASS K-band magnitudes[4], after correcting for Galactic extinction, to compare with the K-band magnitudes derived from the optical magnitudes and colors. The difference is +0.36 magnitudes for M32 and −0.29 for NGC205, illustrating the discrepancy. No $(V-K)_0$ colors were available for NGC147 and NGC185, so we adjusted $K_{2MASS,0}$ by the 0.2 magnitude systematic offset between the two systems found by Ferrarese, Côté & Jordán (2003). To arrive at the LSNR, the bulk nova rates are divided by the K-band luminosities, expressed in $10^{10} L_{\odot,K}$.

We plot our results, and the result for M81 from Neill & Shara (2004a) (see Chapter 3), as open diamonds in Figure 4.9 along with data from Ferrarese, Côté & Jordán (2003), Table 5, plotted as small filled circles. The two discrepant points for M33 are connected with a dotted line. The horizontal dashed line is the average LSNR from Ferrarese, Côté & Jordán (2003).

It is clear that the nova rate in the Local Group dwarf ellipticals is higher than one would expect. If we take the LSNR for M81 in Table 4.6 and apply this to the galaxies studied here, we would expect to detect less than one (0.7) nova yr^{-1} total, in all four galaxies. Instead, we observed two novae in just over four months. We can interpret this in two ways. First, it could be an indication of a higher interacting binary fraction in the dwarf ellipticals and hence a higher nova rate. Another likely explanation stems from the fact that these elliptical systems are small, nearby, and nearly dust free. The incompleteness in these systems, as a result, is likely to be very small. It could be that we are missing the faintest, slowest novae in more distant systems both because current datasets do not go faint enough and as a result of incompleteness caused by dust and steep intensity gradients in the nuclear regions of these galaxies.

4.9 Future Work

It is important to improve the statistics for these low-mass, nearby systems. We will continue to monitor M32, NGC205, NGC147, and NGC185 for several years. We are currently monitoring the LMC and will also survey NGC6822, another low-mass member of the Local Group.

[4]This publication makes use of data products from the Two Micron All Sky Survey, which is a joint project of the University of Massachusetts and the Infrared Processing and Analysis Center/California Institute of Technology, funded by the National Aeronautics and Space Administration and the National Science Foundation.

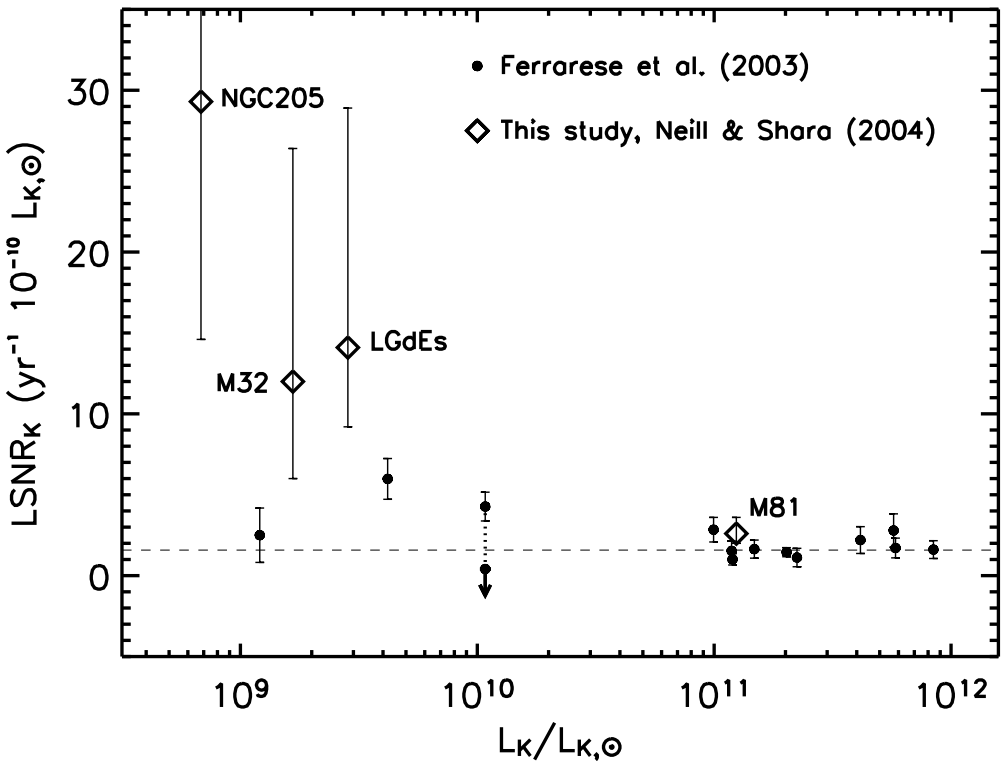

Figure 4.9: LSNR versus K-band luminosity in Solar units. The small filled circles are from data in Ferrarese, Côté & Jordán (2003). As in their Figure 18, the dotted line connects the two (discrepant) values for M33. The large open diamonds are the results from Neill & Shara (2004a) and Table 4.6 of this work. The dashed line is the constant LSNR derived in Ferrarese, Côté & Jordán (2003).

Eliminating systematic errors in bulk nova rates is essential to using the LSNR vs. luminosity diagram to determine the factors that influence the formation and evolution of the close, interacting binaries that produce novae. With large-format cameras and the availability of service telescope time on a nightly basis, we can determine precise nova rates and distributions for these nearby small systems. We must also complement this with the best rates and distributions possible for larger, more distant systems. If the low luminosity nova we discovered in NGC205 represents a new nova population, we must be sure to sample this population in nova surveys of the larger, more distant systems. This will be observationally expensive.

4.10 Conclusions

1. Using the Monte Carlo technique we derive a bulk nova rate for M32 of $2^{+2.4}_{-1.0}$ yr^{-1} and for NGC205 of $2^{+2.2}_{-1.0}$ yr^{-1}. These bulk nova rates are much higher than predicted by extrapolating a constant LSNR determined at high luminosities to low

luminosities.

2. Using $V_{T,0}$ magnitudes and $(V-K)_0$ colors to derive K-band luminosities to normalize these rates produces an LSNR for M32 of $12.0^{+14.4}_{-6.0}$ $yr^{-1}[10^{10}L_{\odot,K}]^{-1}$, and for NGC205 of $29.3^{+32.3}_{-14.7}$ $yr^{-1}[10^{10}L_{\odot,K}]^{-1}$.

3. The nova we discovered in NGC205 may be the lowest luminosity nova ever seen. It is possible this nova represents a population of low-luminosity, low-mass WD novae with $M_V \sim$ -5.0. The implication is that faint novae are being missed in surveys of more distant, larger, and dustier systems producing a systematic underestimate of the nova rates in these systems.

Chapter 5
A Preliminary Survey for Novae In and Between Galaxies in the Fornax Cluster

5.1 Introduction

We now extend our investigation of CVs in different environments to the region in and between the galaxies of the Fornax cluster. We have shown that comprehensive, densely time-sampled surveys will provide a significant advance in our understanding of how novae relate to their underlying stellar population (Neill & Shara 2004a). It is worthwhile at this point to take the preliminary results from our own nova surveys and attempt to to trace the stellar light between galaxies in Fornax.

What can we hope to learn? As an independent check on highly uncertain direct measures of intra-cluster light, we can verify the amount of stellar tidal debris in the cluster. This then places constraints on the importance of tidal stripping in the formation and evolution of galaxy clusters. Our nova results indicate that novae are associated with the older, bulge populations in galaxies. We can use this to attempt to discern the predominant source of the ICL either in bulge- dominated or disk-dominated galaxies.

Another lesson we have learned from our nova studies is that accurate rates and distributions can only be derived from comprehensive, densely time-sampled surveys. Our data set is diverse and very sparsely sampled. We therefore restrict our investigation to a relative comparison of galaxy versus inter-galaxy novae. Our aim is to prove the feasibility of using novae to perform an accurate assessment of the ICL amount and origin.

We have acquired six epochs of survey data of the central 30' square of the Fornax Cluster. Fornax is nearby and has a fairly high surface density of galaxies in the core, increasing the likelihood of tidal stripping. At the distance of Fornax, $(m - M)_0 = 31.35$ (Kissler-Patig et al. 1999), novae will have an average m_B(peak) ~ 23.35 (the brightest novae will have peak brightnesses of $m_B = 21.35$), and are easily detectable. Novae have been observed by Pritchet & van den Bergh (1987) in Virgo cluster galaxies, which are at the same distance as Fornax.

Novae are very bright in Hα (B $-$ Hα $\sim$ 0.5 when the nova erupts, and B $-$ Hα $\sim$ 3 shortly thereafter). Furthermore, novae remain bright in Hα for an extended period of time (months), providing a useful means of discovering them. To a limiting magnitude of $M_{H\alpha}$ = -7.5 ($m_{H\alpha}$ = 23.85 at Fornax) the mean Hα visibility lifetime is 3 months (Ciardullo et al. 1990a). Assuming a nova rate of 24 yr^{-1} per 10^{10} $L_\odot$(B) (Ciardullo et al. 1990b), a luminosity in galaxies of $M_B \sim -22.5$ in the core of Fornax (Ferguson 1989), and a visibility lifetime in Hα of 3 months, we calculate that at any given epoch there should be $\sim$ 100 novae in eruption (with visible Hα emission) in galaxies in the central 1 deg^2 of the Fornax cluster. Since we are surveying the central 1/2 deg^2 we multiply this estimate by 1/4 and predict we will see 25 novae in any

given epoch.

5.2 Observations

The observations that went into this study are a diverse set acquired over the span of more than a decade. The central 30' of Fornax, centered on RA 03:38:13.72, Dec -35:32:52.2 (J2000), was surveyed. This area includes the central dominant (cD) galaxy NGC 1399 and three other elliptical galaxies: NGC 1404, NGC 1387, and NGC 1389. This region was imaged twice in 1993, once in 1995, for five nights in 1999, and once each in 2003 and 2004. The data were acquired during programs for other projects and during engineering time or director's discretionary time. These observations are summarized in Table 5.1.

Because of the long-term nature of the data acquisition, there was no uniform observing strategy employed. We started with the Tek2048 camera, and when the MOSAIC II camera became available (before the 1999 run), we switched to that camera for the remaining epochs. We used primarily standard Johnson B- and R-band filters and narrow-band Hα filters, but for two epochs (b and c, see below) we were constrained to using a T1 filter. Exposure times were restricted by the gaps available in the schedule for other programs. Most of the data were acquired using the CTIO 4m telescope with the exception being the b and c epochs which were acquired with the 1.5m at CTIO.

The data acquired in 1993 and 1995 were taken with the Tek2048 chip. The focal ratios of the 4m and the 1.5m are such that they produce an identical pixel scale for these images of 0".43 per pixel. The resulting field of view is 14'.7 and thus required four pointings to cover the central 30' of the cluster. Sky flats were acquired in each filter to remove the instrumental response.

The data acquired in 1999, 2003, and 2004 were taken with the MOSAIC II camera on the 4m telescope. This camera is a mosaic of eight 2048x4096 pixel CCDs with a pixel scale of 0".27 per pixel. The resulting field of view is 36'.8 and thus only required one pointing. Sky flats were used to remove the instrumental response for the 1999 epochs, and dome flats were used for the 2003 and 2004 epochs.

All data were reduced using the standard tools in IRAF (Tody 1986) or the **mscred** external IRAF package developed by the NOAO MOSAIC instrument team.

5.3 Nova Detection

Because of the diversity of the data sets, several nova detection methods were used. The primary method consisted of performing a spatial registration of the different epochs, and then blinking them against each other. The images were zoomed by a factor of two for the blinking to facilitate detection of faint novae. We required that any candidate nova be visible on each of the individual exposures for the epoch in which it was detected. This eliminated cosmic ray hits from our candidate list. This method worked well for novae outside of the galaxies. For novae in the galaxies,

Table 5.1. Fornax Cluster Observations

Epoch ID	Date	Telescope	Detector	Filter	Exptime
a	NOV-1993	4m-CTIO	Tek2048	B	900s
	"	"	"	T1	900s
	"	"	"	Hα	4500s
b	DEC-1993	1.5m-CTIO	Tek2048	T1	5400s
c	OCT-1995	1.5m-CTIO	Tek2048	T1	9000s
d	05-DEC-1999	4m-CTIO	Mosaic 8K	B	4200s
e	07-DEC-1999	"	"	R	1260s
	"	"	"	Hα	7200s
f	08-DEC-1999	"	"	B	4200s
g	11-DEC-1999	"	"	R	1260s
	"	"	"	Hα	1800s
	"	"	"	B	1800s
h	12-DEC-1999	"	"	R	1260s
	"	"	"	Hα	3600s
	"	"	"	B	3000s
i	27-FEB-2003	4m-CTIO	Mosaic 8K	Hα	6000s
j	14-JAN-2004	4m-CTIO	Mosaic 8K	B	8100s

we employed the spatial median filter technique described in §3.4 with a box size of 17 pixels. The median subtracted image was then blinked in the same way as the unsubtracted images.

For the epochs taken through an Hα - continuum filter pair, we scaled and subtracted the continuum image from the Hα image to accentuate the objects with Hα emission. The a (1993) and the e, g, and h (1999) epochs had this combination which allowed us to blink the Hα bright objects in these epochs.

Figure 5.1 shows the locations of the detected novae on an image from the Digitized Sky Survey[1] covering the central 38' of the Fornax cluster, corresponding to our survey area. The novae are labeled by number and the galaxy identifications are also indicated. Since each nova was discovered using slightly different techniques, each will be discussed in detail below.

Nova 1. This nova was discovered in the unsubtracted T1 image from epoch b. It was easily compared with the T1 image from epoch c which has a deeper frame

[1]The Digitized Sky Survey was produced at the Space Telescope Science Institute under U.S. Government grant NAG W-2166. The images of these surveys are based on photographic data obtained using the Oschin Schmidt Telescope on Palomar Mountain and the UK Schmidt Telescope. The plates were processed into the present compressed digital form with the permission of these institutions.

Table 5.2. Fornax Cluster Nova Positions

	Position (J2000)				
Nova	RA	Dec	Epoch(s)	Galaxy	Distance (arcsec)
1	03:39:06.2	-35:23:48	b	NGC 1399	489
2	03:37:12.1	-35:44:11	a	NGC 1389	37
3	03:38:29.0	-35:29:02	d-h	NGC 1399	121
4	03:36:55.8	-35:28:39	d-h	NGC 1387	108
5	03:39:04.5	-35:34:45	i	NGC 1404	164
6	03:39:18.4	-35:35:55	d-h	NGC 1404	329

limit afforded by the longer exposure time (see Table 5.1). It appears near a faint unresolved object, but is at least 10 times brighter than that object. Figure 5.2 shows the three epochs of T1 images of the region (a, b, and c) and a subtraction of epoch c from epoch b, which removes the other stars in the field and shows Nova 1 quite well.

Nova 2. The 1999 a epoch Hα - T1 image revealed a bright Hα source near the galaxy NGC 1389. Our deep Hα image from from the 1999 e epoch allowed us to easily confirm that this source was transient and an excellent nova candidate, as illustrated in Figure 5.3. In addition, we confirmed that the object was not visible in the b and c epochs in the T1 filter at the candidate's position.

Nova 3. In this case we found a bright Hα source in the Hα - R image from the e epoch near the galaxy NGC 1399. We confirmed its transient nature by the fact that it was undetectable in all other Hα and R or T1 filter epochs. Because we had 5 closely spaced epochs in 1999, we were able to generate a light curve in Hα and B for this nova (see below), which solidified the classification of this object as a classical nova near the peak of its outburst.

Nova 4. This nova is nearly identical to Nova 3 in the way it was discovered, although its magnitude is fainter. The light curve is displayed in the next section and shows an offset between the Hα and B-band brightness of 2 magnitudes, similar to that shown by the novae in M31 (Ciardullo et al. 1990a). Due to its faintness, we were unable to derive a decline rate for this nova.

Nova 5. This nova was discovered in the 2003 i Hα epoch, which did not have a corresponding red continuum image to allow subtraction. It was compared with the deeper 1999 e epoch which proves that the source is transient, as shown in Figure 5.4. It also does not appear on any continuum (B or R or T1-band) image in any other epoch.

Nova 6. We discovered this nova in the B-band image from the 1999 epochs after we obtained the 2004 j B-band epoch. In the 1999 e Hα epoch it fell on a

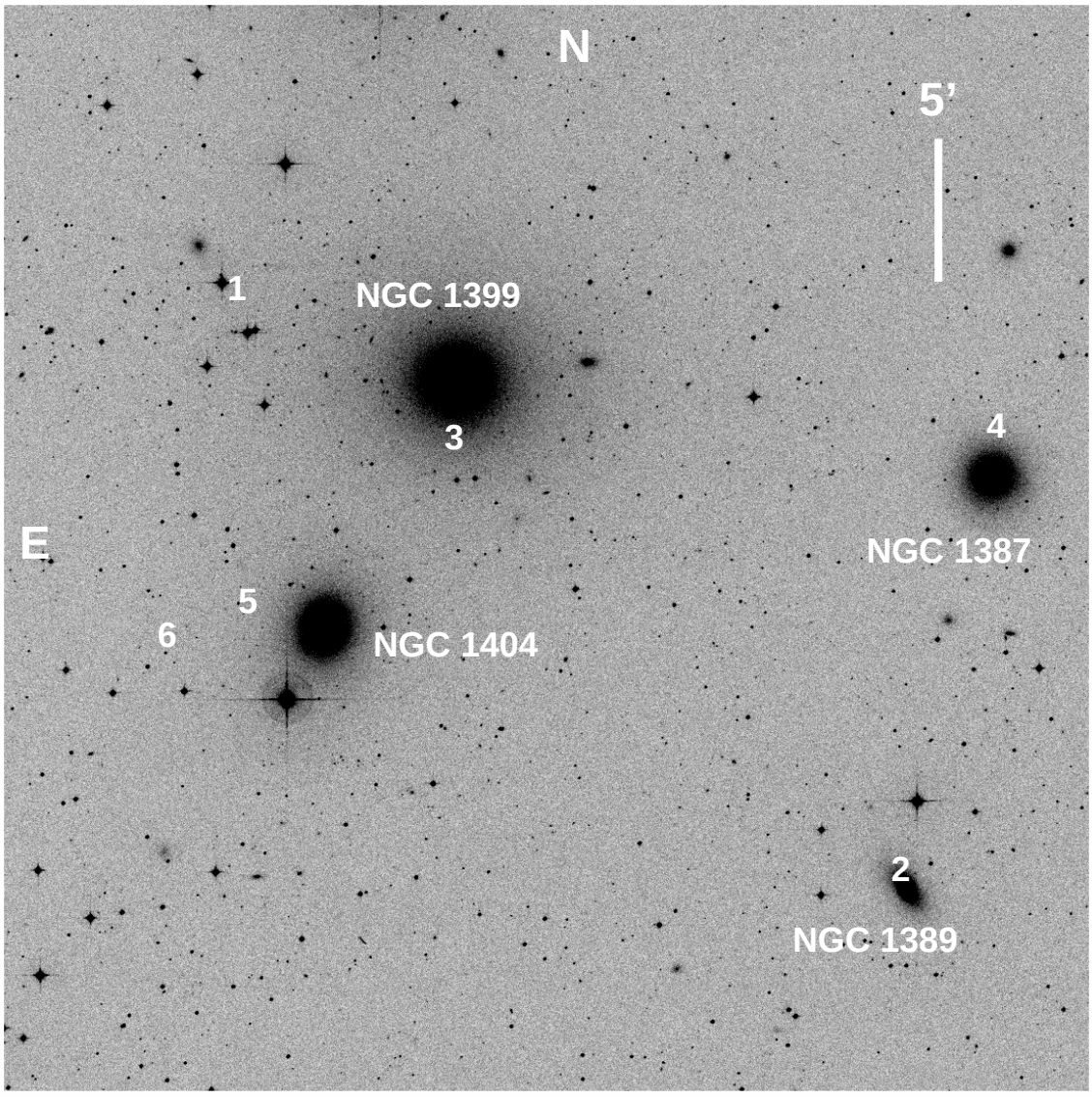

Figure 5.1: Locations of the 6 novae discovered in the Fornax cluster, indicated by nova number. North and East are at their usual orientation as labeled. The field of view is 38’ on a side. The galaxy identifications are indicated, along with a 5’ scale bar in the upper left corner. Note the positions of Nova 1 and Nova 6.

part of the chip that had a readout problem and therefore was missed using the Hα subtraction technique. It was missed in the comparison between the B-band epochs of a and e because the depth of the a epoch B-band image was not sufficient for a good comparison. After compensating for the readout problem, it did show up as a Hα source in the red continuum subtracted image. We were able to generate a B-band light curve (see below) and confirm it as a classical nova. The Hα magnitude is highly uncertain for this object because of the readout problem mentioned above.

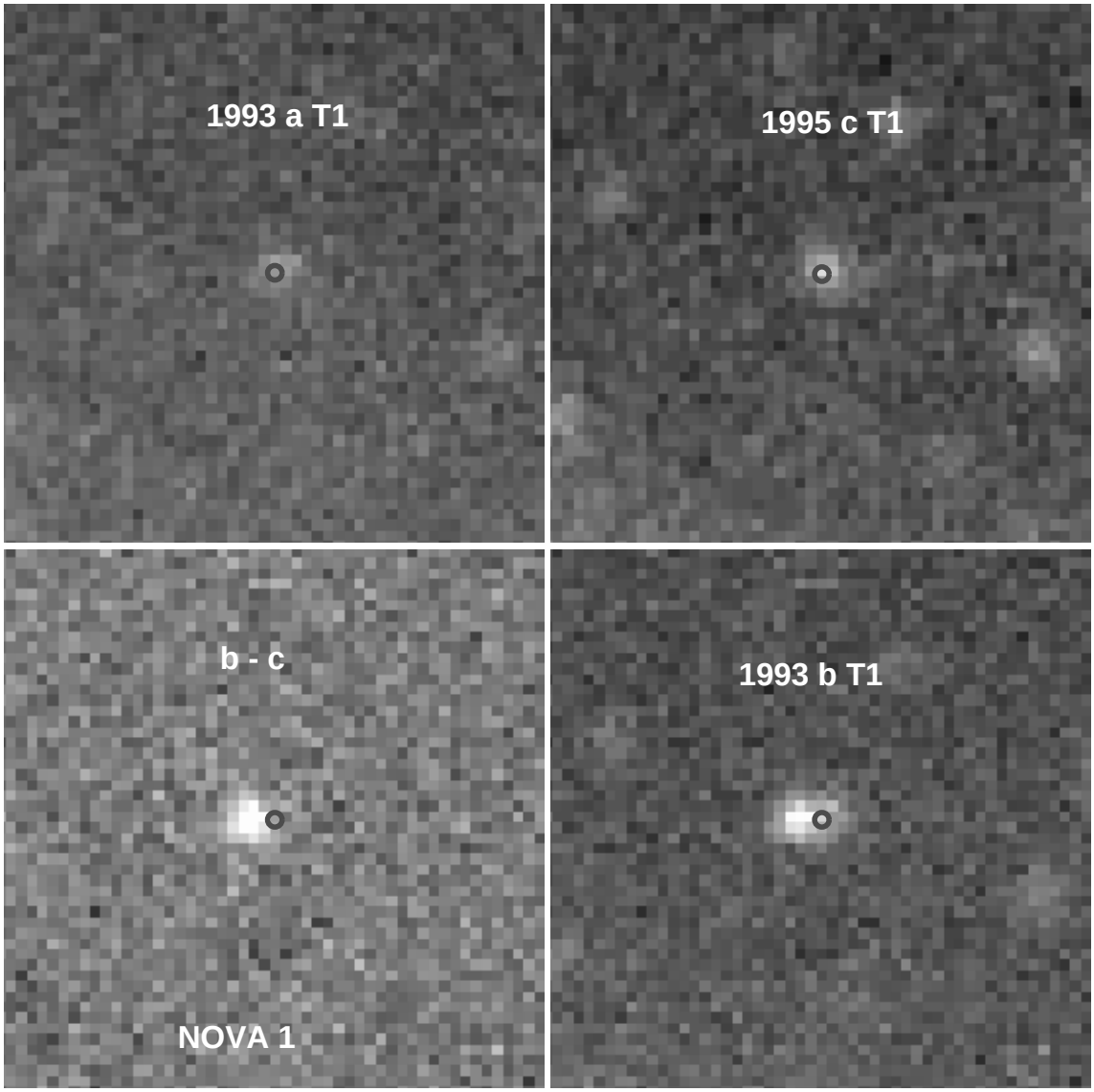

Figure 5.2: Three T1 filter epochs of the region around Nova 1 and a subtraction of epoch c from epoch b. The boxes are 22" on a side and are centered on the faint star whose position is indicated by the small circle. North is up and East is to the left. The subtraction clearly shows that Nova 1 is offset from the faint star.

5.4 Nova Photometry

Nova instrumental magnitudes were derived using DAOPHOT (Stetson 1987) aperture photometry. To account for variable seeing, we set the aperture radii to 1/2 the FWHM of the stellar profile measured from high signal-to-noise, well-isolated stars.

Photometric calibration was achieved using a variety of secondary standards. For B-band calibration we used the Yale/San Juan Southern Proper Motion Program (Platais et al. 1998) which had 7 unsaturated stars in common with our B-band

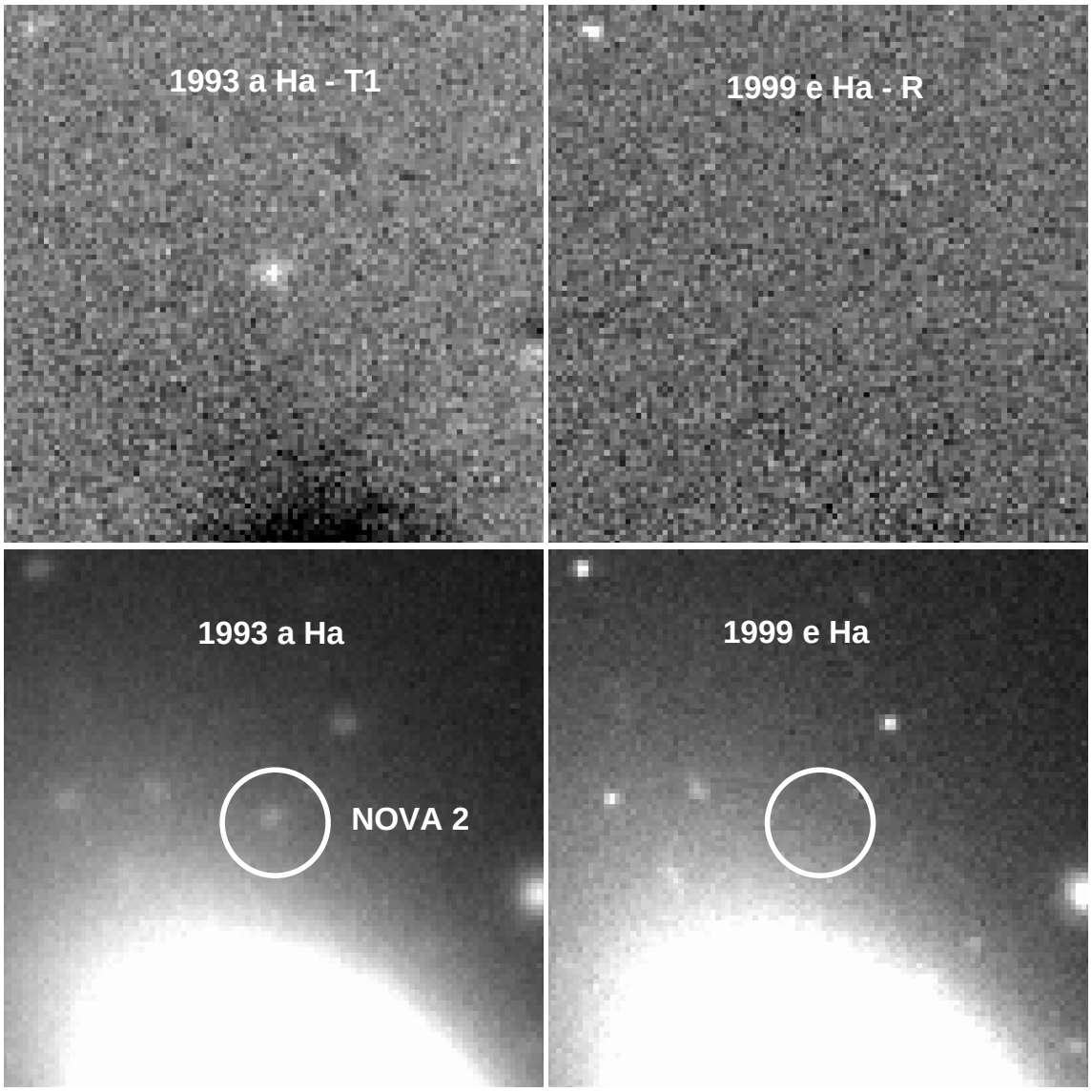

Figure 5.3: Hα - red continuum images from 1993 epoch a and 1999 epoch e are shown in the top two panels showing Nova 2 as a transient Hα bright source. The bottom two panels are the unsubtracted Hα images from the same epochs. North is up and East to the left. The field of view is 27" across.

observations in 1999. This produced a calibration accurate to 0.1 magnitudes. For the calibration of the T1, and Hα photometry we used the R-band magnitudes for the globular clusters published by Kissler-Patig et al. (1999). For the calibration we used measurement apertures that were at least as large as those used to produce the published magnitudes (Grillmair et al. 1994). Since the T1 and the R filter cover a similar wavelength range, we simply forced the T1 magnitudes to the R system. For the Hα magnitudes, we have made the simplifying assumption that the filter bandpass is uniformly filled by the nova light. Without spectra of each nova this avoids highly uncertain corrections for bandpass filling. We then simply calculated the

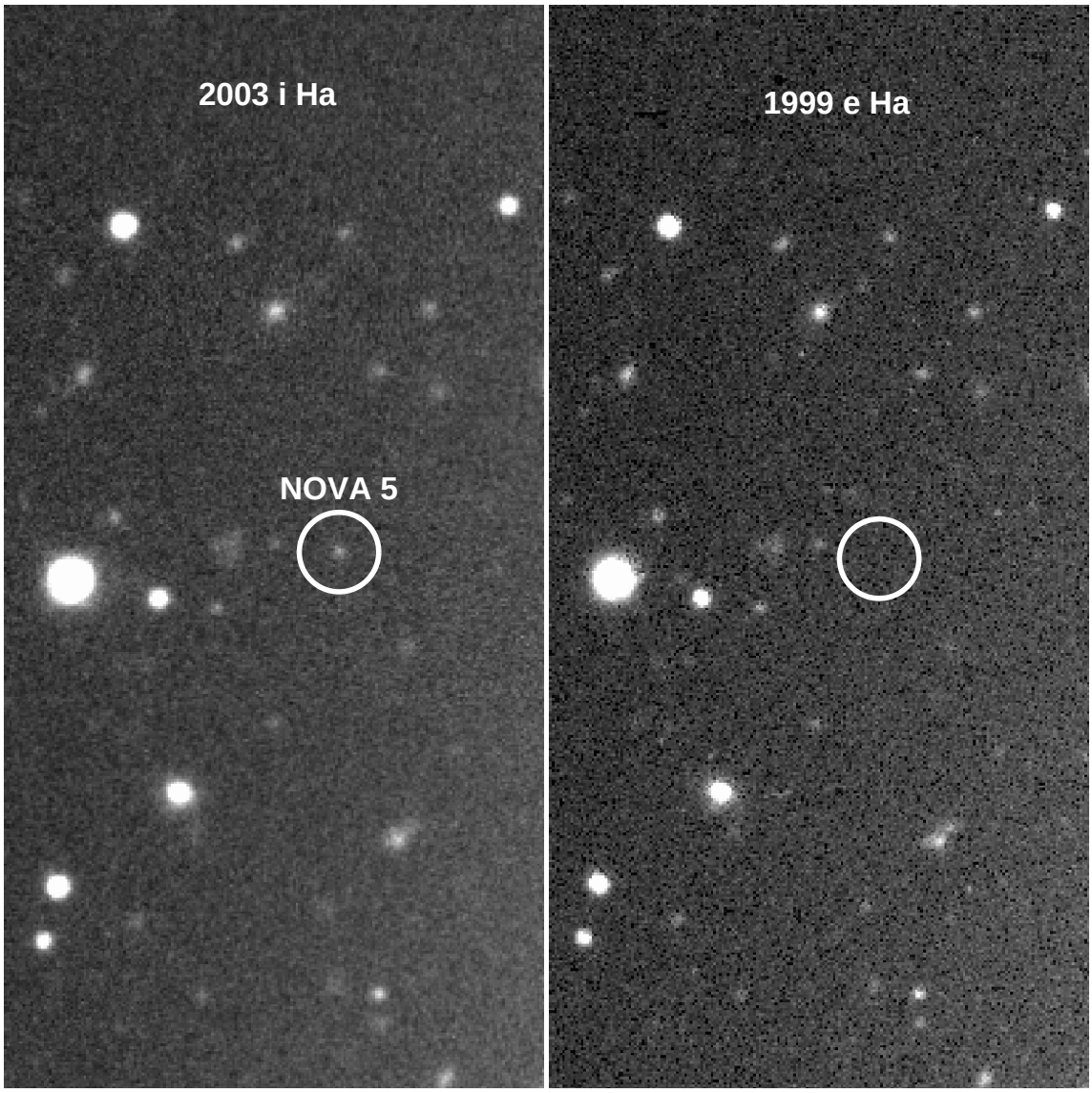

Figure 5.4: Hα images from the 2003 i epoch and the 1999 e epoch, showing that Nova 5 is indeed a transient Hα source. The fields have North up and East to the left and are both 52" wide.

offset between the R system and our instrumental Hα magnitudes using the globular clusters, and applied this offset to force our Hα magnitudes to the R system. In § 3.5 we measured the offset between the Hα and R systems to be -0.26 ± 0.13 magnitudes. Because this was with a narrower filter, and without sources with measured Hα fluxes to verify this, we chose not to apply a correction, and instead assume an external error of 0.25 Hα magnitudes. As such, our Hα magnitudes should not be interpreted as the flux in the line, but as simple filter magnitudes. The number of objects used to perform the calibration varied from 13 to 30. Table 5.3 lists the calibrated magnitudes for each nova. The errors quoted are the internal measurement errors and in most cases are smaller than the external calibration errors.

Table 5.3. Fornax Cluster Nova Photometry

Nova	J. D. (+240000)	Epoch	Filter	m	Err(m)
1	49331.53	b	T1[a]	21.9	0.1
2	49299.84	a	Hα	21.1	0.4
3	51519.07	e	Hα	22.1	0.1
	51523.10	g	Hα	22.0	0.1
	51525.05	h	Hα	22.1	0.1
	51517.05	d	B	22.2	0.1
	51521.04	f	B	23.0	0.1
	51523.13	g	B	23.2	0.2
	51525.10	h	B	>23.0	···
4	51519.07	e	Hα	22.8	0.1
	51523.10	g	Hα	23.1	0.2
	51525.05	h	Hα	22.8	0.1
	51517.05	d	B	>24.9	···
	51521.04	f	B	24.8	0.3
	51523.13	g	B	>23.8	···
	51525.10	h	B	>23.0	···
5	52697.07	i	Hα	22.8	0.1
6	51519.07	e	Hα	24.2	0.5
	51523.10	g	Hα	>23.5	···
	51525.05	h	Hα	>22.8	···
	51517.05	d	B	23.4	0.1
	51521.04	f	B	24.2	0.1
	51523.13	g	B	> 24.3	···
	51525.10	h	B	> 22.7	···

[a]Photometry for this object was forced to the R-band system.

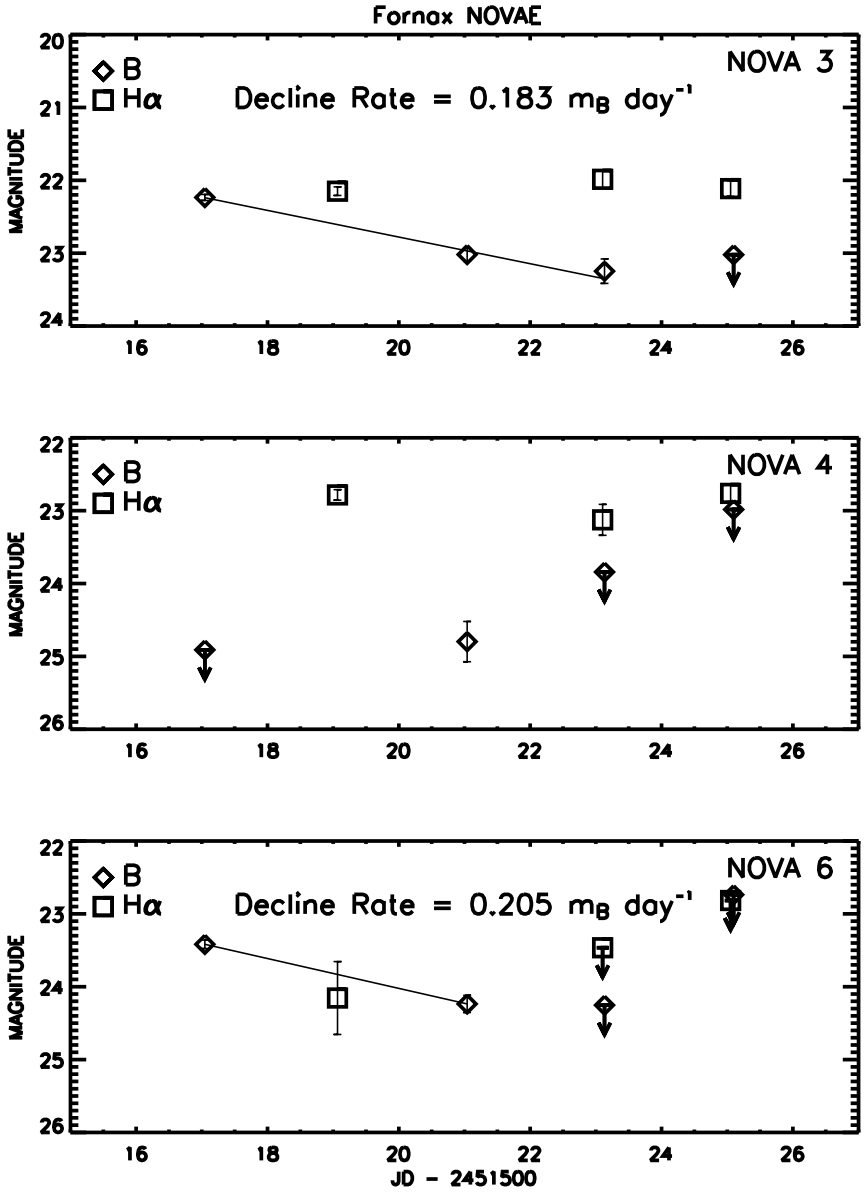

Figure 5.5: Light curves for Fornax Nova 3, Nova 4, and Nova 6. The squares are the Hα magnitudes and the diamonds are the B-band magnitudes. Points with downward pointing arrows are lower limits on the magnitudes. The decline rates were measured for Nova 3 and Nova 6 by using simple linear fits, indicated by the thin solid lines.

5.5 Nova Properties

We were fortunate that three of the novae erupted during the 5 epoch run in 1999. Figure 5.5 shows the light curves derived from the data for Nova 3, Nova 4, and Nova 6 in B and Hα. We were able to fit decline rates for two of these novae in the B-band. The resulting decline rate for Nova 3 is 0.183 m_B day^{-1} and for Nova 4 is 0.205 m_B day^{-1}. These decline rates were derived from simple linear fits and place

both novae in the fast nova category. This is consistent with the brightness of Nova 3 since decline rate is known to correlate with nova brightness (Shara 1981). Given the decline rate of Nova 4, it is clear that we caught this nova several magnitudes down from maximum. If we assume a distance modulus to Fornax of $(M - m)_0 = 31.35$ (Kissler-Patig et al. 1999), then our brightest novae reached $M_B = -9.2$ (Nova 3) and $M_{H\alpha} = -10.2$ (Nova 2). Our faintest novae reached $M_B = -6.6$ (Nova 4) and $M_{H\alpha} = -7.2$ (Nova 6).

These basic properties show that we have sampled a range of B and Hα brightnesses. Clearly there is incompleteness at the faint end and due to the sparse time sampling. As stated in § 5.1, we predicted 25 novae to have visible Hα emission down to the limit of $M_{H\alpha} = -7.5$ in any given Hα epoch, yet we detected only 5 novae in our 3 Hα epochs, a factor of 15 less than we expected. Even with generous corrections for incompleteness, this large discrepancy is hard to explain. One possible explanation is that the tidal debris in the cluster may consist mostly of the disrupted disks of late-type galaxies. The central density of Fornax is such that even the current ellipticals could have recently formed from disk galaxy mergers. Since our earlier results indicate that novae are predominantly associated with older populations, this would be consistent with the low apparent nova rate in the Fornax cluster. Feldmeier, Ciardullo & Jacoby (1998) suggest that the large number of intracluster PNe in Virgo implies that the intracluster stellar population in Virgo is of moderate age. Theuns & Warren (1997) found a similar number of PNe per square arcminute, after accounting for the differences in survey depths, implying that the ICL in Fornax could also be of intermediate age. Perhaps the reason Fornax is currently dominated by early-type galaxies is because the spirals have all been recently cannibalized. The novae we do see would be from the original bulges of the late-type galaxies.

A long-term, densely time-sampled study is required to derive the accurate nova rates in Fornax needed to resolve this issue. Without this kind of data we cannot place accurate constraints on the nova populations in the cluster. However, given that all regions in the survey suffer from the same time sampling limitations, an analysis of the spatial distribution of the novae is worthwhile.

5.6 The Spatial Distribution of the Novae

We deliberately limited ourselves to two simple questions about the spatial distribution of novae in the Fornax cluster. First, assuming that novae follow the bulge light, how many novae did we miss in the centers of the galaxies? Second, based on the light profiles of the galaxies, how many novae are associated with the cluster potential and not with any galaxy?

To answer these questions, we required the light profiles of the four galaxies in our survey region: NGC 1399, NGC 1404, NGC 1389, and NGC 1387. Since NGC 1399 has an extended halo, we used the study of Saglia et al. (2000) for its light profile. For the other profiles, we used our B-band mosaic image from the 1999 epochs. We measured their profiles using the ellipse task in the STSDAS **isophote** package. Isophotes were fit on background subtracted images with the background

being determined by the region in the chip most distant from the galaxy. The task was given the initial center position, position angle (PA), and ellipticity and allowed to vary these parameters at each semi-major axis position, which was set to grow geometrically and not linearly. This allowed the outer isophotes to contain enough signal to produce reasonable fits.

To answer the incompleteness question, we used artificial stars to determine our detection limit for each galaxy. Our goal was to produce a simple correction to the number of novae found in the galaxies. We used the artificial stars to ask the question, how close to the nucleus of the galaxy could the nova that was discovered in the galaxy be found? By comparing this radial limit to the light profile, we know how much light in the galaxy was effectively unsurveyed for novae of the brightness already discovered, and can thus make a correction based on the fraction of the total light unsurveyed.

DAOPHOT was used to generate a point spread function (PSF) and then used to add artificial stars around each galaxy. The galaxy images were then median-filtered, and subtracted, and (as described above) blinked to see where the artificial novae become undetectable. In all cases this limit was determined by the residual light left by the subtraction of the median-filtered image. Thus, the inner profiles of the galaxies strongly affected this detection limit.

Figure 5.6 shows the cumulative light profiles for the four galaxies, normalized to the total light. We set the total light limit at 26 B magnitudes per square arcsecond for the galaxies we measured. The profile of NGC 1404 was contaminated by a very bright star 180" from the galaxy, so we set a limit at that distance of 25 B magnitudes per square arcsecond.

The first thing we notice is the extent of the halo of NGC 1399. Nearly the entire survey area is enclosed by this halo. We will assume that this halo actually traces the inner potential well of the cluster itself as suggested by Merritt (1984). We also see that Nova 2 is clearly associated with NGC 1389 being close to the half-light radius, but the association of the other novae is not straightforward. Nova 4 appears at a radius that encloses over 80% of the light of NGC 1387, while Nova 5 and Nova 6 are even farther outside of NGC 1404. Interpreting the nova placement in NGC 1399 is complicated by the extended halo, although it seems clear that Nova 3 belongs with that galaxy. The extent of the halo of NGC 1399 means that Nova 1 is located just beyond the half-light radius, but clearly it is more properly placed in the cluster rather than that galaxy (see Figure 5.1). To illustrate this situation, we also placed Nova 6 on the NGC 1399 light profile and it appears at a radius that encloses only 65% of the light. To be conservative, we'll assume that 4 of our novae (2, 3, 4, and 5) are associated with the galaxies in the cluster and 2 (1 and 6) are not. But how many novae did we miss in the centers of the galaxies?

To generate a correction for missed novae, we look at the fraction of light unsurveyed, as determined by our detection limits and plotted as the vertical dot-dashed lines in Figure 5.6. For NGC 1399 this fraction of unsurveyed light is 0.15, for NGC 1404 it is 0.4, for NGC 1387 it is 0.3 and for NGC 1389 it is 0.45, giving a total unserveyed light fraction of $1.3/4 = 0.325$. Since we found 1 nova per galaxy, this would essentially add another $0.325 \times 4 = 1.3$ novae to our number associated with

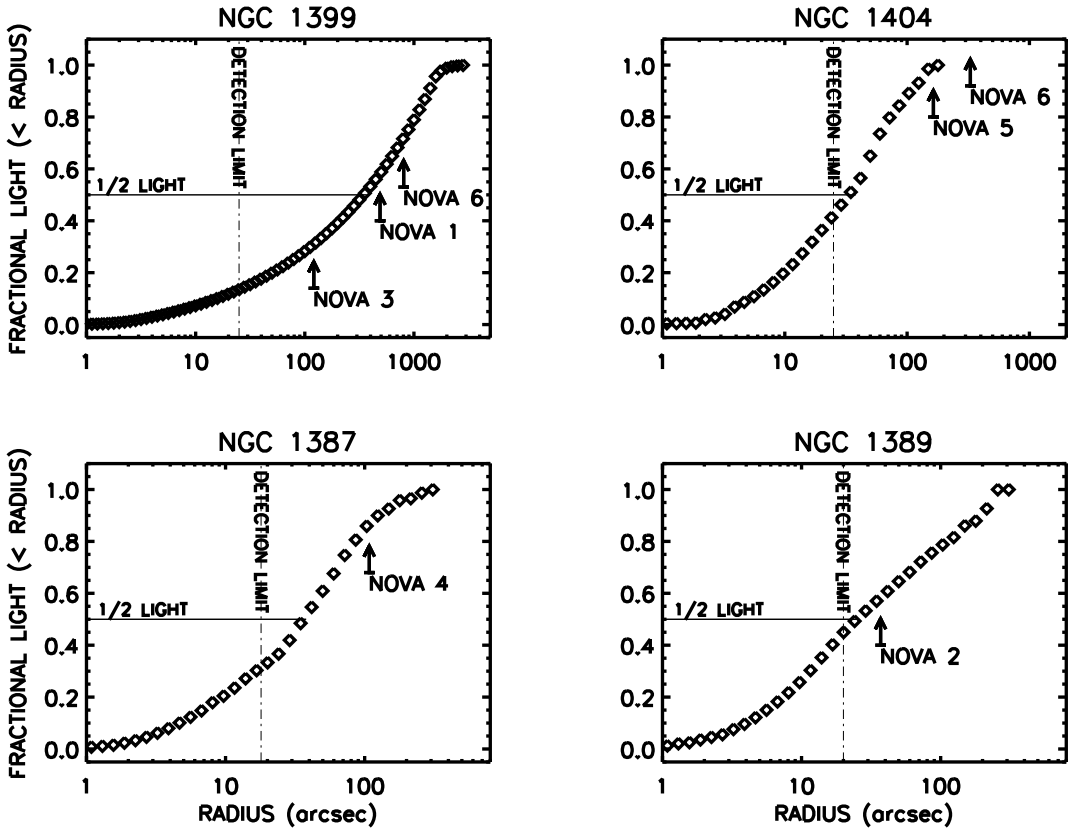

Figure 5.6: Cumulative light profiles for NGC 1399, NGC 1404, NGC 1387, and NGC 1389 in fraction of total light versus radius in arcseconds indicated by the diamonds. The detection limits are indicated by the dot-dashed line and the positions of the novae are indicated by the upward pointing arrows and labeled by the nova id. The 1/2 light level for each galaxy is labeled and indicated with a thin solid horizontal line.

galaxies, giving a final score of 5.3 novae in and 2 novae outside of galaxies in the cluster.

5.7 The Intra-Cluster Light in Fornax

Assuming that novae trace the light, we calculate that the ICL contributes $2/(5.3+2) = 27\%$ of the total light in the Fornax cluster. This is less than the estimate of 40% by Theuns & Warren (1997), who used intergalactic planetary nebulae (PNe), and is close to the estimate of the ICL fraction in Virgo (22%) by Feldmeier, Ciardullo & Jacoby (1998) who also use PNe. We are very aware that we are dealing with small numbers. If we move one nova from the out to the in category, we get an ICL fraction of $1/(6.3+1) = 14\%$ of the total light. If we go the other way and move one nova from the in to the out category (say, Nova 5), we get an ICL fraction of $3/(4.3+3) = 41\%$ in good agreement with the result from Theuns & Warren (1997). All these numbers

are within the range of other measures of ICL; thus, we have demonstrated for the first time that novae can be useful tracers of the ICL.

It is tantalizing that two of the novae (Nova 4 and Nova 5) are beyond the half-light radii of their hosts. This could indicate that tidal stripping is ongoing and that these galaxies are in the process of losing stars in the outer regions. Given our detection limits, it is remarkable that we did not detect more novae closer to the nuclei of these galaxies.

5.8 Future Work

Clearly, a longer-term, densely time-sampled survey in Hα and continuum light of this region would allow us to provide a much more accurate measure of the ICL in Fornax. This kind of survey would not only bolster the statistics by adding more novae, but would also provide light curves which can be used to verify novae and estimate their peak brightnesses. It would also allow us to estimate the nova rates in each galaxy and in the ICL. This would be the first step to estimating the effect of the galaxy cluster environment on close binary stars.

It would be interesting to see if, with a larger number of objects, novae begin to be detected closer to the nuclei of the galaxies. It would be remarkable if it turns out that the novae do not follow the light of the galaxies in Fornax. This would be very different from what is seen in nearby galaxies, and would have very interesting implications for the dynamics of galaxies in clusters.

5.9 Conclusions

1. The number of novae discovered in Fornax is a factor if 15 less than expected, even given generous estimates of incompleteness. One possible explanation is the recent conversion of late-type spirals in the cluster to ellipticals through mergers. This is supported by results from our study of M81 (Neill & Shara 2004a) in which the novae were predominantly associated with the older, bulge population and not with the disk population. Only a longer-term, densely time-sampled survey of Fornax can produce accurate enough nova rates to resolve this.

2. Intra-cluster novae do exist in the Fornax cluster and their distribution is consistent with $\sim$25% of the total light in the cluster being contributed by the ICL. This result is bracketed by studies using PNe in Fornax and Virgo (Theuns & Warren 1997; Feldmeier, Ciardullo & Jacoby 1998).

3. Novae are interesting as tracers of the ICL. Their brightness at peak (M_B up to -10) allows them to be visible out to the Coma cluster with current telescopes. Once our understanding of nova parent populations improve, they may also be useful for constraining the origin of the tidal debris in clusters.

Chapter 6
Concluding Remarks

The aim of this thesis was to explore the relationship between CVs and their environment. In order to overcome the selection biases that have plagued this kind of study in the past, we applied resources that were heretofore unavailable for long-term studies. Given the surprises that resulted, our broadest conclusion is that the systematic application of these long-term, comprehensive surveys will produce drastic changes in our understanding of the workings of environment on CV formation and evolution. As large-format CCD cameras covering degree-sized fields of view begin to be deployed on robotically controlled and/or queue scheduled telescopes, the kind of surveys we conducted for this study will become commonplace. We can look forward to high-quality observational constraints on CV formation and evolution theory in the near future.

More specifically, we have shown that a dwarf nova that formed in a globular cluster has an orbital period that falls within the normal range for DN in the Milky Way. We have also provided evidence that this DN may be in the process of being ejected from the cluster, which supports the idea that globular clusters are important sources of CVs.

We have performed the first densely time-sampled, comprehensive, long- term nova survey of an external galaxy and shown that the novae in M81 are predominantly associated with the older, bulge stellar population. This disagrees with the most basic prediction of nova formation and evolution theory (Yungelson, Livio & Tutukov 1997) which predicts more novae in the younger disk population. A consistent picture of novae as associated with older stellar populations may be emerging, bolstered by recent longer estimates of the magnetic breaking evolution timescale for CVs (Andronov, Pinsonneault & Sills 2003) which may also explain why fewer short-period CVs than predicted are seen. It appears that observations are only beginning to provide meaningful constraints on CV evolution theory.

We have shown the extent to which completeness may be a factor in determining nova rates in external galaxies by surveying four local group dwarf ellipticals. These systems are nearby, have little or no dust, and must have nova completenesses approaching 100%. We found by using the comprehensive, densely time-sampled technique, that the nova rate per unit light for these systems is much higher than for more complex, distant galaxies. Either these systems produce more close binaries, or incompleteness in larger, more complex galaxies produces systematically underestimated nova rates.

We have discovered a remarkably low luminosity nova in NGC205, which has intriguing implications for nova rates measured in external galaxies. Recent theoretical calculations show that novae do occur in systems with WD masses down to $0.4 M_{\odot}$ with properties similar to NGC205 Nova 1 (Shara 2004). If this object represents an entire class of novae, then our surveys must take these objects into account when attempting to trace extragalactic binaries with novae.

We have shown that intra-cluster novae apparently exist in the Fornax cluster. As a proof-of-concept, we have shown that the spatial distribution of the novae in Fornax is consistent with $\sim$25% of the total light in the cluster arising from the ICL. We have discovered an intriguingly low nova rate in Fornax that may have implications for the stellar populations in the cluster.

As better samples of novae from different populations become available, we will be able to delineate the relationship between novae and their underlying stellar population. If we are lucky, at some point we will be able to invert this problem and use novae to probe distant stellar populations. With the exception of Type Ia supernovae, novae are the most distant observable close binary systems and are at least 1000 times more common than SN Ia's. Only by acquiring the comprehensive, densely time-sampled data sets like those presented here will we be able to move close binary theory toward the level of understanding enjoyed by single star theory today.

Bibliography

Aaronson, M. 1978, ApJ, 221, L103

Andronov, N., Pinsonneault, M., & Sills, A. 2003, ApJ, 582, 358

Arp, H. C. 1956, AJ, 61, 15

Baraffe, I. & Chabrier, G. 1996, ApJ, 461, L51

Bochkarev, N. G., Karitskaya, E. A., & Shakura, N. I. 1979, SvA, 23, 8

Boughn, S. P., Kuhn, J. R., & Uson, J. M. 1990, IAU Symp. 139: The Galactic and Extragalactic Background Radiation, 139, 357

Ciardullo, R., Ford, H., & Jacoby, G. 1983, ApJ, 272, 92

Ciardullo, R., Ford, H. C., Neill, J. D., Jacoby, G. H., & Shafter, A. W. 1987, ApJ, 318, 520

Ciardullo, R., Jacoby, G. H., Ford, H. C., & Neill, J. D. 1989, ApJ, 339, 53

Ciardullo, R., Shafter, A. W., Ford, H. C., Neill, J. D., Shara, M. M., & Tomaney, A. B. 1990a, ApJ, 356, 472

Ciardullo, R., Tamblyn, P., Jacoby, G. H., Ford, H. C., & Williams, R. E. 1990b, AJ, 99, 1079

della Valle, M., Rosino, L., Bianchini, A., & Livio, M. 1994, A&A, 287, 403

della Valle, M. & Livio, M. 1998, ApJ, 506, 818

de Vaucouleurs, G., de Vaucouleurs, A., Corwin, H. G., Buta, R. J., Paturel, G., & Fouque, P. 1991, Third Reference Catalogue of Bright Galaxies (New York: Springer)

Dressler, A. 1984, ARA&A, 22, 185

Fabian, A. C., Pringle, J. E., & Rees, M. J. 1975, MNRAS, 172, 15P

Feldmeier, J. J., Ciardullo, R., & Jacoby, G. H. 1998, ApJ, 503, 109

Ferguson, H. C. 1989, AJ, 98, 367

Ferguson, H. C., Tanvir, N. R., & von Hippel, T. 1998, Nature, 391, 461

Ferrarese, L., Côté, P., & Jordán, A. 2003, ApJ, 599, 1302

Filippenko, A. V. & Chornock, R. 2003, IAU Circ., 8086, 3

Freedman, W. L. et al. 2001, ApJ, 553, 47

Frogel, J. A., Persson, S. E., Matthews, K., & Aaronson, M. 1978, ApJ, 220, 75

Gray, D. F. 1976, The Observation and Analysis of Stellar Photospheres (New York: Wiley-Interscience)

Grillmair, C. J., Freeman, K. C., Bicknell, G. V., Carter, D., Couch, W. J., Sommer-Larsen, J., & Taylor, K. 1994, ApJ, 422, L9

Grillmair, C. J. et al. 1996, AJ, 112, 1975

Grindlay, J. E., Heinke, C., Edmonds, P. D., & Murray, S. S. 2001, Science, 292, 2290

Han, M., Hoessel, J. G., Gallagher, J. S., Holtsman, J., & Stetson, P. B. 1997, AJ, 113, 1001

Hatano, K., Branch, D., Fisher, A., & Starrfield, S. 1997, ApJ, 487, L45

Hjellming, M. S. & Taam, R. E. 1991, ApJ, 370, 709

Horne, J. H. & Baliunas, S. L. 1986, ApJ, 302, 757

Hurley, J. R. & Shara, M. M. 2002, ApJ, 570, 184

Hut, P. 1985, IAU Symp. 113: Dynamics of Star Clusters, 113, 231

Jacoby, G. H., Ciardullo, R., Booth, J., & Ford, H. C. 1989, ApJ, 344, 704

Jarrett, T. H., Chester, T., Cutri, R., Schneider, S. E., & Huchra, J. P. 2003, AJ, 125, 525

Kissler-Patig, M., Grillmair, C. J., Meylan, G., Brodie, J. P., Minniti, D., & Goudfrooij, P. 1999, AJ, 117, 1206

Knigge, C., Shara, M. M., Zurek, D. R., Long, K. S., & Gilliland, R. L. 2002, Stellar Collisions, Mergers and their Consequences, ASP Conference Proceedings, Vol. 263. , ed. M. M. Shara, San Francisco, Astronomical Society of the Pacific, p.137

Kolb, U. 1993, A&A 271, 149.

Kolb, U. & Baraffe, I. 1999, MNRAS, 309, 1034.

Kukarkin, B. V. & Mironov, A. V. 1970, AZh, 47, 1211

Lee, M. G., Freedman, W. L., & Madore, B. F. 1993, AJ, 106, 964

Lee, M. G. 1996, AJ, 112, 1438

Magnier, E. A., Lewin, W. H. G., van Paradijs, J., Hasinger, G., Jain, A., Pietsch, W., & Truemper, J. 1992, A&AS, 96, 379

Magrini, L., Perinotto, M., Corradi, R. L. M., & Mampaso, A. 2001, A&A, 379, 90

Margon, B., Downes, R. A., & Gunn, J. E. 1981, ApJ, 247, L89

Merritt, D. 1984, ApJ, 276, 26

Miller, G. E. 1983, ApJ, 268, 495

Mink, D. J. 2002, ASP Conf. Ser. 281: Astronomical Data Analysis Software and Systems XI, 11, 169

Moses, R. N. & Shafter, A. W. 1993, Bulletin of the American Astronomical Society, 25, 1248

Naylor, T. et al. 1989, MNRAS, 241, 25P

Neill, J. D., Shara, M. M., Caulet, A., & Buckley, D. A. H. 2002, AJ, 123, 3298

Neill, J. D. & Shara, M. M. 2004a AJ, 127, 816

Neill, J. D. & Shara, M. M. 2004b AJ, submitted

Neill, J. D. , Shara, M. M., & Oegerle, W. R. 2004c in preparation

Nowotny, W., Kerschbaum, F., Olofsson, H., & Schwarz, H. E. 2003, A&A, 403, 93

Oosterhoff, P. T. 1941, Annalen van de Sterrewacht te Leiden, 17, 41

Partridge, R. B. 1990, IAU Symp. 139: The Galactic and Extragalactic Background Radiation, 139, 283

Patterson, J. 2004, private communication

Perelmuter, J. & Racine, R. 1995, AJ, 109, 1055

Platais, I., et al. 1998, AJ, 116, 2556

Pooley, D., Lewin, W. H. G., Homer, L., Verbunt, F., Anderson, S. F., Gaensler, B. M., Margon, B., Miller, J., Fox, D. W., Kaspi, V. M., & van der Klis, M. 2002, ApJ, 569, 405

Press, W. H. & Rybicki, G. B. 1989, ApJ, 338, 277

Prialnik, D., & Kovetz, A. 1995, ApJ, 445, 789

Pritchet, C. J. & van den Bergh, S. 1987, ApJ, 318, 507

Richstone, D. O. 1976, ApJ, 204, 642

Rosino, L. 1973, A&AS, 9, 347

Saglia, R. P., Kronawitter, A., Gerhard, O., & Bender, R. 2000, AJ, 119, 153

Sandage, A. 1961, in The Hubble Atlas of Galaxies (Washington: Carnegie Institution) atlas page 19.

Sandage, A. & Tammann, G. A. 1981, Carnegie Inst. of Washington, Publ. 635

Sandage, A. 1984, AJ, 89, 621

Sandquist, E. L., Bolte, M., Stetson, P. B., & Hesser, J. E. 1996, ApJ, 470, 910

Scargle, J. D. 1982, ApJ, 263, 835

Schlegel, D. J., Finkbeiner, D. P., & Davis, M. 1998, ApJ, 500, 525

Shafter, A. W., Ciardullo, R., & Pritchet, C. J. 2000, ApJ,530, 193

Shafter, A. W. & Irby, B. K. 2001, ApJ, 563, 749

Shara, M. M. 1981, ApJ, 243, 926

Shara, M. M., Potter, M., & Moffat, A. F. J. 1987, AJ, 94, 357

Shara, M. M., Potter, M., & Moffat, A. F. J. 1990, AJ, 99, 1858

Shara, M. M., Sandage, A., & Zurek, D. R. 1999, PASP, 111, 1367

Shara, M. M. 2004, private communication

Simien, F. & de Vaucouleurs, G. 1986, ApJ, 302, 564

Stetson, P. B. 1987, PASP, 99, 191

Stetson, P. B. 2000, PASP, 112, 925

Theuns, T. & Warren, S. J. 1997, MNRAS, 284, L11

Tody, D. 1986, Proc. SPIE, 627, 733

Tomaney, A. B. & Shafter, A. W. 1992, ApJS, 81, 683

Vilchez-Gomez, R., Pello, R., & Sanahuja, B. 1994, A&A, 283, 37

Warner, B. 1995, Cataclysmic Variable Stars, Cambridge Astrophysics Series (Cambridge, New York: Cambridge University Press)

Webbink, R. F. 1990, Accretion-Powered Compact Binaries, ed. C. W. Mauche, Cambridge University Press, Cambridge, p.177

Weisz, D. & Li, W. 2003, IAU Circ., 8069, 2

Yungelson, L, Livio, M., & Tutukov, A. 1997, ApJ, 481, 127

Zurek, D. 2001, private communication